# FEATURE BASED COSTING OF EXTRUDED PARTS

BY

JOSE TORRE NIETO

THESIS

Submitted in partial fulfillment of the requirements
for the degree of Master of Science in Mechanical Engineering
in the Graduate College of the
University of Illinois at Urbana-Champaign, 2010

Urbana, Illinois

Adviser:

Associate Professor Michael L. Philpott

# ABSTRACT

This thesis presents the creation of a model to predict the manufacturing cost of parts made by the extrusion process. Feature Based Costing (FBC) techniques have been used to develop the cost model, which is intended to be used early in the design phase of a part, when the geometry and the material are being defined in a Computer Aided Design (CAD) software by the designer. The cost model was developed specifically for hot extruded parts made of aluminum alloys, extruded in the forward direction using single-hole dies, as this was found to be the case for the majority of extrusion work in the industry.

As the cost model is developed, the main Geometric Cost Drivers (GCDs) and Non-Geometric Cost Drivers (NGCDs) of a part made by the hot extrusion process are identified. The main outputs of the model include the Piece Part Cost (broken down into its various recurring costs components), the Amortized Investment (i.e. Amortized Tooling Cost) and ultimately the Manufacturing Cost. The Piece Part Cost estimation includes an algorithm for selecting the optimal combination of press and billet size to extrude a given shape. Extrusion speed, cycle time and yield are all calculated by the model as well. The Piece Part Cost Model was validated against actual quotes data from extruders in the US for a number of different designs. The model predictions were shown to correlate within 3% to the actual quotes.

Unlike the Piece Part Cost, the Tooling Cost part of the model is of empirical nature, obtained by Multivariate Regression techniques from actual quotes data provided by extruders in the US. The Tooling Cost Model was validated statistically, and it was shown to explain 84% of the variance observed in the actual quotes. Finally, the complete Manufacturing Cost Model developed herein was successfully implemented in a Computer Spreadsheet, which is included as a supplemental file for this thesis, representing a fantastic tool for design engineers, manufacturing engineers and any other Design for Manufacture (DFM) practitioners in general.

*This work is dedicated to the memory of my mother.*

# ACKNOWLEDGEMENTS

This project could not have been completed without the valuable contributions and support of numerous persons who made it possible. I wish to thank the following people and organizations in particular:

- My advisor, Dr. Mike Philpott for the outstanding guidance, availability and support in this research project. Your practical engineering mindset has greatly inspired me during my graduate studies.
- The extrusion industry professionals who kindly provided valuable information for this research: Greg Lea (Aluminum Extruders Council), Hans-Uwe Rode (SMS Meer), Scott Burket (UBE), Terry Mullins (TCE), James Way (Bonnell), and Shane Carpenter (Bonnell).
- The sponsors of my graduate program: Fulbright, COMEXUS, the US Department of State, and the University of Illinois at Urbana-Champaign (UIUC).
- My recommendation letters' writers for my Fulbright Fellowship and UIUC Admission: Ed Rainous (General Electric), Jeff Herbert (General Electric), Dr. Gabriel Viesca (General Electric), Carlomagno Rivas (General Electric), Juan Asencio (General Electric) and Dr. Ricardo Ramírez (Tec de Monterrey). I simply cannot express how grateful I am with all of you.
- My parents, brother and sister, for all the values you taught me and for making me the person I am.
- Finally, most of all, my lovely wife Cynthia for your encouragement in pursuing graduate education abroad. Your relentless support, love and patience have been the key for the successful completion of this project. It is mainly because of you that my graduate school experience was so memorable.

# TABLE OF CONTENTS

# CHAPTER 1: INTRODUCTION AND STATE OF THE ART

## 1.1 Introduction

The manufacturing industry is one of the main drivers of today's global economy, representing approximately 20% to 30% of the value of all goods and services produced in industrialized countries [1]. The product design process is a critical activity for manufacturers, as it has been estimated that about 70% to 80% of the cost of product development and manufacture is determined at the initial design stages [1]. Ironically, in most manufacturing organizations, design and manufacture are separate areas and information has to be passed across the boundaries, often resulting in costly design iterations, long product development cycle times and high manufacturing costs [2]. Thus, modern approaches like Concurrent Engineering (CE) and Design for Manufacture (DFM) represent very attractive options for successfully integrating design and manufacturing functions in the industry, with the objective of minimizing the time and costs involved in taking a product from the conceptual design phase to production and introduction into the marketplace.

From a typical engineering perspective, every single product must be designed to perform a specific function in an efficient way and withstand certain operating conditions without failure during its entire useful life. Historically, design engineers have tended to focus on such technical aspects only, leaving the business part of the process to "other people" and neglecting important "downstream" considerations that affect the usability and cost of the product during its lifetime [3]. In response, Westney [4] states that "*successful engineers today understand that technical work is merely part of a cost-driven business process. In most companies, the successful project is not necessarily the one that has the most sophisticated design, but more likely it is the one that makes the most money. Modern engineers know that a project that was a technical success will be judged a business failure if costs are not analyzed and controlled*".

Manufacturing cost is considered as the most complete measure of manufacturability of a product [3]. Thus, computer systems that provide cost estimations on alternative designs can offer "*a highly useful measure of which design alternative is preferable*" [3], representing a fantastic tool for design engineers, manufacturing engineers and any other DFM practitioners in general. Surprisingly, there are still some manufacturing processes for which cost estimates rely strongly on expert's opinion and/or historical records. For instance, according to Greg Lea, a consultant to the extrusion industry with more than 15 years of experience in process optimization, the quoting methods used by extruders are not very sophisticated, as there are no analytical or empirical cost models that are standards within the industry; instead, most companies use their own pricing methods.

Having the preceding ideas as motivation, the objective of this thesis is to create a model to predict the manufacturing cost of parts made by the Extrusion process. The cost model is intended to be used early in the design phase of a part, when the geometry and the material are being defined in a CAD software by the designer. Extrusion is a continuous manufacturing process that competes with Roll Forming (another continuous process) and with non-continuous processes like Stamping and Hydroforming, and is used in a wide range of applications in the automotive, aerospace, energy and construction industries, to name a few [5],[6]. Before getting into manufacturing cost estimation ground, it is deemed necessary to present some background information and state of the art review on the extrusion process technology. That is indeed the objective of the following section.

## 1.2 Extrusion Process Background and State of the Art

Extrusion is a Bulk Deformation Process used to produce long lengths of solid or hollow products with constant cross-section. In the most basic form of extrusion, a round billet is placed in a chamber and forced through a die opening by a ram. The die design is what determines the cross section of the profile. The extruded product can then be cut off to desired lengths in a subsequent operation.

### *1.2.1 Extrusion Processes Types*

Depending on the direction of metal flow, extrusion processes can be either **Forward** (also called Direct), **Backward** (also called Indirect) or **Lateral**. A schematic of these processes is shown in Figure 1.1, and examples of each type of extrusion are depicted in Figure 1.2. Forward Extrusion is the most common of these three methods [6]. Besides the direction of metal flow, extrusion processes can be classified according to their characteristics in the following types: Hot Extrusion, Cold Extrusion, Impact Extrusion, Hydrostatic Extrusion, Coextrusion and Equal Channel Angular Extrusion (ECAE). All these processes differ in equipment, tooling and operating conditions, and all of them have advantages and drawbacks in relation to the others.

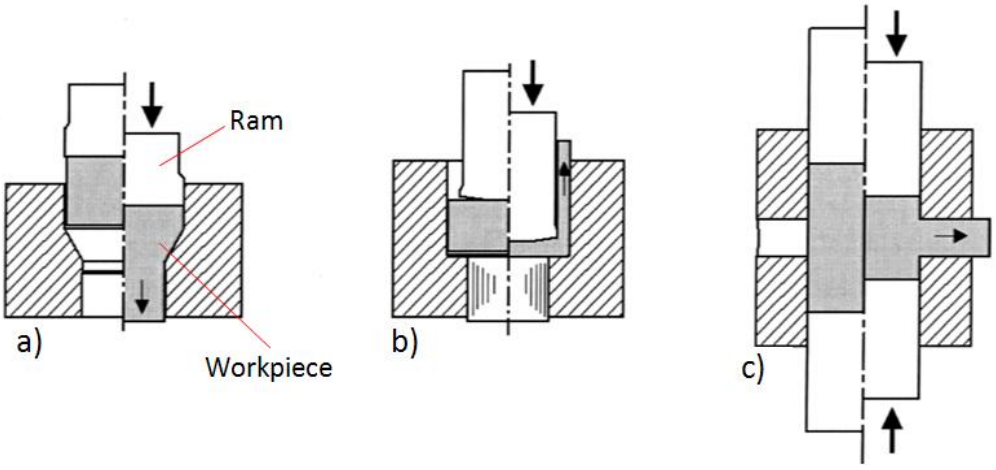


**Figure 1.1** Extrusion types by direction of metal flow: a) Forward, b) Backward, c) Lateral [6].


**Figure 1.2** Parts made by (a) forward extrusion, (b) backward extrusion, and (c) lateral extrusion [6].

**Hot Extrusion** is the most typical extrusion process used in the industry [6]. As the name implies, this process is carried out at elevated temperatures, generally greater than 60% of the absolute melting temperature of the metal [6]. Depending on the material being worked, hot extrusion can be either lubricated or non-lubricated. Aluminum Alloys are generally non-lubricated, while Steel, Titanium, and Copper Alloys are typically lubricated [6].

In **Cold Extrusion,** the starting material (billet/slug) is at room temperature. However, during the process the material undergoes deformation heating to several hundred degrees. Typically, a punch is used to apply pressure to the billet enclosed, partially or completely, in a stationary die, as shown in Figure 1.3. Aluminum and aluminum alloys, copper and copper alloys, carbon steels, alloy steels, and stainless steels can be cold extruded [6]. Compared to hot extrusion, the advantages of cold extrusion are: dimensional precision, improved surface finish, no oxides layers formed, cold work benefit, high production rates and relatively low costs [1]. The drawbacks are higher loads, higher lubrication cost, limited deformation, and limited shape complexity [6].

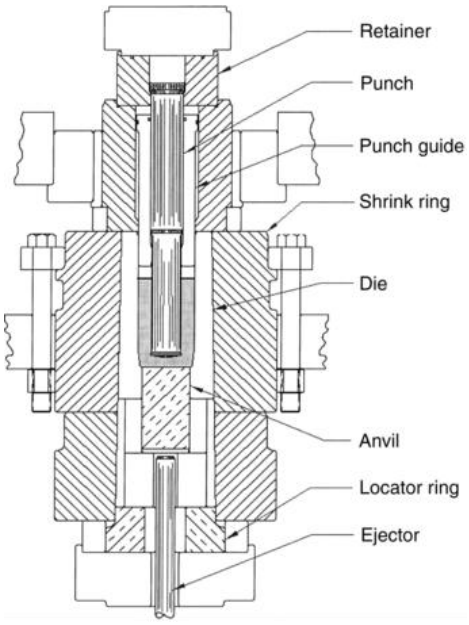


**Figure 1.3** Typical setup for backward cold extrusion [6].

**Impact Extrusion** is often included in the category of cold extrusion and it is very similar to a backward extrusion. The difference is that in impact extrusion, the punch descends at a high speed and strikes the workpiece, which flows upward through a small clearance between the punch and the die cavity. This method is commonly used for producing very thin wall tubular sections made of non-ferrous alloys [1].

In **Hydrostatic Extrusion**, the pressure required for deformation of the workpiece is supplied by means of a fluid surrounding the billet. This process is usually performed at room temperature and since hydrostatic pressure increases the ductility of materials, a variety of high strength materials, including brittle ones can be successfully extruded by this method [1],[6]. Unfortunately, hydrostatic extrusion requires vast experience in designing the complex tooling involved, so its application in the industry has been limited [1].

**Coextrusion** is the simultaneous extrusion of two or more metals to form an integral product, as illustrated in Figure 1.4. The simultaneous deformation of the core and sleeve (at a temperature appropriate to the metal system) results in the formation of an interfacial bond. This process has found interesting applications in the "canned" extrusion of powder or difficult-to-form materials, multifilamentary superconductors, and ceramic composite precursors [6]. However, while much qualitative understanding of coextrusion has been gained through research and development efforts in the last years, many aspects of this process have not been fully understood yet, hence its limited usage in the industry [6].

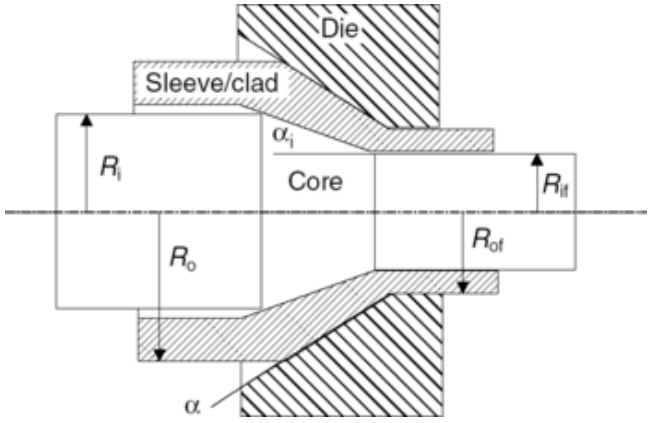


**Figure 1.4** Schematic of Coextrusion Process [6].

**Equal Channel Angular Extrusion (ECAE)** is one of the so-called Severe Plastic Deformation (SPD) Processes [7], which aim to produce ultra-fined grain (UFG) materials. As opposed to the traditional extrusion methods, ECAE is not intended to change the billet shape and dimensions. Its only purpose is to provide superior mechanical properties to the billet (via an UFG microstructure) which can then be further processed by other traditional methods [6]. Figure 1.5 shows a schematic of the ECAE process, in which pure shear deformation can be repeatedly imposed on the material so that an intense plastic strain is produced without any change in the cross-sectional dimensions of the workpiece [7]. Insufficient information on engineering aspects and commercialization still limits the interest of ECAE in the industry [6].

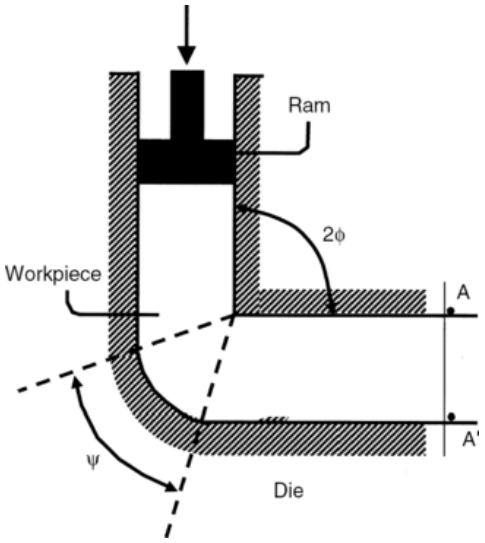


**Figure 1.5** Equal Channel Angular Extrusion (ECAE) [6].

### *1.2.2 Materials in Extruded Products*

As it was mentioned above, hot extrusion is the most common type of extrusion process used in the industry. Practically all metals can be extruded, but extrudability varies with the deformation properties of the metal. Soft metals are easy to extrude, while high-strength metals require higher billet temperatures and extruding pressures as well as higher-rated presses and dies [6]. **Aluminum** and **aluminum alloys** are the most ideal materials for extrusion, and they are the most commonly extruded. Most commercially available aluminum

alloys in the 1xxx, 3xxx, 5xxx, and 6xxx series are easily extruded. The high-strength aluminum alloys in the 2xxx and 7xxx series are more difficult to extrude [6].

**Lead** and **tin** exhibit high ductility and are therefore easy to extrude; the same applies to **magnesium** and **magnesium alloys**, which show almost the same extrudability as aluminum. **Zinc** and **zinc alloys** are also broadly used in extruded products, although they require forming pressures that are higher than those necessary for lead, aluminum, and magnesium. **Copper** and **copper alloy** extrusions are used a lot for wire, rods, bars, pipes, tubes, electrical conductors and connectors. Depending on the copper alloy, its extrudability ranges from easy to difficult [6].

The hot extrusion of **steels** requires the use of a high-temperature lubricant (typically glass) to avoid the severe tooling wear that can result from the high temperatures required for the billet (1100 to 1260 °C) [6]. A similar lubrication method is used to extrude **titanium alloys**, which in some cases may be even more difficult to extrude than steels. **Nickel alloys** can be very difficult to extrude as well, with billet temperatures exceeding 1000 °C [6].

**Metal powders** can be extruded by cold and hot processes, depending on the characteristics of the powders. Some of the metal powders extruded are aluminum, copper, nickel, stainless steels, beryllium, and uranium [6]. The powders are usually compacted into billets that are heated before being extruded. In many cases, the powders are encapsulated in protective metallic cans, heated, and extruded with the cans, in a genuine coextrusion fashion [6].

### *1.2.3 Extrusion Complexity Parameters*

In order to provide an idea of how easy or difficult it is to manufacture a given part by extrusion, geometric and material parameters have been defined in the industry to characterize design configurations. In the geometry side, there are two different metrics that have been widely adopted in the industry:

a) The **Circumscribing Circle Diameter** (CCD) is defined as the diameter of the circle circumscribing the cross section of the shape to be extruded, as shown in Figure 1.6. This parameter is an indicator of the size of an extruded shape.

b) The **Shape Factor** is the amount of surface generated per pound (or kg) of metal extruded [8]. Thus, this parameter can be determined by dividing the perimeter of the cross section by the weight per unit length (lb/ft or kg/m) of the extrusion [8]. In general, the smallest the shape factor, the simplest it is to extrude that shape. The shape factor affects the production rate as well as the cost of manufacturing and maintaining the dies [6]. An extrusion cost generally can be expected to increase as the shape factor increases [8]. Hence, it is used by many extruders as a basis for pricing and provides the designer with a means of comparing the relative complexities of alternate designs [6].

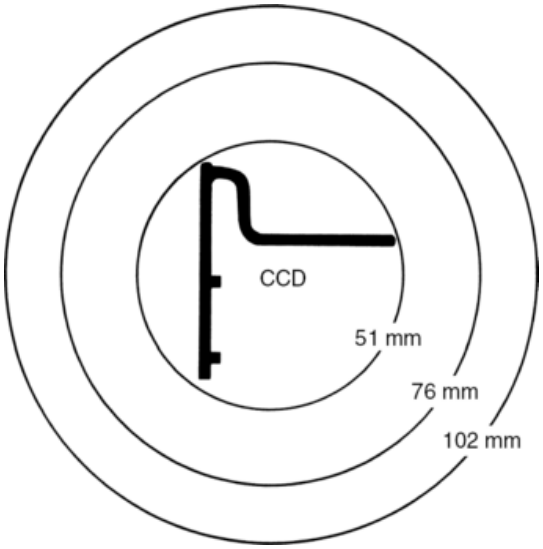


**Figure 1.6** Definition of Circumscribing Circle Diameter (CCD) [6].

In the material properties side, several methods have been proposed for extrudability evaluation; however, no specific method has been adopted as a single, accepted test [6]. The **maximum exit speed**, which ensures obtaining a product without surface tearing, has been frequently suggested. This parameter has the advantage of being both a metallurgical and

productivity measurement. Extrudability (expressed as exit speed) data can be found in the literature for different aluminum alloys [6].

### *1.2.4 Conventional Hot Extrusion Equipment and Tooling*

Hot extrusion is typically carried out in Horizontal, Direct-Drive Hydraulic Presses [6], like the one illustrated in Figure 1.7. Besides the press, there are many other pieces of auxiliary equipment and accessories that are vital to the success of the hot extrusion process. Prior to extrusion, the billet is heated in either a gas billet furnace or an electrical induction heater. The heated billet must then be quickly transferred to and loaded into the press. After the shape is extruded, it typically undergoes a water quenching. A puller system and a runout table -usually about 30 to 40 m long- are used to support and guide the product during extrusion. A stretcher is used to straighten the extruded product, and a cutoff saw is used to cut parts to the required length. Figure 1.8 shows a layout of such an extrusion installation [6].

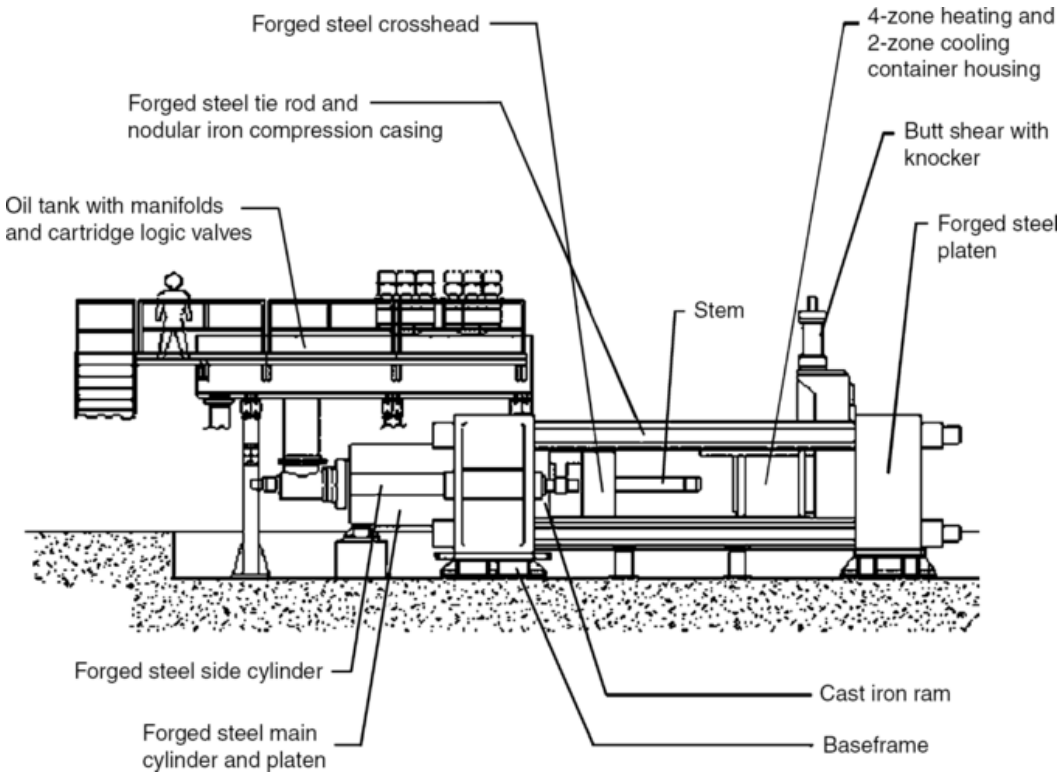


**Figure 1.7** Schematic of a direct-drive, direct hydraulic extrusion press [6].

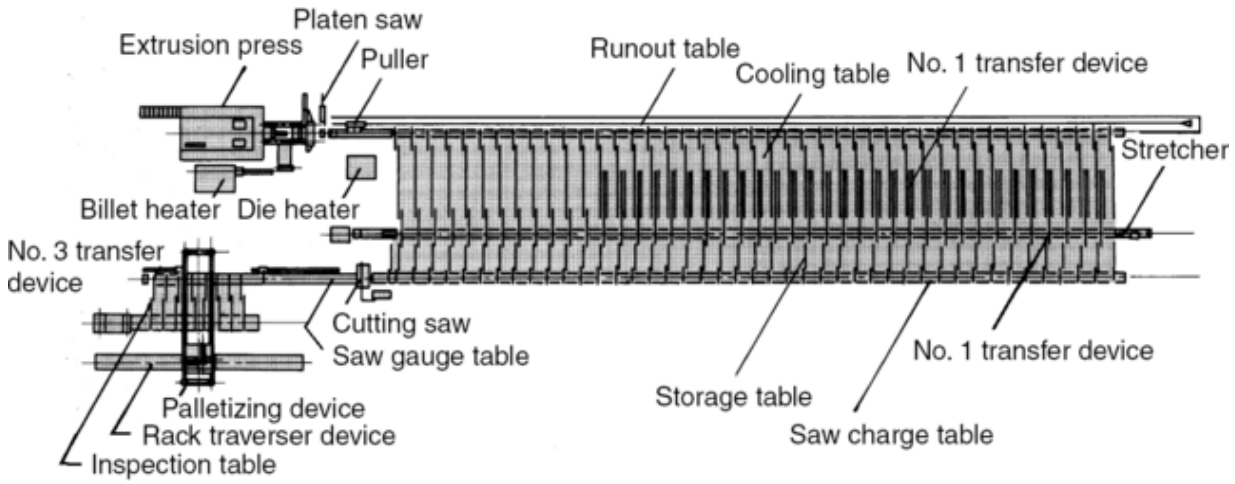


**Figure 1.8** Layout of a typical aluminum hot extrusion installation [6].

The main tooling for hot extrusion is depicted in Figure 1.9, which includes containers, liners, stems, dummy blocks, mandrels, dies of various kinds, and their associated support hardware [6]. The die design (and its cost) is strongly dependent on the type of material and geometry being extruded [6].

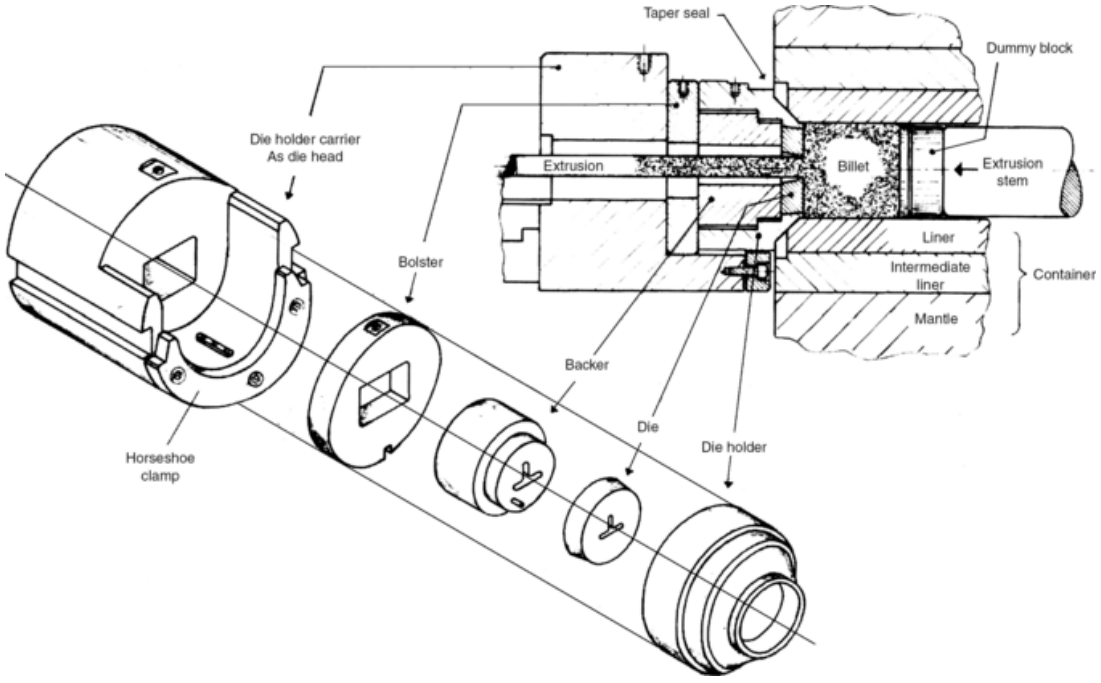


**Figure 1.9** Schematic showing various extrusion process tooling [6].

### *1.2.5 State of the Art Technologies in Extrusion*

Despite being an old bulk deformation process, extrusion is an active area of research around the world. The majority of the investigators' work in the recent years has been related to developing new processes, new materials, and advanced numerical process simulation techniques. One of the most active topics today is related to the development of new SPD process. Improved and augmented versions of ECAE, like Cross-Equal Channel Angular Pressing (Cross-ECAP) [9], or ECAE-Forward Extrusion for consolidation of aluminum powders show promising results [10].

On the non-SPD processes side, an innovative process called Friction Coextrusion has been developed recently at The Welding Institute (TWI) in the UK [6]. This process involves solid state welding of the materials being coextruded, by means of frictional heat generated by spinning the workpieces. Other innovative processes being developed include Semisolid Metal Extrusion of recycled aluminum scrap [11] and direct extrusion using multi-step pocket dies [12].

Regarding new materials, the feasibility of extruding Metal Matrix Composites, Metal Powders, Intermetallics and other modern materials is being investigated [13],[14],[15]. Finally, numerical simulations of several extrusion processes using sophisticated Finite Element Models (FEM) have been the focus of numerous researchers [9], [12], [16], [17]. The results provided by those simulations have increased the understanding of material behavior in the extrusion process and have enabled the optimization of die designs and process parameters.

# CHAPTER 2: MANUFACTURING COST ESTIMATION FUNDAMENTALS

## 2.1 The Importance of Manufacturing Cost Estimation

Manufacturing Cost Estimation may be defined as "*an attempt to forecast the expenses that must be incurred to manufacture a product*" [18]. The process of cost estimation is based on a detailed plan for the manufacturing operations sequence, labor, equipment and tooling required to produce any particular item [19]. In order to provide some context to the ideas presented herein, it is important first to distinguish the difference between the Manufacturing Cost and the Total Cost of a product. The traditional cost and price structure for a manufactured product is shown in Figure 2.1, where it can be seen that General and Administrative (G&A) Costs, Engineering and Development Costs and other expenses are usually not considered part of the Manufacturing Cost [18], [19], but they are important elements of the Total Product Cost. The selling price of the product is obtained by adding the desired profit margin to the total product cost. In Design for Manufacture, the term "Cost Estimating" is typically used to refer to the prediction of the manufacturing cost of a product [18], [19].

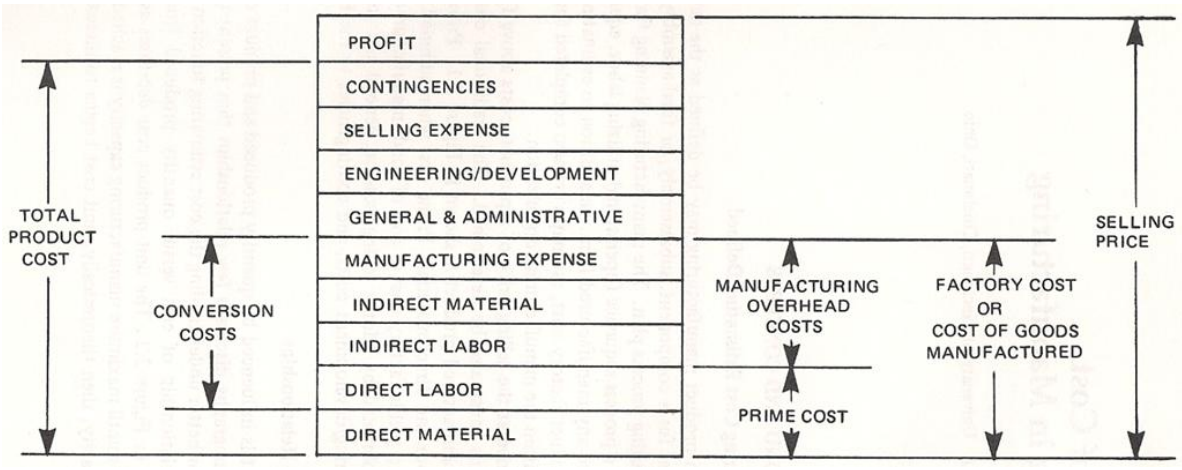


**Figure 2.1** Structure of a cost estimate for a manufactured product [19].

Cost Estimating is a vital function in manufacturing organizations, as many decisions are based on cost estimates for specific products [19]. There are numerous important applications of Cost Estimating, like the establishment of bid price recommendations for customer quotations, the assessment of quotations from suppliers, the economic analysis of make-or-buy a part, the evaluation of product design alternatives, long-term financial planning, and manufacturing costs control, among others [19]. It is important to remark that the more complete the design information is in a request for quotation, the more accurate the cost estimation will be. Indeed, in some cases contingency allowances are used to account for lack of design information for quoting [18], [19].

## 2.2 Manufacturing Cost Analysis Approach

Cost estimating methodologies range from simple parametric systems based on a single attribute, like weight, to the complete and detailed routing of the part through a production system [20]. Wilson [18] distinguishes between Preproduction Cost Analysis and Postproduction Cost Analysis, the former being comprised by Material Cost, Tooling Cost and Processing Cost, and the latter being comprised by Material, Labor, Overtime, Setup Time, Tooling, Maintenance, Indirect Labor, Supplies, Scrap/Rework, Savage Material, Down-time, Energy, Floor Space and Depreciation [18]. Malstrom [19] considers the Factory Cost to be the sum of the Prime Cost (Direct Labor + Direct Material) and the Factory Expenses (rent, heat, electrical utilities, water, gas, expendable factory supplies, and indirect labor). It is clear that, despite the variety of approaches for manufacturing cost estimation, most of them consider a series of common factors in the cost equation.

One of the most common cost estimation methodologies adopted in the industry is the so called *Activity Based Costing* (ABC) [20]. This methodology provides cost estimates by routing parts through the production system and attempting to determine the actual cost of manufacture, considering every single detail and breaking down all the overhead expenses involved (power, gas, water, floor space, depreciation, maintenance, supplies, etc.). In theory,

ABC should be the most accurate method for cost prediction; however, since the processing times and labor handling times must be estimated based on the experience of a manufacturing engineer or a cost estimating engineer, and given the difficulty to accurately break down the various overhead costs incurred on manufacturing a part, the ABC approach often provides inaccurate cost estimates, as well as being a very time consuming task [20].

A novel approach developed by Philpott, et al [20] is called *Feature Based Costing* (FBC) and it consists of a methodology for automatically estimating the manufacturing cost of parts in real time, in a software interface integrated into a CAD system. The method extracts parametric features of a current design from the CAD model. Manufacturing cost drivers are identified on the basis of those parametric features, and then translated into costs using physics based manufacturing process models. In this way, a designer is able to obtain cost estimates feature by feature as a part is being designed. Philpott, et al [20] claim that *"because cost estimates are typically achieved in less than 2 seconds, the designer is able to complete the design task without being hindered by the cost estimating system. Also, because the methodology provides for much higher speeds than other existing cost estimating systems, it is now possible to perform a large number of what-if design experiments. In this manner, a unique vehicle is provided for achieving an optimized economic solution during the early design phases of a project*". Based on all these advantages and its great research potential, the FBC approach has been adopted in the work presented in this thesis.

### *2.2.1 Cost Accounting Taxonomy in FBC*

The cost accounting taxonomy used in FBC [20] is based on Recurring and Non-Recurring Costs, as depicted in Figure 2.2. As the name implies, the Recurring Costs are all those costs that are incurred on a regular basis throughout the production life of the product and constitute the so called "Piece Part Cost". On the other hand, the Non-Recurring Costs are all those costs that are incurred only once in the production life of the product and can be treated as an initial investment. The manufacturing cost is given by:

$$Manufacturing\ Cost = Piece\ Part\ Cost + Amortized\ Investment \quad (2.1)$$

where the Piece Part Cost is:

$$Piece\ Part\ Cost = \sum Recurring\ Costs \quad (2.2)$$

and the Amortized Investment is:

$$Amortized\ Investment = \frac{\sum Nonrecurring\ Costs}{Total\ Production\ Volume} \quad (2.3)$$

where the Total Production Volume is:

$$Total\ Production\ Volume = Annual\ Prod.Volume \times Production\ Years \quad (2.4)$$

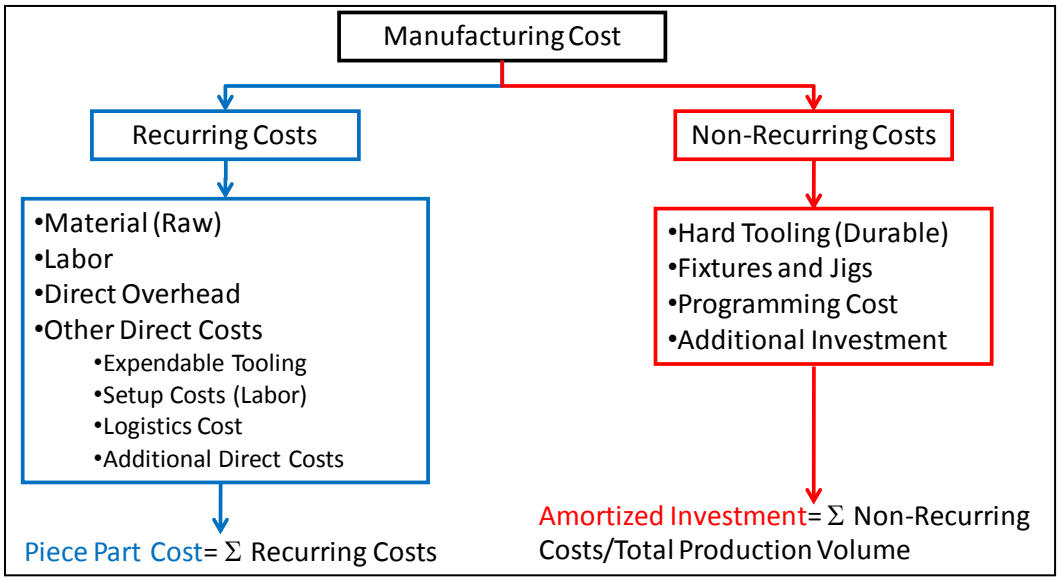


**Figure 2.2** Taxonomy used in FBC.

Additionally, a "Fully Burdened Cost", which is similar to the previously mentioned "Total Product Cost" (Figure 2.1), can be calculated as:

$$Fully\ Burdened\ Cost = Manufacturing\ Cost + Period\ Overhead\ Cost \quad (2.5)$$

where the term "Period Overhead" is a synonym for Indirect Overhead and it includes all the costs that are not directly associated with the manufacture of the product, as shown in Figure 2.1. Conversely, Direct Overhead[1] accounts for the cost of all services and facilities required to keep the operator working. This includes items like utilities, maintenance, toolroom, equipment amortization, and rent [18]. Moreover, some process operations like cleaning, washing, painting, drying and plating are often considered overhead items as well, since it is difficult to specifically estimate these items on a unit basis [18]. Many accounting departments simplify the overhead charge by lumping all the costs aforementioned and dividing the sum by the anticipated production hours, obtaining an overhead rate [18] that is used in a similar way than the labor rate, as explained in the next section.

### *2.2.2 Recurring Costs Estimation Overview*

The first step in the cost estimation activity is to make a manufacturing process map for the part [18]. This is the starting point to understand the sequence of operations and estimate the Manufacturing Cycle Time. Once this has been done, the Labor and Overhead Costs are readily calculated by multiplying the cycle time by the labor and overhead rates, respectively, as follows:

$$Labor\ Cost = Crew\ Size \times Cycle\ Time \times Labor\ Rate \quad (2.6)$$

$$Overhead\ Cost = Cycle\ Time \times Overhead\ Rate \quad (2.7)$$

where the term "Crew Size" refers to the number of operators involved in the manufacturing process, and it may or may not be an integer number, depending on the tasks being performed in parallel by the workers (e.g. an operator working on two production lines in parallel would be considered as 0.5 in the crew size of each line).

[1] The terms "Direct Overhead" and "Overhead" are sometimes used interchangeably in the literature. The same thing will be done in this thesis.

The Setup Cost (under the "Other Direct Costs" category) accounts for all the time (called "setup time") spent in recurring "nonproductive" tasks that are necessary for the suitable operation of the plant, like switching tools and fixtures, calibrating equipment, running production trials, etc. The setup cost is calculated by multiplying the setup time by the labor and overhead rates, and then adding the two products. The number of operators (a.k.a. Crew Size) involved in the setup operations must be considered as well, so the setup cost is calculated as:

$$Setup\ Cost = Setup\ Time \times (Crew\ Size \times Labor\ Rate + Overhead\ Rate) \quad (2.8)$$

where the setup time is usually calculated as:

$$Setup\ Time = \frac{Setup\ Time\ per\ Batch}{Batch\ Size} \quad (2.9)$$

where the term "Batch" is defined here as a continuous production lot of a certain number of identical parts (a.k.a. "Batch Size").

The Material Cost is calculated based on the weight of the total raw material used to produce a part (considering scrap and recycled material) multiplied by the price per kilogram (or pound) of the alloy. The term "Yield" is widely used in the industry to refer to the ratio of net mass (of good parts) produced to the total gross mass of material consumed in the process. Hence, the material cost can be estimated by:

$$Material\ Cost = \frac{Part\ Mass}{Yield} \times Material\ Price\ per\ unit\ mass \quad (2.10)$$

where:

$$Yield = \frac{Net\ Mass\ Produced}{Gross\ Mass\ Consumed} = \frac{Net\ Mass\ Produced}{Net\ Mass\ Produced + Scrap\ Mass} \quad (2.11)$$

### *2.2.3 Non-Recurring Costs Estimation Overview*

In FBC, the cost of major equipment like presses, machining centers, furnaces, motors, pumps and other auxiliary systems is usually not accounted for as a non-recurring cost, but as part of the overhead rate calculated by the accounting department of the manufacturing organization. The same thing applies for plant layout setup costs like foundation, services (electrical, gas, water, lighting, ventilation) and equipment installation. However, the costs of tooling, fixtures and jigs required to produce a new part are included in the non-recurring costs, amortized by the total production volume. In many modern shops, the cost of tooling is calculated in the same manner as the main product, using detailed estimates of material, labor and overhead [21]. On the contrary, in many other companies the tooling cost is still estimated based on experience, thumb rules, or empirical equations obtained from historical data.

For those manufacturing processes that require computer programming of the equipment as part of the initial setup to produce a new part (e.g. CNC Machining, Robot Welding, Laser Cutting, etc), the amortized Programming Cost incurred can be estimated by:

$$Programming\ Cost = \frac{Programming\ Time \times Labor\ Rate}{Total\ Production\ Volume} \quad (2.12)$$

Finally, whatever the method for estimating the tooling and other non-recurring costs is, it is very important to realize that the total production volume is a major factor in determining the amortized cost per part of the initial investment, as it was shown by equation 2.3. The larger the production volume is, the less significant the non-recurring costs per part will be, and vice versa.

# CHAPTER 3: ALUMINUM HOT EXTRUSION PROCESS

## 3.1 Why Aluminum Hot Extrusion?

Among the different types of existing extrusion processes, Hot Extrusion is the most commonly used in the industry [6]. Aluminum and aluminum alloys are the most ideal materials for extrusion, and they are the most commonly extruded [6]. The most important and common method used in aluminum extrusion is the Direct (or Forward) Process [22]. The majority of the commercially available aluminum alloys in the 1xxx, 3xxx, 5xxx, and 6xxx series are easily extruded [6]. Of these, the predominant alloy group by commercial volume (covering about 80% of all extruded products) is the 6xxx series alloys [23], with Aluminum 6063 being by far the first in the list, followed by Aluminum 6061 [24], [25]. The high-strength aluminum alloys in the 2xxx and 7xxx series are more difficult to extrude, but still can be extruded with the proper procedures [22].

The hot extrusion process map for aluminum alloys is illustrated in Figure 3.1, where a typical installation layout is shown. The seven main steps of the process [6] consist of: 1) Preheating the Billet, 2) Extrusion, 3) Quenching, 4) Stretching, 5) Cut-off, 6) Artificial Aging and 7) Quality Control. The following sections explain the details of each of the steps in the process.

## 3.2 Billet Preheating

The preheating of the billet is done either in a Gas Furnace or in an Electrical Induction Heater [6]. The Induction Furnace is the most technically efficient unit for billet heating available [26]. The basic structure of a low-frequency induction heater consists of a horizontal coil in which three or four billets are heated to the desired temperature in a continuous cycle [26]. The typical billet temperatures for the so called soft and medium-grade aluminum alloys (most of 1xxx, 3xxx, 5xxx, 6xxx series) are shown in Table 3.1, while Table 3.2 shows the same information for the so called hard aluminum alloys (2xxx, 7xxx and some 5xxx series) [22]. In

order to make sure the billet has attained thermal equilibrium (i.e. a steady state temperature profile) in the time available between extrusions, the electrical power of the coil is increased as necessary [26]. The time required to heat the billet is mainly a function of the thermal conductivity of the alloy, the billet dimensions and the electrical power input. The time between loading the billet and its removal can vary from 3 to 20 minutes [26]. In some cases, depending on the press capacity, several furnaces are installed to feed one press [26]. On the other hand, the high-speed gas furnace represents a cheaper energy alternative, but cannot equal the heating speed of the induction furnace, with heating period times being three to five times longer [26].

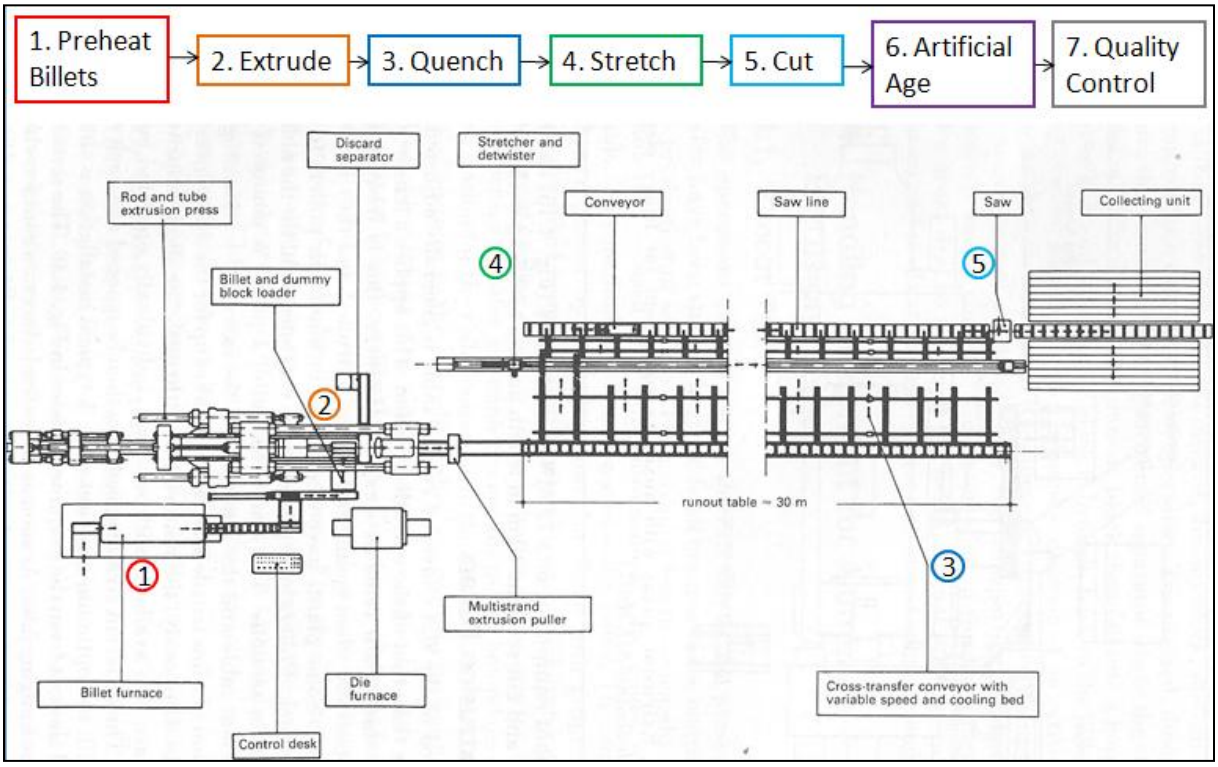


**Figure 3.1** Process Map and Layout for an Aluminum Hot Extrusion Installation [26].

**Table 3.1** Typical billet temperatures of soft and medium-grade aluminum alloys [22].

| Alloy | Type | Billet temperature °F | Billet temperature °C | Exit speed ft/min | Exit speed m/min |
|---|---|---|---|---|---|
| 1060 | Non-heat-treatable | 788 | 420 | 164–328 | 50–100 |
| 1100 | Non-heat-treatable | 806 | 430 | 164–262 | 50–80 |
| 3003 | Non-heat-treatable | 842 | 450 | 98–230 | 30–70 |
| 5052 | Non-heat-treatable | 842 | 450 | 16–33 | 5–10 |
| 5154, 5254, 5454 | Non-heat-treatable | 860 | 460 | 20–49 | 6–15 |
| 6061 | Heat treatable | 806–932 | 430–500 | 16–82 | 5–25 |
| 6063 | Heat treatable | 896–932 | 480–500 | 115–262 | 35–80 |
| 6066 | Heat treatable | 797–860 | 425–460 | 66–115 | 20–35 |
| 6101 | Heat treatable | 896–932 | 480–500 | 115–262 | 35–80 |
| 6463 | Heat treatable | 896–932 | 480–500 | 115–262 | 35–80 |
| 7003 | Heat treatable | 824–977 | 440–525 | 16–69 | 5–21 |
| 7005 | Heat treatable | 824–977 | 440–525 | 16–46 | 5–14 |

**Table 3.2** Typical billet temperatures of hard aluminum alloys [22].

| Alloy | Type | Billet temperature °F | Billet temperature °C | Exit speed ft/min | Exit speed m/min |
|---|---|---|---|---|---|
| 2014–2024 | Heat treatable | 788–842 | 420–450 | 5–11 | 1.5–3.5 |
| 5083, 5086, 5456 | Non-heat-treatable | 824–842 | 440–450 | 7–20 | 2–6 |
| 7001 | Heat treatable | 700–780 | 370–415 | 2–5 | 0.5–1.5 |
| 7075, 7079 | Heat treatable | 572–860 | 300–460 | 3–7 | 0.8–2 |
| 7049, 7150, 7178 | Heat treatable | 572–824 | 300–440 | 2.5–6 | 0.8–1.8 |

Note: Temperatures and extrusion speeds are dependent on the final shape and the extrusion ratio, and it may be necessary to start with lower billet temperatures than mentioned in the table. Source: Ref 11

## 3.3 Extrusion

The second step in the process map of Figure 3.1 is the Extrusion operation, which begins with loading the preheated billet in the press container, then extruding it until a specified billet butt thickness is left over. Stopping extrusion at a specified butt thickness prevents oxide and other metallic or nonmetallic inclusions from flowing into the extrusion [22]. According to industry practice, standard butt thickness for direct extrusion is kept to ~10% of the billet length [22], [27]. Next, the press container and the ram are retracted and the butt is cutoff by a shear and then recycled. Once the container and ram have returned to their original positions, the process is repeated. In order to improve productivity, a “billet-on-billet” extrusion process is generally used to produce continuous lengths of a given section [22]. In this process, the butt discard is removed as mentioned before, and then the following billet is welded (in a solid state weld, with the aid of temperature and pressure) to the one remaining in

a welding or feeder plate, as shown in Figure 3.2. Aluminum alloys are well suited to this process, as they are easily welded at the extrusion temperature and pressure [22]. The billet-on-billet method makes extrusion a continuous manufacturing process, in which the length of the continuous extrudate is limited only by the length of the runout table (shown in Figure 3.1), which is usually between 30-40 m [6].

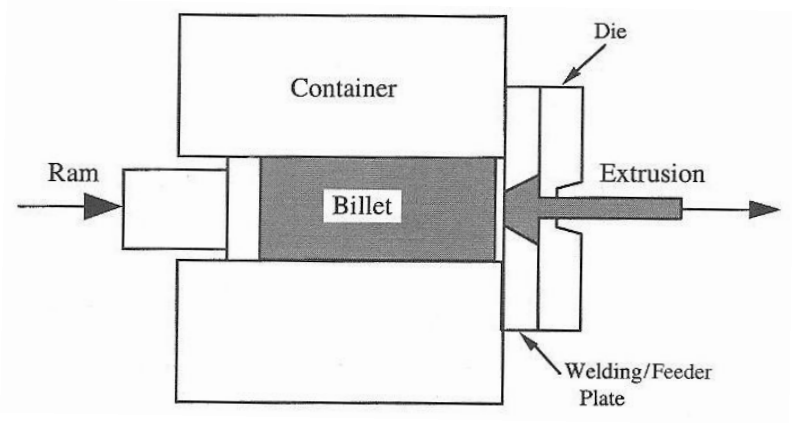


**Figure 3.2** Billet-on-billet extrusion using welding plate in front of the die [22].

Today, extrusion plants extruding 6xxx shapes at high productivity are using mechanical or automatic puller systems (single or double) that grip the extruded section as it exits the press on the runout table, taking it through the air or water quench system [22]. The puller is synchronized with the press cycle, and it stops automatically when the press is stopped at any time during the extrusion process [22].

## 3.4 Quenching

The third step in the process map of hot extrusion is the quenching operation, which is typically performed on the runout table [6], [22]. Water-spray systems are gradually replacing tank-type water quench and over-table and under-table cooling fans [22]. High-pressure, high velocity sprays have been developed to quickly cool difficult shapes well below critical temperatures to attain higher mechanical properties and desired finish [22]. High-pressure

Spray Quench (Figure 3.3) offers the maximum cooling rate in a profile while also minimizing distortion, thus allowing maximum extrusion speed with minimum space requirements [28].


**Figure 3.3** High-Pressure Spray Quench, from Granco Clark [28].

## 3.5 Stretching

After quenching, the extruded material generally requires straightening to remove the distortion and residual stresses generated during the cooling operation. The sections are transferred from the runout and cooling table to the stretcher bed to be straightened by stretching 1 to 3% [22]. The stretcher capacity has to be greater than the required stretching force, which is the product of the cross sectional area of the shape times the yield strength of the alloy [22]. Current technology for precise control of gripping pressure prevents the stretcher both from excessively distorting the extrusion and from allowing slippage at the grip, hence, minimizing scrap and manual intervention [29]. A modern stretcher is shown in Figure 3.4, where the significant deformation imposed on the gripped part of the extrusion is evident. Note that, depending on the size of the cross section, more than one extrusion at a time can be straightened by the stretcher. Nowadays, stretching equipment offers one, two, or no-man operational modes, reducing labor costs of the extruder [29].


**Figure 3.4** Granco Clark's Controlled Vertical Crush Stretcher (CVCS) in operation [29].

## 3.6 Cutoff

Sawing is the next operation after stretching. A high-speed circular cutoff saw is normally used to trim stretcher grip marks, front and back end allowances and to cut the extrusion to the finished lengths [22]. The sawing principle is illustrated in Figure 3.5, where it can be seen that the sections are moved against a gage stop, which is set to the required length of the product. Saw chips are collected by using a high-pressure vacuum connected to the machine [22]. Also, as in the stretching operation, the sawing operation can cut off a batch of extrusions simultaneously, depending on the size of the section, the alloy and the capacity of the saw [30].

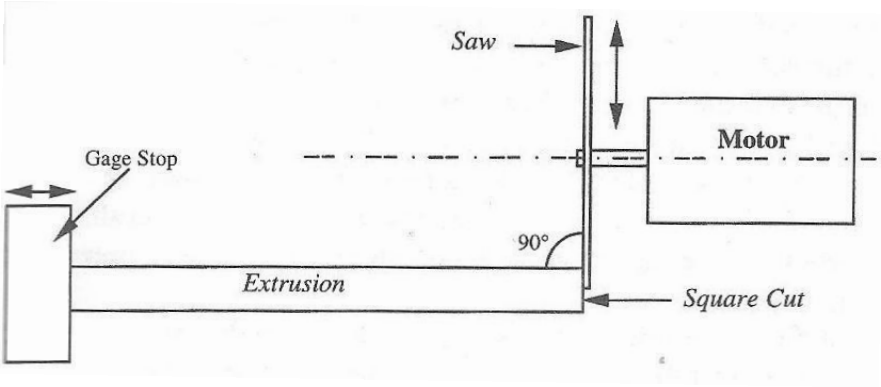


**Figure 3.5** Sawing Principle [22].

## 3.7 Artificial Aging

Artificial Aging is the final stage of the heat treatment process and is used to achieve the desired temper for the alloy. Typical Heat Treatment parameters for some 6xxx alloys are shown in Table 3.3, while the same information for some hard alloys is shown in Table 3.4. It is important to remark that precipitation hardening is a two stage-process, starting with Solution Heat Treatment and followed by Precipitation Heat Treatment (aging). For the soft and medium-grade aluminum alloys the Solution Heat Treatment stage is carried out inside the press during the hot extrusion and the subsequent quenching [22]. Thus, when the extrusion exits the press, its temperature shall be no lower than the one specified in Table 3.3 for the Solution Heat Treatment to be effective. Otherwise, a separate out-of-the line Solution Heat Treatment needs to be carried out, reducing the productivity of the process. That is sometimes the case for aluminum extrusions made of hard alloys [22].

**Table 3.3** Typical Heat Treatment Parameters of some 6xxx alloys [22].

| | Solution heat treatment | | | Precipitation heat treatment | | | |
|---|---|---|---|---|---|---|---|
| | Temperature | | | Temperature | | | |
| Alloy | °F | °C | Temper | °F | °C | Time, h | Temper |
| 6005 | 985 | 530 | T1 | 350 | 175 | 8 | T5 |
| 6061 | 985 | 530 | T4 | 350 | 175 | 8 | T6 |
| 6063 | 970 | 520 | T4 | 350 | 175 | 8 | T6 |
| | | | | 360 | 182 | 6 | T6 |
| 6066 | 990 | 530 | T4 | 350 | 180 | 8 | T6 |
| 6070 | 1015 | 545 | T4 | 320 | 160 | 18 | T6 |
| 6262 | 1000 | 540 | T4 | 350 | 175 | 12 | T6 |

**Table 3.4** Typical Heat Treatment Parameters of some hard alloys [22].

| | Solution heat treatment | | | Precipitation heat treatment | | | |
|---|---|---|---|---|---|---|---|
| | Temperature | | | Temperature | | | |
| Alloy | °F | °C | Temper | °F | °C | Time, h | Temper |
| 2014 | 935 | 500 | T4 | 320 | 160 | 18 | T6 |
| 2024 | 920 | 495 | T3 | 375 | 190 | 12 | T81 |
| 7001 | 870 | 465 | W | 250 | 120 | 24 | T6 |
| 7075 | 870 | 465 | W | 250 | 120 | 24 | T6 |

Artificial Aging is done in ovens that are separate from the main extrusion installation. Suppliers of auxiliary equipment sometimes offer Handling Systems that include conveyors, rack stackers and destackers. The extruded product then moves through the entire aging cycle with no manual intervention required (Figure 3.6), enhancing productivity, reducing labor costs, and maintaining profile quality [31], [32]. Moreover, some aging equipment suppliers offer "Continuous Aging Ovens" with the capability of processing continuous production flow for higher productivity [33].

**Figure 3.6** Racked extrusions going into the Aging Oven, from GiA CLECIM Press [32].

# CHAPTER 4: EXTRUSION RECURRING COSTS ESTIMATION

## 4.1 Press Selection

The first step in the process of estimating the recurring costs of manufacturing a part by extrusion is to select the size of the press that is necessary to do the job. Not only will the press size have an impact on the overhead rate of the extruder, but it will also affect the cycle time of production, as it will be shown later in this chapter.

### *4.1.1 Extrusion Pressure Calculations*

While there are numerous models in the literature for predicting the pressure that is necessary to extrude a part, one of the most commonly used in practice due to its simplicity [6], [34] is:

$$p_o = \sigma_f \left( \ln R + \frac{2 m_f L_o}{D_o} \right) \quad (4.1)$$

where $p_o$ is the pressure required to extrude a round billet into a solid round bar with an Extrusion Ratio of $R=A_o/A_f$ ($A_o$ being the billet cross sectional area, and $A_f$ being the extrusion cross sectional area); $\sigma_f$ is the flow stress of the material at the extrusion temperature and strain rate; $L_o$ and $D_o$ are the billet length and diameter respectively and $m_f$ is a friction factor that ranges from zero to one ($m_f$=0 for a frictionless case, and $m_f$=1 for a sticking friction case). In non-lubricated extrusion (as it is the case for aluminum alloys), sticking friction at the billet-container interface is generally assumed (worst-case scenario), and therefore $m_f$=1. The flow stress $\sigma_f$ of the material can be estimated by the typical hot working constitutive equation:

$$\sigma_f = C \dot{\varepsilon}^m \quad (4.2)$$

where $C$ and $m$ are temperature dependent material properties called Strength Coefficient and Strain Rate Sensitivity Exponent, respectively. These properties may be obtained directly from

sources like [35]. However, if *C* and *m* are not directly available (as is generally the case), they can be obtained mathematically by using two different hot work flow stress-strain rate data points (available from sources like [26], [36], [37] or [38]) into equation 4.2 and solving the resulting 2x2 simultaneous equations system for *C* and *m*. Interpolations may be necessary to estimate *C* and *m* for the corresponding billet temperature of the alloy. Alternatively, if only one flow stress-strain rate data point is available for the alloy, the value of *m* may be assumed to be 0.125 (as observed in experimental data for a variety of aluminum alloys [26]) and the value of *C* can be readily calculated by using equation 4.2.

The strain rate $\dot{\varepsilon}$ is calculated as an average effective value by the following expression [1], [6]:

$$\dot{\varepsilon} = \frac{6v_o \ln R}{D_o} \quad (4.3)$$

where $v_o$ is the extrusion ram speed, which is related to the extrusion exit speed $v_f$ and the extrusion ratio *R*, by the mass conservation principle in the following form:

$$v_o = \frac{1}{R} v_f \quad (4.4)$$

where the extrusion exit speed ($v_f$) is dictated by the extrudability of the alloy (i.e. the maximum exit speed it can sustain without surface tearing), as it was mentioned before in Section 1.2.3. This is a critical parameter for the process, and as such, will be addressed in more detail in Section 4.1.2.

So far, the estimation of the extrusion pressure has been idealized to the case of a simple bar with a solid round cross section. For the more general case of extruding other shapes, an additional factor is usually introduced in the equation for extrusion pressure, in the form of a "complexity index" of the shape [39], as follows:

$$p = K_{shape}\ p_o \quad (4.5)$$

where $p$ is the actual pressure required to extrude a given shape, $p_o$ is the theoretical pressure defined in Equation 4.1 and $K_{shape}$ is an empirical complexity index of the shape that accounts for various factors neglected in the theoretical equation 4.1, like redundant work of deformation, additional friction in the die bearing length, non-sticking friction in the billet-container interface and additional shearing taking place on the extrusion of shapes of higher complexity than a simple solid round bar [26]. The empirical complexity index $K_{shape}$ is defined in [39] as:

$$K_{shape} = 0.95 + 0.05\left(\frac{P_{ext}}{P_o}\right)^{1.5} \quad (4.6)$$

where $P_{ext}$ is the external perimeter of the extruded cross section, and $P_o$ is the perimeter of an equivalent solid round section with the same cross sectional area ($A_f$) as the actual shape, and can be mathematically derived as:

$$P_o = 2\sqrt{\pi\, A_f} \quad (4.7)$$

The empirical equation for $K_{shape}$ is an improved version of an older expression of the same form, but with different numerical coefficients [39] and it has been obtained by statistical regression techniques to provide the best fit to numerous experimental results obtained by extruding a variety of shapes made of Al 6063, ranging from simple solid sections to fairly complex hollow profiles, using single-hole dies and multi-hole dies [34]. Considerable research work has been done in the past [40],[41] to obtain similar correction factors for other alloys, like Al 1050 and Al 6082; however, the experimental data available is mostly for solid sections only, so it lacks the robustness of the more recent experiments documented in [34]. Therefore, in the absence of similarly validated expressions for $K_{shape}$ for other than Al 6063 alloys, the complexity index will be assumed to be a function of geometry only, hence extending the use of equation 4.6 to any other material extruded without a lubricant, as is the case for aluminum alloys.

Before using the empirical equation for $K_{shape}$ along with the rest of the equations presented so far, an additional adjustment must be made, since the regression analysis performed in [39] to obtain equation 4.6 assumed a constant flow stress for Al 6063 of $\sigma_f$ =40 MPa in the calculation of the theoretical extrusion pressure ($p_o$, equation 4.1). That assumption is certainly invalid, as the flow stress is sensitive to the strain rate value. Furthermore, a flow stress of 40 MPa for Al 6063 at ~460°C is very high and uncommon, as it would require a strain rate of about 50 $s^{-1}$ [42], which is considerably higher than the typical strain rates obtained in hot extrusion of soft aluminum alloys (~1-3 $s^{-1}$). Fortunately, the complexity index can still be used if the following mathematical adjustment is made, resulting in an adjusted index, $K_{shape\_adj}$:

$$p_{specimens} = K_{shape}\ p_o(\sigma_f = 40\ MPa) = K_{shape_{adj}}\ p_o\left(\sigma_{f_{specimens}} = C\dot{\varepsilon}_{specimens}{}^{m}\right)$$

$$K_{shape_{adj}} = \left(\frac{40\ MPa}{C\dot{\varepsilon}_{specimens}{}^{m}}\right)K_{shape} \quad (4.8a)$$

where $\sigma_{f_{specimens}}$ and $\dot{\varepsilon}_{speciments}$ are the average effective flow stress and strain rate of the specimens tested by Qamar, et al in the study documented in [34]. The flow stress and the strain rate of such specimens were not calculated in [34]; however, all the necessary information to do so is available. A calculation of the strain rates (using equation 4.3) indicated that $\dot{\varepsilon}_{specimens}$ ≈0.27-0.40 $s^{-1}$. The values of *C* and *m* for Al 6063 at the billet temperature used in the experiments (~460°C) are *C*=28.8 MPa and *m*=0.161, as obtained mathematically from flow stress data available in [36]. Then, the calculation of the flow stress (using equation 4.2) revealed that $\sigma_{f_{specimens}}$ ≈23-25 MPa, which is a relatively narrow range. Considering the average value of $\sigma_{f_{specimens}}$ =24 MPa, the equation for the adjusted complexity index, $K_{shape\_adj}$ can be rewritten as:

$$K_{shape_{adj}} = \left(\frac{40\ MPa}{24\ MPa}\right)K_{shape}$$

$$K_{shape_{adj}} = 1.67K_{shape} \quad (4.8b)$$

It is important to remark that equation 4.8b is valid for any material (not only Al 6063) extruded in non-lubricated conditions, as it is just the result of a numerical correction to $K_{shape}$ (which as mentioned before, it is assumed to be a function of geometry only). Finally, the revised version of equation 4.5 for the actual extrusion pressure becomes:

$$p = K_{shape_{adj}}\ p_o \quad (4.9)$$

The extrusion pressure $p$ is an important parameter for the selection of the press required to do the job. In doing so, one approach is to convert the extrusion pressure $p$ to an extrusion force $F$, multiplying it by the billet cross sectional area ($F=pA_o$). The selected press must have a force capacity that is equal or greater than the extrusion force required (i.e. $F_{press} \geq F$). An alternative approach is to convert the press force capacity to a "specific pressure", dividing it by the billet cross sectional area ($p_{press}=F_{press}/A_o$) and then comparing it against the extrusion pressure required, to verify if the press can do the job (i.e. $p_{press} \geq p$). Either way, it is a good practice to use a press with extra load capacity than the one required, as this provides margin for using lower billet temperatures and higher extrusion speeds [6].

### *4.1.2 Extrusion Exit Speed Estimation*

As it was mentioned before, the extrusion exit speed is a crucial parameter in the extrusion process, having both technical and economical relevance. Besides its influence on the strain rate (and thus on the flow stress and extrusion pressure), the extrusion exit speed has a direct impact on the productivity of the process (i.e. on the cycle time), so it is desirable to maximize it without compromising the quality of the extruded part.

During the extrusion operation, the billet exhibits a significant increase in temperature from its preheated value, due to bulk deformation work and heat generation by friction. If the exit temperature resulting from the initial billet temperature and the extrusion speed is too close to the solidus temperature of the alloy, the surface tears and roughens and is unacceptable [26]. This problem is known as "Hot Shortness" or "Speed Cracking" and is one of

the most common producibility issues in hot extrusion [43]. On the other hand, as the temperature of the billet increases with higher extrusion speeds, the flow stress of the metal is reduced, resulting in a lower extrusion load for the press, which is always desirable. This trade-off is illustrated in Figure 4.1, in the form of a Limit Diagram for Extrusion Speed, based on the extrusion capability of the press (which increases with temperature) and the metallurgical capability against hot shortness of the alloy (which is reduced with temperature). The maximum extrusion speed depicted in Figure 4.1 is a theoretical value that would be obtained only if the optimal exit temperature is maintained, which is hardly ever the case [26]. The typical actual extrusion exit speeds attainable for different aluminum alloys are shown in Table 4.1 and Table 4.2 for soft and hard alloys respectively [22], and represent a direct indication of the extrudability of each alloy [6].

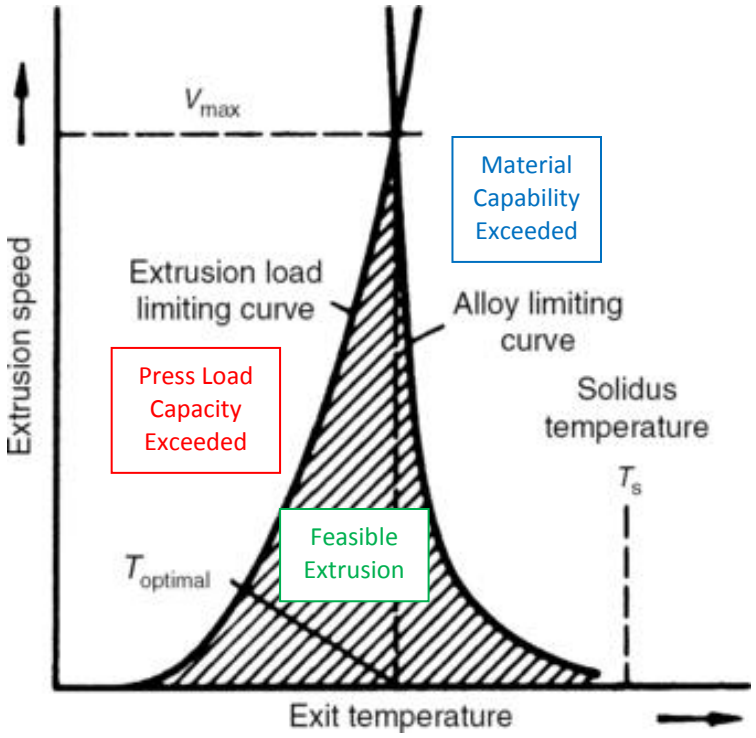


**Figure 4.1** Limit Diagram for Extrusion Speed [26].

**Table 4.1** Typical exit speed of soft and medium-grade aluminum alloys [22].

| Alloy | Type | Billet temperature | | Exit speed | |
|---|---|---|---|---|---|
| | | °F | °C | ft/min | m/min |
| 1060 | Non-heat-treatable | 788 | 420 | 164–328 | 50–100 |
| 1100 | Non-heat-treatable | 806 | 430 | 164–262 | 50–80 |
| 3003 | Non-heat-treatable | 842 | 450 | 98–230 | 30–70 |
| 5052 | Non-heat-treatable | 842 | 450 | 16–33 | 5–10 |
| 5154, 5254, 5454 | Non-heat-treatable | 860 | 460 | 20–49 | 6–15 |
| 6061 | Heat treatable | 806–932 | 430–500 | 16–82 | 5–25 |
| 6063 | Heat treatable | 896–932 | 480–500 | 115–262 | 35–80 |
| 6066 | Heat treatable | 797–860 | 425–460 | 66–115 | 20–35 |
| 6101 | Heat treatable | 896–932 | 480–500 | 115–262 | 35–80 |
| 6463 | Heat treatable | 896–932 | 480–500 | 115–262 | 35–80 |
| 7003 | Heat treatable | 824–977 | 440–525 | 16–69 | 5–21 |
| 7005 | Heat treatable | 824–977 | 440–525 | 16–46 | 5–14 |

**Table 4.2** Typical exit speed of hard aluminum alloys [22].

| Alloy | Type | Billet temperature | | Exit speed | |
|---|---|---|---|---|---|
| | | °F | °C | ft/min | m/min |
| 2014–2024 | Heat treatable | 788–842 | 420–450 | 5–11 | 1.5–3.5 |
| 5083, 5086, 5456 | Non-heat-treatable | 824–842 | 440–450 | 7–20 | 2–6 |
| 7001 | Heat treatable | 700–780 | 370–415 | 2–5 | 0.5–1.5 |
| 7075, 7079 | Heat treatable | 572–860 | 300–460 | 3–7 | 0.8–2 |
| 7049, 7150, 7178 | Heat treatable | 572–824 | 300–440 | 2.5–6 | 0.8–1.8 |

Note: Temperatures and extrusion speeds are dependent on the final shape and the extrusion ratio, and it may be necessary to start with lower billet temperatures than mentioned in the table. Source: Ref 11

The extrusion exit speed ranges indicated in Table 4.1 and Table 4.2 are dependent on the shape of the cross section and the extrusion ratio [22]. The normally acceptable extrusion ratio range for soft alloys is $R$=10-100, and for hard alloys is $R$=10-35 [22], [44]. Thus, a model to estimate the maximum extrusion exit speed based on the alloy, extrusion ratio and geometrical properties of the cross section seems adequate. One of the simplest, yet reasonably accurate models to predict the exit temperature of an extrusion is the one developed by Stüwe [45] and reported in [26] and [42]. He assumed that the increase in temperature of the emerging extrusion consisted of three components:

1. A temperature increase caused by the work of deformation that is almost entirely converted into heat (adiabatic):

$$\Delta T_1 = \frac{\sigma_f \ln R}{\rho c_p} \quad (4.10)$$

where $\rho$ and $c_p$ are the density and specific heat of the material, respectively.

2. A temperature increase at the billet surface caused by friction at the container wall, assuming adiabatic deformation:

$$\Delta T_2 = \frac{\sigma_f}{4\rho c_p}\sqrt{\frac{v_f}{R}\frac{L_o}{\alpha}} \quad (4.11)$$

where $\alpha$ is the thermal diffusivity of the material and is equal to $k/\rho c_p$ ($k$ being the thermal conductivity of the material).

3. A temperature increase at the extrusion surface caused by friction at the die land:

$$\Delta T_3 = \frac{\sigma_f}{4\rho c_p}\sqrt{\frac{v_f\ s}{\alpha}} \quad (4.12)$$

where $s$ is the die land length or bearing length, and according to extrusion die design practice for aluminum sections, should be at least 3 mm or twice the wall thickness, whatever is longer [26].

The exit temperature of the extrusion can be readily calculated as:

$$T_{exit} = T_{billet} + \Delta T \quad (4.13)$$

where $T_{billet}$ is the temperature of the preheated billet, and $\Delta T$ is the sum of the three temperature increase components described before.

The model illustrated in equations 4.10-4.13 relates the extrusion exit speed to the exit temperature. In order to avoid hot shortness in the extrusion, the exit temperature must be lower than the solidus temperature of the alloy by a certain margin, as it was shown in Figure 4.1. However, such margin doesn't seem to be documented in the literature, suggesting that the industrial practice may be based on historical data and/or error-trial procedures, as press operators have traditionally used surface cracking observations to regulate the press speed [42]. In the absence of a documented criterion to limit the exit temperature to a certain value

below the solidus temperature of the alloy, a pseudo-limit for the exit temperature can be obtained using the following approach:

1) Assume the upper limit of the range for maximum exit speed of the alloy (e.g. 80 m/min for Al 6063, from Table 4.1) corresponds to the simplest shape (solid round section) with the most favorable values of extrusion ratio and die land length (i.e. the ones that minimize $\Delta T$). The most favorable die land length is obviously the minimum possible within the feasible range ($s$=3 mm), while the most favorable extrusion ratio is not trivial, but it turns out to be the maximum within the allowable range ($R$=100 for soft alloys, and $R$=35 for hard alloys), as shown in more detail in APPENDIX A: EXIT TEMPERATURE VS. EXTRUSION RATIO.
2) Calculate the pseudo-limit for the exit temperature ($T_{exit}$) with equations 4.10-4.13 using the real billet dimensions ($L_o$ and $D_o$) and the assumed (most favorable) values for $R$, $s$ and $v_f$ described in step 1, as input. The billet preheat temperature ($T_{billet}$) may be assumed to be the average of the typical range for the alloy (Table 3.1 and Table 3.2).

Once the pseudo-limit for the exit temperature has been obtained by the approach mentioned above[2], it can be used as a calibrated limit for the exit temperature of any shape under any extrusion conditions (i.e. any $R$ and $s$). Finally, the following non-linear equation (based on the models presented before) can be solved numerically[3] for the extrusion exit speed of the actual shape and conditions:

$$\frac{\sigma_f(v_f)\ln R}{\rho c_p} + \frac{\sigma_f(v_f)}{4\rho c_p}\sqrt{\frac{v_f}{R}\frac{L_o}{\alpha}} + \frac{\sigma_f(v_f)}{4\rho c_p}\sqrt{\frac{v_f\ s}{\alpha}} - (T_{exit} - T_{billet}) = 0 \quad (4.14)$$

[2] The pseudo-limit for the exit temperature may result in a value that is higher than the solidus temperature of the alloy, since the model in equations 4.10-4.12 is a simplification of the real thermomechanical phenomenon, and therefore it is not 100% accurate. However, the pseudo-limit is just a mathematical reference to calculate the exit speed of the actual shape, based on the assumptions mentioned above.

[3] A closed-form solution for $v_f$ in Equation 4.14 cannot be obtained, so it must be solved numerically or graphically. The MS Excel Solver Analysis Pack has the capability to obtain a numerical solution.

where $v_f$ is the only unknown variable and it represents the maximum extrusion exit speed allowable to avoid hot shortness issues in the actual shape under the actual extrusion conditions. As it will be explained shortly, this may or may not be the actual extrusion exit speed, as the maximum ram speed capacity of the press may be the limiting factor. Thus, in order to differentiate the hot shortness speed limit from the press speed limit, the maximum extrusion exit speed obtained from equation 4.14 will be called $v_{f\_hs}$ (hot shortness exit speed limit). The ram speed hot shortness limit can then be calculated as:

$$v_{o_{hs}} = \frac{1}{R} v_{f_{hs}} \quad (4.15)$$

The press limit for ram speed will be called $v_{o\_press}$ and it is a technical parameter of the press selected. This parameter must be compared against $v_{o\_hs}$ in order to estimate the actual extrusion ram speed, as follows:

$$v_o = MIN\left(v_{o_{hs}}, v_{o_{press}}\right) \quad (4.16)$$

this means that the minimum between the hot shortness limit and the press limit for ram speed will dictate the actual extrusion ram speed. Finally, the actual extrusion exit speed can be calculated as:

$$v_f = R\, v_o \quad (4.17)$$

It is important to remark that the extrusion speed is not constant through the process, because friction and temperature vary during the extrusion cycle [6]. Indeed, many modern extrusion plants use *Isothermal Extrusion Technology* [22], [26] to maintain the exit temperature as uniform as possible through the process by controlling the extrusion speed. Nevertheless, the method presented in this section is a reasonable estimate of the extrusion exit speed, a parameter that is necessary for the extrusion pressure calculations covered in Section 4.1.1, as well as for the cycle time estimation to be presented in Section 4.2.

### *4.1.3 Press Selection Algorithm*

The model presented in Sections 4.1.1 and 4.1.2 to predict the extrusion pressure and speed represents the basis for the press selection process, which is described in detail in this section, in the form of an algorithm that should be easily implemented in a computer program.

Before getting into the algorithm details, it is necessary to mention the way extrusion presses are typically specified in the industry, as well as the press size range available in the market nowadays. The main technical specifications of extrusion presses consist of the following:

1. Billet Diameter
2. Extrusion Force
3. Billet Length (Maximum and Minimum)
4. Extrusion Ram Speed (Maximum)
5. Dead-Cycle Time (Non-extrusion time per billet)

Additionally, press manufacturers usually specify the material type that can be extruded by the press (e.g. Aluminum Alloys, Copper Alloys, Steel, etc), as well as the direction of extrusion (i.e. direct, indirect, or both). A survey of the direct extrusion presses available in the market for aluminum alloys revealed that the typical press sizes range from those having a container (or billet) diameter of 3.5 inches (90 mm) to 18 inches (457 mm), and an extrusion force of 700 US ton (6.3 MN) to 9000 US ton (80 MN). Larger presses are not very common, but they do exist in the market, with container diameters up to 29 inches (736 mm) and extrusion force capacities up to 16000 US ton (142 MN) [1], [6], [46].

Regarding maximum extrusion ram speed, the survey showed that most of the presses in the market are in the range of 20-25 mm/s, although a few presses reach up to 50 mm/s. A table of technical specifications of presses obtained in the survey is included in APPENDIX B: EXTRUSION PRESS DATABASE. The dead-cycle time for the majority of the presses was not directly specified by the press manufacturer, so it was estimated based on the method presented in Section 4.2.1. Similarly, the minimum billet length was not specified for most of

the presses; however, based on data provided by *SMS* (a recognized press manufacturer), showing that the minimum billet length is 50% of the maximum billet length for all their presses, it may be assumed that such ratio is the same for presses from any other manufacturer, unless otherwise specified.

The main goal of the press selection algorithm proposed here is to find the smallest press capable of extruding the part being designed, at the maximum extrusion ram speed available, to maximize the productivity of the plant and minimize the manufacturing cost. The press selection is subject to the following constraints:

1) The CCD must not exceed 85% of the billet diameter[4] ($D_o$), according to best practices documented by the extrusion division of the DGM (German Metallurgical Society) [26]. Thus, $D_o \geq CCD/0.85$.
2) The extrusion ratio ($R$) must be within the feasible range for the material being extruded (i.e. $10 \leq R \leq 100$ for soft aluminum alloys, and $10 \leq R \leq 35$ for hard aluminum alloys [22], [44]).

In addition, as it will be discussed later in Section 4.2.2, it is always desirable to use the maximum billet length allowable by the press, to maximize the productivity of the process. Therefore, the press selection algorithm must consider the maximum billet length allowed by the press ($L_{o\_max}$) in the extrusion pressure calculations (i.e. $L_o$=$L_{o\_max}$). If the extrusion pressure required is too high so that no press in the database has enough capacity to extrude the part, then the billet length $L_o$ can be reduced from $L_{o\_max}$, until the extrusion pressure required is reduced to achievable levels. However, the billet length must not be reduced below the minimum billet length ($L_{o\_min}$) allowable on each press.

The proposed press selection algorithm is depicted in the form of a Flow Diagram in Figure 4.2, Figure 4.3, and Figure 4.4. Due to the complexity of the press selection process, the

[4] On the other hand, the greater the clearance between the *CCD* and $D_o$, the higher the tendency for contamination from the skin of the billet [22].

algorithm contains several iterative loops. In order to identify the variables that change from one iteration to the other, the following index nomenclature was introduced:

- The index *i* represents the $i^{th}$ iteration as a result of increasing $D_o$.
- The index *j* represents the $j^{th}$ iteration as a result of changing the press selected within a group of presses with the same $D_o$.
- The index *k* represents the $k^{th}$ iteration as a result of reducing $L_o$.
- The index *l* represents the $l^{th}$ iteration to find a numerical solution for the hot shortness extrusion exit speed limit ($v_{f\_hs}$).

The nomenclature of all the variables used in the Flow Diagram is the same as the one introduced before, in Sections 4.1.1 and 4.1.2. A few new variables were introduced as follows: $R_{min}$ and $R_{max}$ are the minimum and maximum extrusion ratio allowable on the material, $THK_{max}$ is the maximum wall thickness of the part, $v_{f\_max}$ is the upper limit of the range for maximum exit speed of the alloy (from Table 4.1 or Table 4.2), $s_{round}$ is the die land length assumed in the calculation of the pseudo-limit for the exit temperature in a solid-round bar (as discussed in Section 4.1.2), $\sigma_{f\_round}$ is the flow stress calculated for such solid-round bar, and $\sigma_{f\_hs}$ is the flow stress calculated for the actual cross-section at the hot shortness extrusion speed.

As it can be seen in the first part of the Flow Diagram (Figure 4.2), the billet length ($L_o$) is assigned a value of $L_o=L_{o\_max}*0.95^{(k-1)}$. Thus, when $k$=1 (first iteration), $L_o=L_{o\_max}$, as intended. If no press in the database has enough force capacity to extrude the section with $L_o=L_{o\_max}$, the selection process is then restarted with $k=k+1$. In that way, when $k$=2, $L_o=L_{o\_max}*0.95$; then when $k$=3, $L_o=L_{o\ max}*0.95^2$, and so on, reducing the billet length progressively by 5% after each global iteration, until a press with enough force capacity is found. Since the minimum billet length allowable in the press ($L_{o\_min}$) is generally assumed to be $0.5*L_{o\_max}$, the iterative process cannot continue if $k$=15, as it would result in a billet length $L_o$ shorter than $0.5*L_{o\_max}$ (i.e. when $k$=15, $L_o=L_{o\_max}*0.95^{14} = 0.49*L_{o\ max}$). To prevent that from happening, a constraint of $k \leq 14$ was introduced in the algorithm as a condition to continue with the iterative process.

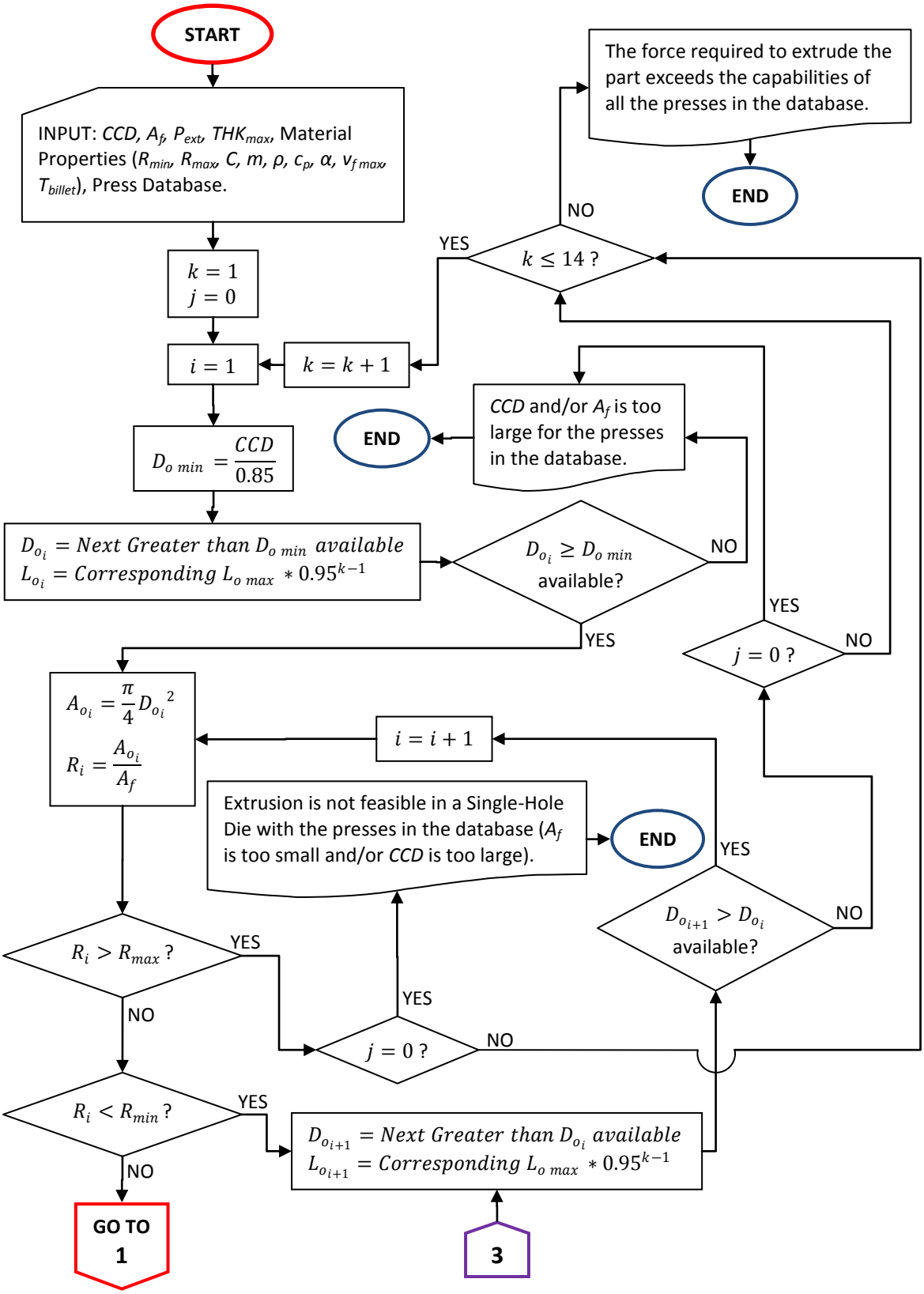


**Figure 4.2** Flow Diagram of Press Selection, Part 1.

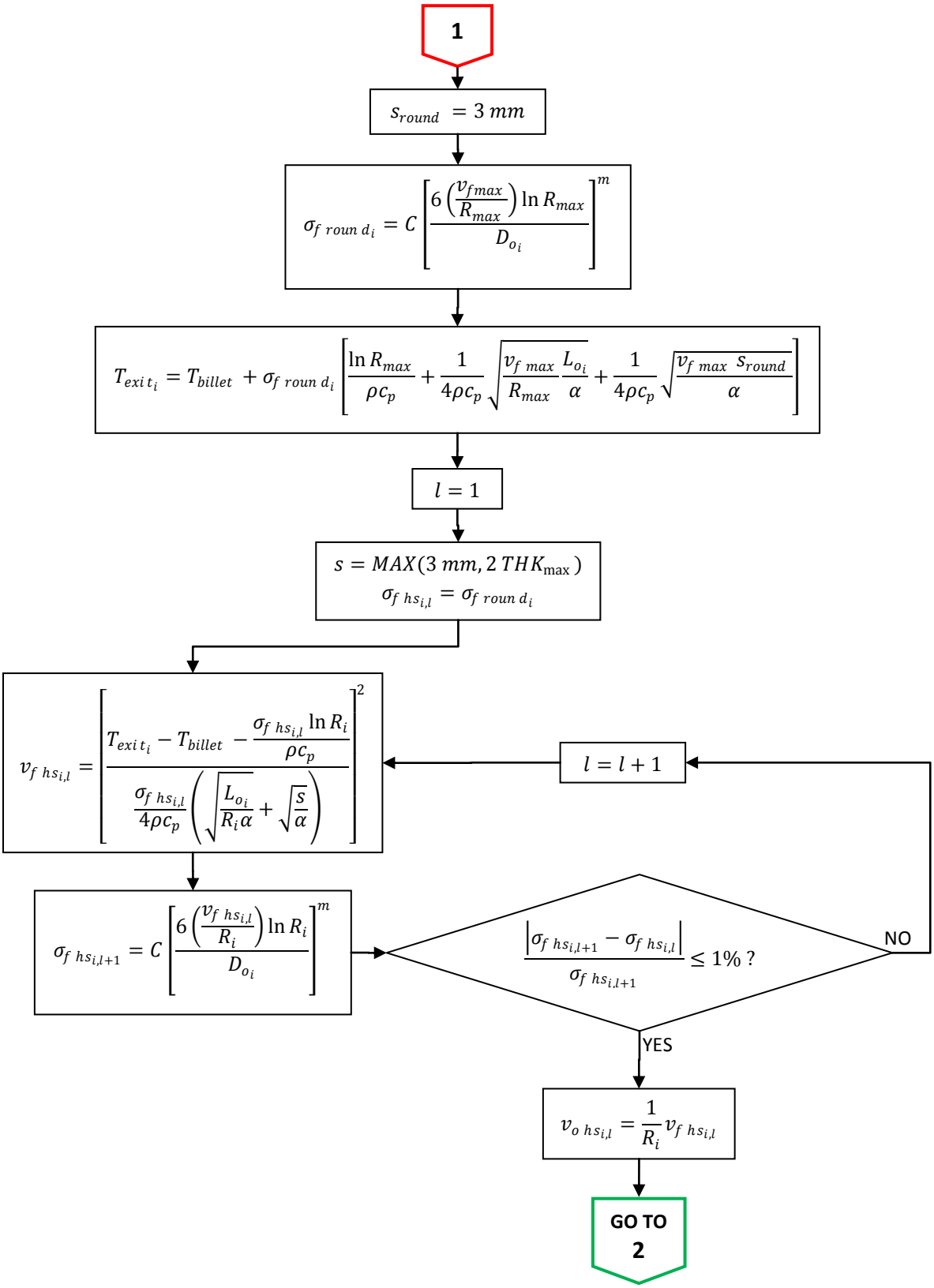


**Figure 4.3** Flow Diagram of Press Selection, Part 2.

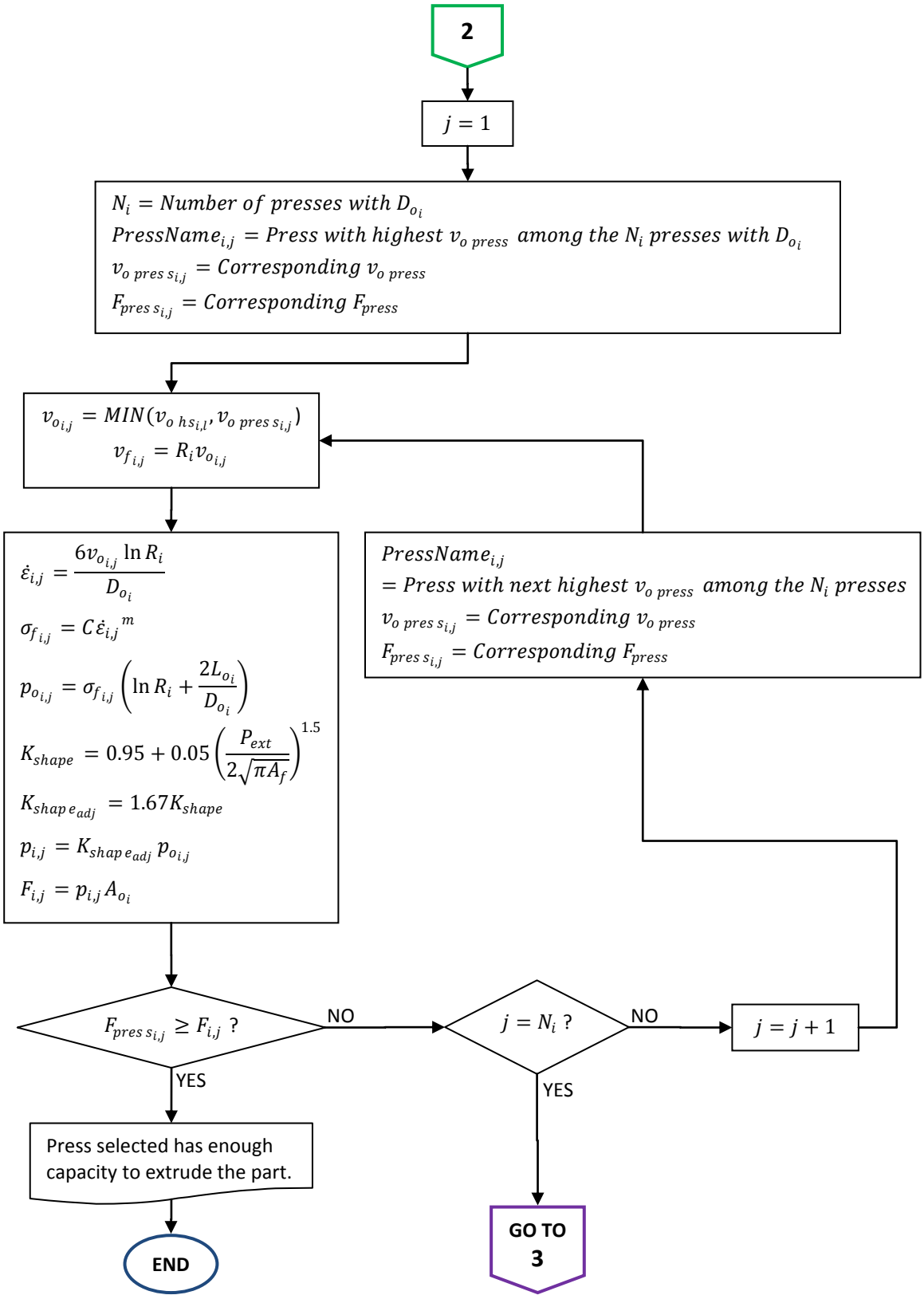


**Figure 4.4** Flow Diagram of Press Selection, Part 3.

In Part 2 of the Flow Diagram (Figure 4.3), the extrusion exit speed limit for hot shortness ($v_{f\_hs}$) is obtained using the approach described before in Section 4.1.2. A numerical iterative process is included to find the value of $v_{f\_hs}$, assuming a 1% error tolerance as a convergence criterion for the numerical solution. The equation for $v_{f\_hs}$ in the Flow Diagram is simply the result of solving equation 4.14 for $v_{f\_hs}$, using a guess value for the flow stress $\sigma_{f\_hs}$ in the first iteration ($\sigma_{f\_hs} = \sigma_{f\_round}$), and then iterating as necessary. Since the flow stress is not very sensitive to the strain rate (i.e. $m \approx 0.125$), a couple of iterations should suffice to converge into a numerical solution for $v_{f\_hs}$.

The proposed press selection algorithm (presented in Figure 4.2, Figure 4.3, and Figure 4.4) can be greatly simplified if the trends of Press Specific Pressure ($p_{press}$) vs. Billet Diameter ($D_o$) and Extrusion Pressure ($p$) vs. Billet Diameter ($D_o$) are examined in more detail. The typical variation of Press Specific Pressure vs. Billet Diameter is plotted in Figure 4.5, as obtained from the survey of presses in the market (see APPENDIX B: EXTRUSION PRESS DATABASE). In that figure, it can be visualized that larger presses (i.e. presses with a larger billet diameter) tend to have lower specific pressures. On the other hand, an inspection of Equations 4.1 to 4.9 reveals that the extrusion pressure ($p$) tends to increase logarithmically as the billet diameter ($D_o$) increases[5]. Therefore, the extrusion force margin (i.e. $F_{press} - F$, or $p_{press} - p$) tends to decrease with increasing billet diameter. In other words, contrary to natural intuition, moving to a press with a larger billet diameter (and consequently a higher extrusion force) will usually not provide a more favorable extrusion force margin. Thus, the optimum billet diameter is the smallest one that complies with the previously mentioned constraints for extrusion ratio ($R \geq 10$) and CCD clearance ($D_o \geq CCD/0.85$).

The assumptions and approach described above greatly simplify the press selection algorithm by removing the iterative loops containing the "$i$" index and making the billet diameter ($D_o$) a dependent variable, rather than an independent one. This simplification makes it much easier to implement the algorithm in a spreadsheet environment, since the only

[5] This is true assuming that the $L_o/D_o$ ratio remains more or less constant for every press. Indeed, that is usually the case, as $L_o/D_o$ is generally around 4 [22].

independent variable left in the press selection process is the billet length ($L_o$). However, it must be noted that the press specific pressure data presented in Figure 4.5 contains a great deal of scatter, suggesting that the decreasing trend assumption is not always valid. Having said that, the recommended press selection algorithm is still the one shown in the Flow Diagram of Figure 4.2, Figure 4.3, and Figure 4.4, but the simplifications described above can be adopted with caution if a less sophisticated computer program is desired (e.g. spreadsheet).

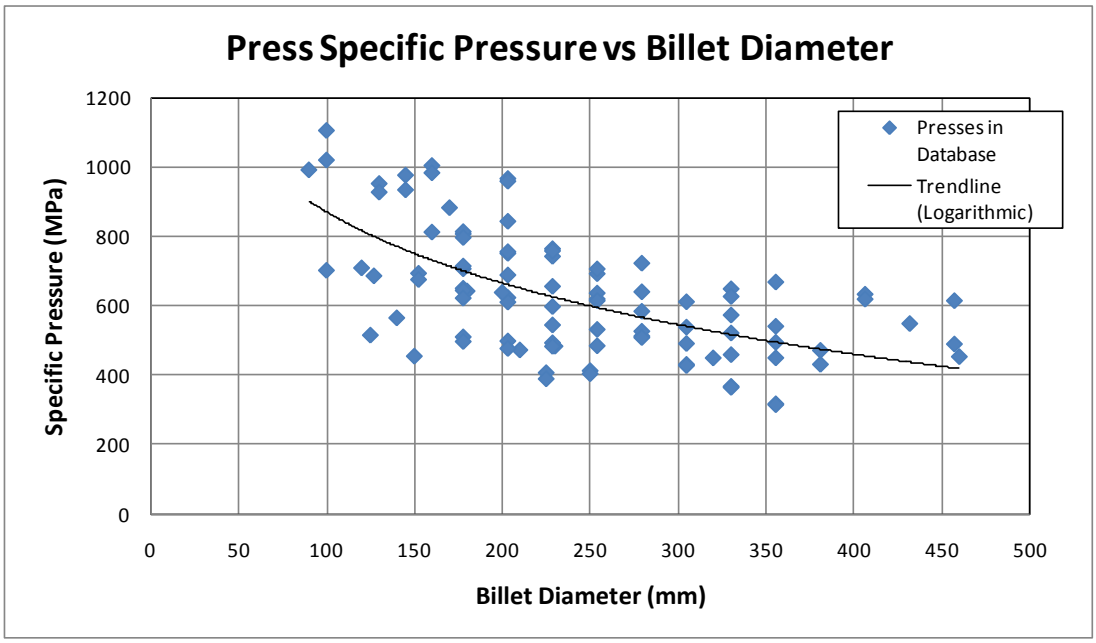


**Figure 4.5** Survey of Press Specific Pressure vs. Billet Diameter.

Finally, it is imperative to mention that the proposed algorithm assumes the use of a Single-Hole Die. If the section has a small CCD and a relatively simple shape, the extruder has the option of putting multiple holes in a die (i.e. use a Multi-Hole Die) to extrude various strands of metal simultaneously and increase productivity [26]. However, from a FBC standpoint, the "optimal press selection problem" becomes much more complex if the use of Multi-Hole Dies is considered. The complication resides in the fact that an additional independent variable is introduced in the "optimization problem": the number of holes in the die, $N_{holes}$. This variable affects the definition of the extrusion ratio, which then becomes $R=A_o/(N_{holes}*A_f)$ [22]. Another complication is the introduction of an additional constraint: the

"Table Weight" (which is the weight per unit length of each extrusion multiplied by the number of holes) must not exceed the capability of the runout table and handling equipment in the extrusion plant.

Moreover, according to Greg Lea, a consultant to the extrusion industry with more than 15 years of experience in process optimization, the decision on whether or not to use a Multi-Hole Die, and the number of holes to put on it, is usually an engineering judgment call made by the extruder when the die is designed, as several factors are involved, like the Table Weight, the CCD vs. the container diameter of the extruder press(es), the finish requirements, the runout handling system (i.e. puller or conveyer), and the production volume (i.e. a small volume may not be worth the higher difficulty implicated in producing multiple strands in a die). Consequently, for the sake of FBC, the press selection algorithm assuming a Single-Hole Die seems adequate, leaving the Multi-Hole Die option up to the extruder.

## 4.2 Cycle Time

As it has been mentioned before, extrusion is a continuous manufacturing process and as such, an extrusion plant can be visualized as a "production pipe" where metal is flowing continuously at a certain mass flow rate, as illustrated in Figure 4.6. If the steady state mass flow rate of the production line is known, then the cycle time to produce a part can be readily calculated. In order to determine the mass flow rate of a production line, the individual operation that constitutes the bottleneck of the entire process must first be identified and then analyzed to calculate the cycle time.

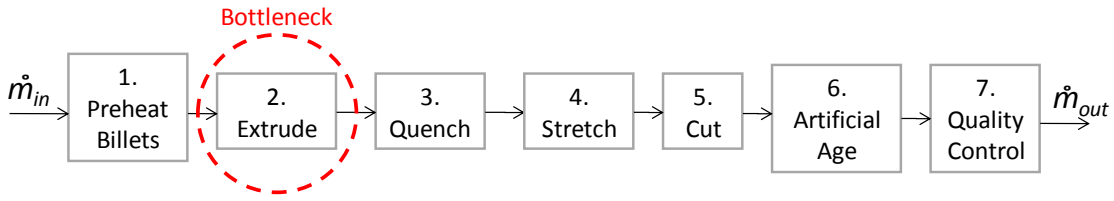


**Figure 4.6** Extrusion Production vs. Pipe Flow Analogy.

Although the aging heat treatment is in general the most time consuming part of the production system, other process steps may actually be the bottlenecks of the line [23]. The press operation is usually the one dictating the output of the line, as it is noncontinuous and considerable time is spent on changing dies, loading billets in the container and performing maintenance tasks [23]. Furthermore, according to best practices documented for economical production in extrusion plants, any bottlenecks in die preparation, billet heating, stretching or sawing must be located and eliminated; at the end, the press should be the bottleneck [26]. In other words, the auxiliary equipment of the plant must be able to keep up with the press. Indeed, extruded products with short lengths are usually cut as a secondary operation, to avoid backing up the whole production line [47]. The minimum cut length that can be achieved in the extrusion line seems to be in the order of 6 to 8 ft (1.83 to 2.44 m), based on discussions held with manufacturing personnel from *Bonnell Aluminum Inc* (a recognized aluminum extruder in the US) and confirmed by Greg Lea (Consultant). Wider saw tables tend to be more forgiving on this matter, and therefore some extruders like *Tri-City Extrusion Inc* are able to cut shorter lengths in the extrusion line, in the order of 3 ft (914 mm).

### *4.2.1 Press Cycle Time Elements*

The cycle time of a press is comprised by the following three major tasks [23]:

1) Extrusion Time: The time spent pushing a billet through the die at the desired (steady state) extrusion speed.
2) Ram Acceleration Time: The time spent per charge on reaching the desired (steady state) extrusion speed.
3) Dead-Cycle Time: The non-extrusion (idle) time per billet spent on cutting off the butt discard after extrusion, inserting a new billet in the container, upsetting the billet, and performing the “burp” cycle (decompression).

Additionally, the setup time (e.g. time to change dies) is sometimes included as part of the cycle time and applied the corresponding labor and overhead rates; however, in this thesis

the setup time is considered as a separate item, in order to follow the cost taxonomy described in Section 2.2. At the end, the estimated piece part cost must be the same, regardless of the taxonomy used.

The extrusion time per billet is calculated as:

$$t_{ext_{billet}} = \frac{L_f}{v_f} \quad (4.18)$$

where $v_f$ is the actual extrusion exit speed, and $L_f$ is the extruded length of the billet, given by the following equation:

$$L_f = R(1 - b_d)L_o \quad (4.19)$$

where $b_d$ is the butt discard fraction of the billet that is not extruded (typically 10%, as discussed in Section 3.3).

The ram acceleration time is a function of many parameters like the extrusion ratio, the billet temperature, and the extrudability of the alloy [22]. Although no model seems to be available in the literature, the ram acceleration time can be assumed to be in the order of 7 seconds [23] in the absence of data.

The dead-cycle time is dictated by the technology of the selected press, although the size of the billet has indirect implications as well. The survey of technical specifications of presses available in the market suggested a strong correlation between the dead-cycle time and the press force capacity, as shown in Figure 4.7, where data from two different press manufacturers (*SMS* and *UBE*) is compared and fitted to appropriate polynomial equations. It is clear from Figure 4.7 that the dead-cycle time increases with the size of the press in an almost linear relationship. Since the majority of the presses in the collected database contain no explicit information on its dead-cycle time, the regression equation obtained from the *SMS*

data[6] may be assumed to predict the dead-cycle time of any modern aluminum extrusion press with reasonable accuracy. Thus, in the absence of explicit data, the empirical equation for dead-cycle time is:

$$t_{dead_{billet}} \approx 0.0015F_{press}^{\ 2} + 0.0338F_{press} + 11.776 \quad (4.20)$$

where $t_{dead\_billet}$ is the dead-cycle time (sec) per billet and $F_{press}$ is the press force (MN) capacity.

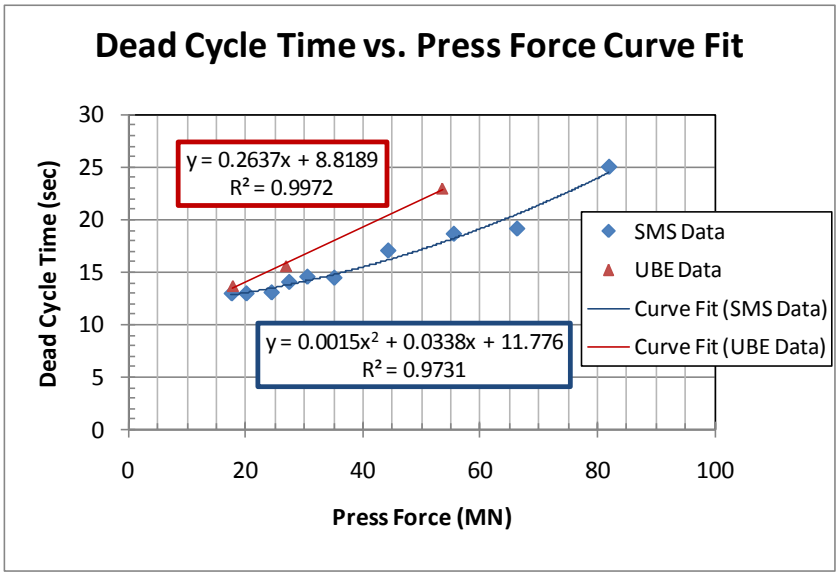


**Figure 4.7** Dead-cycle time vs. Press Force (Courtesy of *SMS* and *UBE*).

### *4.2.2 Cycle Time Calculations*

The equations in the previous section predict the cycle time on a "per billet basis", without considering the effect of "unproductive mass flow rate" resulting from defective parts and scrap losses generated after the press. The incorporation of such unproductive mass flow rate into the cycle time model can be performed easier if the calculations are carried out on a "per batch run[7] basis", and then translated into a "per part basis". The cycle time per batch is:

---

[6] The regression equation obtained from SMS data is considered to be more accurate than the one obtained from UBE, as more data points were available.

[7] For the purpose of cost estimating, a batch run is defined here as a continuous production lot of a certain number of identical parts.

$$t_{cycle_{batch}} = t_{ext_{billet}}\, n_{billets_{batch}} + \left(t_{accel_{billet}} + t_{dead_{billet}}\right) N_{billets_{batch}} \quad (4.21)$$

where $t_{ext\_billet}$, $t_{accel\_billet}$ and $t_{dead\_billet}$ are the extrusion, acceleration and dead-cycle times per billet, respectively, calculated as described in the previous section; $n_{billets\_batch}$ is the number of billets extruded per batch run, including the fraction of the last billet pressed in the lot (not extruded completely). Thus, $n_{billets\_batch}$ is a non-integer number, and its calculation will be explained shortly. On the other hand, $N_{billets\_batch}$ is an integer number[8], and is defined as:

$$N_{billets_{batch}} = ROUNDUP\left(n_{billets_{batch}}\right) \quad (4.22)$$

Note that the acceleration and dead-cycle times per billet in equation 4.21 are multiplied by $N_{billets\_batch}$ because the last billet in the batch takes the regular acceleration and dead-cycle time of any other charge, regardless of the fraction of the billet that is extruded. Conversely, the extrusion time per billet in equation 4.21 is multiplied by $n_{billets\_batch}$ because the pressing time of the last billet in the batch depends on how much of the billet is extruded before stopping the press. Incomplete extrusion of the last billet in the batch is due to the fact that the total length extruded in a batch run is not necessarily a multiple of the extruded length of one billet. One might be tempted to adjust the billet length to avoid this; however, from a cycle time and productivity perspective, the optimal billet length is always the longest allowable in the selected press [22], to minimize the number of times the ram acceleration and dead-cycle time occur. Thus, the model in equation 4.21 assumes that the extruder either stops the press after a certain fraction of the last billet has been extruded, or it has the capability to cut off the last billet of the batch to the necessary length before loading it into the press.

The calculation of $n_{billets\_batch}$ must contain the adverse effect of defective parts and scrap losses after the press upon the productivity of the plant. It is a common practice to assume that the first and the last meter of the total continuous extrusion are of inferior quality and therefore scrapped [23]. Indeed, the ends of each continuous extrusion are crushed by the

[8] The nomenclature followed in this thesis for naming the quantity variables is to use *N* for integer quantities and *n* for non-integer quantities.

jaws in the stretcher anyway, and such crushed length varies from 1 to 3 m [42]. It is important to remark that the "total continuous extrusion" term mentioned before does not refer to the extruded length of one billet ($L_f$), but to the total continuous length of billet-on-billet extruded section before it is cut by a flying hot saw in the runout table, as illustrated in Figure 4.8. Obviously, the continuous extrusion length must be equal or shorter than the runout table length, which typically ranges from 30 to 40 m, as mentioned in Section 3.3.

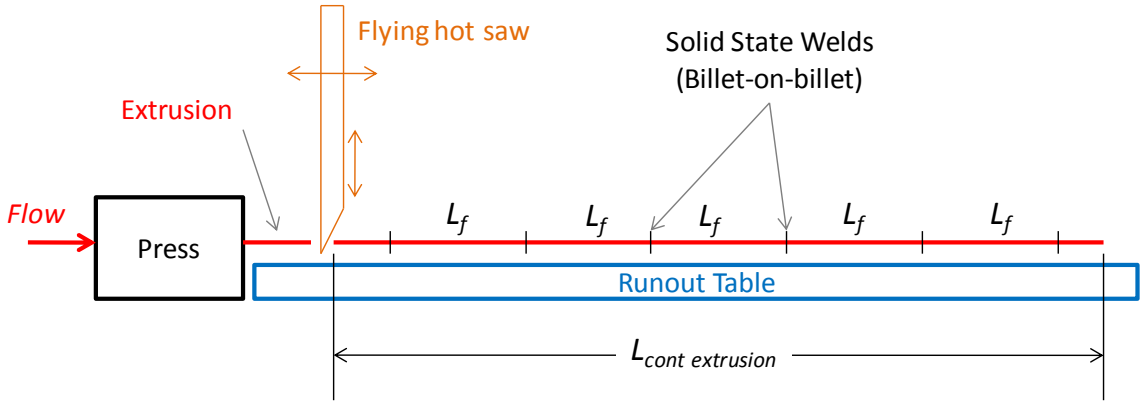


**Figure 4.8** Schematic of Continuous Extrusion Length.

The estimation of $n_{billets\_batch}$ must also contain quality scrap resulting from defective parts. Typically, expected quality scrap losses may be assumed to be in the order of 6% [23], which means that about 6 out of 100 parts in a lot would be rejected and scrapped in the quality inspection. Hence, the gross production must be increased accordingly so that at the end of the process, the net production of (good) parts per batch meets the intended volume. Having said that, the number of billets per batch, $n_{billets\_batch}$ can be calculated as follows:

$$n_{billets_{batch}} = \frac{N_{parts_{batch}}}{Y_{quality}\ n_{parts_{billet}}} \qquad (4.23)$$

where $N_{parts\_batch}$ is the number of good parts per batch (a.k.a. the batch size), which is obviously an integer number and is an input for the FBC model; $Y_{quality}$ is the expected yield of the quality inspection process (~94%, as mentioned above), and $n_{parts\_billet}$ is a non-integer number representing the number of parts produced from one billet, which can be calculated as:

$$n_{part\ s_{billet}} = \frac{N_{part\ s_{ext}}}{n_{billet\ s_{ext}}} \quad (4.24)$$

where $N_{parts\_ext}$ is an integer number representing the number of parts produced from one continuous extrusion length, and $n_{billets\_ext}$ is a non-integer number that represents the number of billets welded together in one continuous extrusion length, including the fractions at the front and rear ends, as depicted in Figure 4.8. The equations to calculate both $N_{parts\_ext}$ and $n_{billets\_ext}$ will be presented shortly.

So far, the scrap material on the ends of each continuous extrusion length (~ 2 m, as discussed before) has not been considered in the calculations; however, it can be included in the number of parts per continuous extrusion ($N_{parts\_ext}$), as follows:

$$N_{part\ s_{ext}} = ROUNDDOWN\left(\frac{L_{runout\ \ table} - L_{scrap}}{L_{part}}\right) \quad (4.25)$$

where $L_{runout\ table}$ is the length of the runout table (which can be assumed to be 35 m, as the average of the typical runout tables in the industry), $L_{scrap}$ is the length of the scrap material on the ends of each continuous extrusion (assumed to be ~2 m), and $L_{part}$ is the length of the part, which must be no shorter than 3 ft (914 mm), as it was discussed previously in Section 4.2. The length of each continuous extrusion becomes then:

$$L_{cont\ ext} = N_{part\ s_{ext}}\ L_{part} + L_{scrap} \quad (4.26)$$

and finally the number of billets per extrusion is readily calculated as:

$$n_{billet\ s_{ext}} = \frac{L_{cont\ ext}}{L_f} \quad (4.27)$$

The use of equations 4.22-4.27 provides all the necessary input for equation 4.21 to calculate the cycle time per batch ($t_{cycle\_batch}$). Once this has been done, the cycle time per part $t_{cycle}$ is easily calculated as:

$$t_{cycle} = \frac{t_{cycl\ e_{batc\ h}}}{N_{part\ s_{batc\ h}}} \quad (4.28)$$

## 4.3 Labor and Overhead Costs

Once the cycle time has been estimated, the labor and overhead costs calculation is fairly simple, as described previously in Section 2.2.2. The labor cost per part is:

$$L_{cost} = n_{operators} \; L_{rate} \; t_{cycle} \quad (4.29)$$

where $n_{operators}$ is the effective number of operators (or crew size) working in the extrusion line, $L_{rate}$ is the labor rate of the operators (in US dollars per hr), and $t_{cycle}$ is the cycle time per part.

The crew size in aluminum extrusion plants has been reduced significantly over the years, as new technology has increased automation and process control. In the early 1970's, a typical crew size consisted of seven operators [21], [26]. However, by the mid 1980's, a highly automated aluminum extrusion line operated by a three-man crew became a reality [6], and this seems to be the standard today. Fully automated presses use a three-man crew as follows: One man as a press supervisor and operator; a second man for operating, die preparation at the press and support of stretcher head stock; and a third man for supervising the saw and the stacking and aging unit [42]. Thus, in the absence of more recent data, it may be assumed that $n_{operators}$ =3 in the labor cost calculation.

The labor rate is highly variable as it is dependent on the geographical location of the manufacturer (e.g. US vs. China) and other economic variables that are beyond the scope of this thesis. For simplicity, an average labor rate for extrusion line operators in the US will be assumed, as reported by the *US Bureau of Labor Statistics* in [48]. This source estimates a national average labor rate of $14.92 per hour for "Extruding and Drawing Machine Setters, Operators, and Tenders, Metal and Plastic" (Occupation Code 51-4021).

On the other hand, the overhead cost per part is calculated by:

$$OH_{cost} = OH_{rate} \; t_{cycle} + OH_{upcharge} \, m_{part} \quad (4.30)$$

where $OH_{rate}$ is the overhead rate (in US dollars per hr) determined by the accounting department of the manufacturer; $OH_{upcharge}$ is an additional overhead charge, priced per unit

mass (in USD/kg or USD/lb), and $m_{part}$ is the mass of the part (=$\rho A_f L_{part}$). Note that Equation 4.30 differs from the previously introduced definition of overhead cost (in Equation 2.7) in that an additional overhead charge ($OH_{upcharge}$) was introduced. This charge accounts for a series of costs that are incurred on a per unit mass basis, rather than on a per unit time basis. Some examples of such costs in the extrusion process are: Press and Tooling Maintenance, Expendable Tooling, and Cleaning/Inspection Consumables [23], [25]. As it will be shown later in more detail in CHAPTER 6: COST MODEL VALIDATION, the overhead upcharge ($OH_{upcharge}$) is dependent on the size of the press (billet diameter) selected to extrude the part, with larger presses having a higher overhead upcharge. For now, the reader can think of the variable $OH_{upcharge}$ as a known input that depends on the billet diameter selected.

Conversely, the overhead rate ($OH_{rate}$) is dependent on a number of costs lumped together by the accounting department of the manufacturing organization, as mentioned before in Section 2.2.1. In the absence of specific data from extruders, it may be assumed that the sum of labor and overhead rates is around $60 per hour, based on expert opinion (Dr. Mike Philpott, Associate Professor, University of Illinois at Urbana-Champaign). Hence, the overhead rate may be assumed to be ≈$45 per hour.

## 4.4 Material Cost

The Material Cost is calculated based on the weight of the total raw material used to produce a part, multiplied by the price per unit mass of the alloy. As it was explained in Section 2.2.2, in order to calculate the raw material used to produce a part, the Yield must first be estimated based on all the scrap mass generated in the entire process. The schematic in Figure 4.9 illustrates a mass balance for the extrusion line, where the different major sources of scrap material are shown, consisting of the following:

a) Mass of Billet Butt Discard ($m_{butt}$): The mass of all the discarded butts of the billets.

b) Mass of Crushed Ends in Stretcher ($m_{crushed}$): The mass of all the front and rear ends of inferior quality (with a length of ~1 m per side, or $L_{scrap}$~2 m) and crushed by the stretcher on each continuous extrusion length.

c) Mass of Non-conforming Parts ($m_{NC\ parts}$): The mass of all parts rejected in the Quality Inspection Process (~6% of all parts).

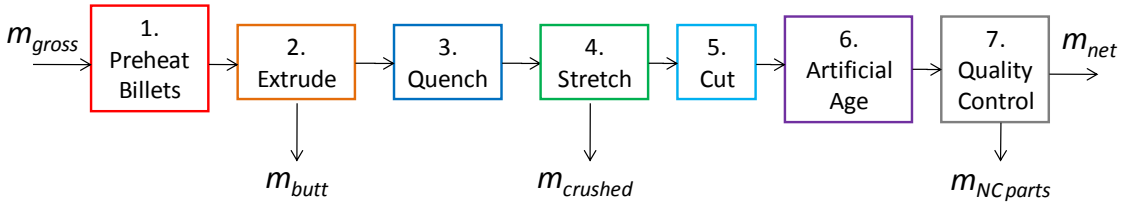


**Figure 4.9** Mass Balance for Yield and Raw Material Calculations

The scrap mass calculations are easier if they are performed on a per batch basis. First, the mass of billet butt discard per batch can be estimated as:

$$m_{butt_{batch}} = b_d m_{billet}\, ROUNDDOWN\left(n_{billets_{batch}}\right) + b_{df}\, m_{billet} \qquad (4.31)$$

where $m_{billet}$ is the mass of one billet (=$\rho A_o L_o$), $b_d$ is the regular butt discard fraction (~10%, as discussed before), $n_{billets\_batch}$ is the number of billets extruded per batch (calculated per the methods covered in Section 4.2.2), and $b_{df}$ is the butt discard fraction of the last billet in the batch (the one that is not completely extruded), which can be calculated as:

$$b_{df} = ROUNDUP\left(n_{billets_{batch}}\right) - n_{billets_{batch}} \qquad (4.32)$$

Secondly, the mass crushed in the stretcher per batch can be calculated as:

$$m_{crushed_{batch}} = N_{ext_{batch}} \rho A_f L_{scrap} \qquad (4.33)$$

where $\rho$ is the density of the material, $A_f$ is the cross sectional area of the extrusion, $L_{scrap}$ is the assumed crushed length (~2 m), and $N_{ext\_batch}$ is an integer number representing the number of continuous extrusion lengths per batch, and is calculated by the following expression:

$$N_{ext_{batch}} = ROUNDUP\left(\frac{N_{parts_{batch}}}{N_{parts_{ext}}}\right) \quad (4.34)$$

where $N_{parts\_batch}$ is the Batch Size (an input for the FBC model) and $N_{parts\_ext}$ is the number of parts per continuous extrusion length, calculated as described previously in Section 4.2.2.

The third scrap source is the mass of the nonconforming parts, which can be calculated on a per batch basis by the following equation:

$$m_{NC\ parts_{batch}} = N_{NC\ parts_{batch}}\, m_{part} \quad (4.35)$$

where $m_{part}$ is the mass of the part ($=\rho A_f L_{part}$) and $N_{NC\ parts\_batch}$ is the expected number of nonconforming parts per batch rejected in the quality inspection. The latter is obviously an integer number, and it can be calculated from the following:

$$N_{parts_{batch}} = Y_{quality}\left(N_{parts_{batch}} + N_{NC\ parts_{batch}}\right) \quad (4.36a)$$

where $Y_{quality}$ is the expected yield of the quality inspection process (~94%, as mentioned before) and $N_{parts\_batch}$ is the number of (good) parts per batch (i.e. the Batch Size, an input to the FBC model). Solving equation 4.36a for $N_{NC\ parts\_batch}$ and rounding the result to the closest integer, gives the approximate number of nonconforming parts per batch:

$$N_{NC\ parts_{batch}} = ROUND\left(\frac{N_{parts_{batch}}}{Y_{quality}} - N_{parts_{batch}}\right) \quad (4.36b)$$

Now that the different types of scrap generated in the process have been calculated, the total scrap mass per batch is obtained by adding them up:

$$m_{scrap_{batch}} = m_{butt_{batch}} + m_{crushed_{batch}} + m_{NC\ parts_{batch}} \quad (4.37)$$

The total raw mass (or gross mass) per batch is then:

$$m_{raw_{batch}} = m_{net_{batch}} + m_{scrap_{batch}} \quad (4.38)$$

where $m_{net\_batch}$ is the net mass of good parts produced per batch, simply calculated by:

$$m_{net_{batch}} = N_{parts_{batch}} m_{part} \quad (4.39)$$

Once the total raw mass and net mass per batch have been calculated, the Yield can be estimated by the following:

$$Yield = \frac{m_{net_{batch}}}{m_{raw_{batch}}} \quad (4.40)$$

As a reference to verify the accuracy of the Yield estimated by the method presented above, aluminum extrusion plants usually operate with a scrap percentage ranging from 17 to 27% in relation to the billets used [26]. A series of Yield calculations performed for different geometries and batch sizes using the equations presented in this section have predicted Yields in the order of 73 to 80%, which correspond to scrap percentages of 20 to 27%. Thus, the model predicts Yield values that are in good agreement with the typical range observed in industry.

Finally, the Material Cost per part can be calculated by:

$$M_{cost} = \frac{m_{part}}{Yield} M_{price} \quad (4.41)$$

where $M_{price}$ is the price per unit mass (in USD/kg or USD/lb) of the raw material. This price is constantly fluctuating, so a current price at the time of cost estimation must always be consulted.

Unless secured by a Forward Metal Buy Purchase Agreement, extruders in the US usually quote raw material price based on the previous month's average "US Midwest Price" in effect at the time of shipment. Such price can be consulted in metal pricing publications by *American Metal Market (AMM)* [49], or *Platts* [50]. The former reports the so-called "AMM Free Market Price" for Aluminum on a daily basis, but monthly averages are available as well. Likewise, Platts reports a "MW US Transaction Price" for Aluminum on a weekly basis, where daily and weekly average prices can be consulted. Both "AMM Free Market Price" and Platts' "MW US Transaction Price" represent the "US Midwest Price" mentioned above, as both of them are obtained using a similar methodology: they start with a baseline price for High Grade

(HG) Aluminum (99.7% purity) from the *London Metal Exchange* (LME) [51], and then add a "Midwest Premium" which is an estimated US free-market charge for prompt delivery to a typical-freight consumer in the US Midwest (arrival within 30 days) [52]. The Midwest Premium is determined based on physical business reported by a daily survey of major buyers and sellers, using a representative survey sample of producers, traders and different types of end users (sheet mills, extruders, automotive companies, etc.) [52]. Hence, the "US Midwest Price" of HG Aluminum is estimated by the following:

$$US\ Midwest\ Price = LME\ HG\ Price + Midwest\ Premium \quad (4.42)$$

Additionally, a "Billet Upcharge" is added to the base metal price by the aluminum ingot supplier. An estimate of this upcharge can also be consulted in metal pricing publications by AMM [49], or Platts [50]. The former reports this upcharge in the so-called "6063 Extrusion Billet Upcharge", while the latter reports it in the so-called "US Spot 6063 Billet Upcharge". The Billet Upcharge is applied over the US Midwest Price for primary, North American General Purpose 6063 Billet, to Aluminum Association specifications [52]. This type of upcharge is not reported in AMM or Platts for any other aluminum alloy than Al-6063, suggesting that there is either not enough data to do so, or the upcharge for billets made of other aluminum alloys is similar to the one for Al-6063. Hence, in the absence of more specific data for other aluminum alloys, it may be assumed that they have a similar Billet Upcharge than Al-6063. Having said that, the price of the raw material (i.e. billet) for extruders in the US can be estimated as:

$$M_{price} = US\ Midwest\ Price + Billet\ Upcharge \quad (4.43a)$$

Or in an expanded way, substituting Equation 4.42 in 4.43a:

$$M_{price} = LME\ HG\ Price + Midwest\ Premium + Billet\ Upcharge \quad (4.43b)$$

where the LME HG Price can be obtained from LME [51], and both the Midwest Premium and the Billet Upcharge can be consulted in AMM [49] or Platts [50]. As a reference, the monthly average official LME HG Aluminum Price in September 2009 was \$1.834/kg (\$0.832/lb) [51], while the monthly average Midwest Premium in the same month was \$0.119/kg (\$0.054/lb)

[49], and the monthly average 6063 Billet Upcharge in the same period was $0.209/kg ($0.095/lb) [49], making the raw material price ($M_{price}$) equal to $2.162/kg ($0.981/lb), with all prices being in US dollars.

## 4.5 Other Direct Costs

### *4.5.1 Setup Cost*

As it was explained before in Section 2.2.2, the Setup Cost is associated to the Setup Time spent in recurring "nonproductive" tasks that are necessary for the suitable operation of the extrusion line, like switching tooling, calibrating equipment, running production trials, etc. The time spent changing dies between batch runs (to produce a different part) is a natural setup time source in extrusion plants. The die change time depends on the design of the press; for presses with a "Single Die Slide", the die change time is about 4 minutes [26], while for presses with a "Double Die Slide", the effective die change time is only about 1 minute [26], since much of the actual die change time occurs within the dead cycle, and the only lost time is that taken to lead out the front end of the extrusion [53]. A survey of commercial extrusion presses available in the market has revealed that the majority of them have a double die slide; hence, in the absence of data, it may be assumed that the die change time is 1 minute per batch. Even though the die change time is relatively short, it occurs with a relatively high frequency, as a typical production schedule in an aluminum extrusion plant includes about 10 die changes per 8 hr shift (i.e. 10 production batches per shift) [26].

Another common setup time source in manufacturing processes involves production trials. In extrusion, it is usually necessary to try one or two billets with each new die [26]. Therefore, extrusion die trials is in fact a non-recurrent cost, as it is incurred only once in the production life of the part. Furthermore, there are dies that do not need trials [26], so the benchmark productivity practice in the extrusion industry today is to request a complete elimination of die trials to the die supplier and die corrector [54]. Thus, the time spent in die trials will not be considered in this thesis.

The setup cost per part is calculated by multiplying the setup time per part by the labor and overhead rates, and then adding the two products, as follows:

$$S_{cost} = t_{setup_{part}} \left( n_{operators} \, L_{rate} + OH_{rate} \right) \quad (4.44)$$

where $t_{setup\_part}$ is the setup time per part, calculated as:

$$t_{setup_{part}} = \frac{t_{setup_{batch}}}{N_{parts_{batch}}} \quad (4.45)$$

where $t_{setup\_batch}$ is the setup time per batch, which may be assumed to be ~1 minute, as discussed above.

### *4.5.2 Waste Time Cost*

So far, the cost model has considered an ideal plant where everything runs smoothly and no interruptions occur, resulting in maximum productivity of the extrusion line. In reality, the equipment, the crew and the synchronization of the entire plant are not 100% efficient, therefore an additional amount of time is necessary to achieve the production volume intended. Such time will be referred here as "Waste Time", and it includes the time spent in various unproductive tasks like the following [26], [53]: Downtime, "full table" (i.e. downstream equipment unable to keep up with press output), waiting for billet (i.e. upstream equipment unable to keep up with press output), polishing die, operating the press manually instead of automatically, extrusion falling off the runout table, time lost at beginning and end of shift, etc.

Since a thorough study of waste time would not be feasible (falling more into an Activity Based Costing approach), a more practical, yet reasonably accurate estimation of waste time can be carried out by "calibrating" the cost model with benchmark productivity data available in the literature. Fielding, et al [53] have stated that from 1969 to 2000, the benchmark productivity on a typical 8-inch (203 mm) billet diameter press extruding Al 6xxx has increased from 2400 lb/hr (1089 kg/hr) to 6000 lb/hr (2721 kg/hr). Using this data as a benchmark, the

cost model can be calibrated by including the waste time in the productivity[9] calculation, as follows:

$$Productivity = \frac{m_{net_{batch}}}{t_{cycle_{batch}} + t_{setup_{batch}} + t_{waste_{batch}}} \quad (4.46)$$

where $m_{net\_batch}$ is the net mass of good parts produced per batch, calculated using equation 4.39; $t_{cycle\_batch}$ is the cycle time per batch, $t_{setup\_batch}$ is the setup time per batch, and $t_{waste\_batch}$ is the waste time per batch. In order to estimate $t_{waste\_batch}$, it may be assumed that a benchmark plant would be capable of extruding a typical batch size of an "average shape" from an 8-inch billet of Al-6063 with a productivity of 6000 lb/hr (2721 kg/hr). By "average shape", it is meant a section with average values on all the extrusion parameters that vary within a typical range (e.g. for Al-6063: $R$≈55, $v_f$≈57 m/min). Also, as it was mentioned before, a typical batch size in extrusion plants is one that is produced in 0.8 hrs (10 batches in an 8-hr shift). Using these assumptions, a numerical calculation of the necessary waste time per batch to achieve a productivity of 6000 lb/hr (2721 kg/hr) was performed, using equation 4.46 along with the Extrusion Speed and Cycle Time Models presented in Sections 4.1.2 and 4.2. The details of the calculations are included in APPENDIX C: WASTE TIME ESTIMATION; the results indicate that a waste time per batch of 6.8 minutes (≈7 minutes) gives the benchmark productivity of 6000 lb/hr (2721 kg/hr). Thus, for any other section of any other size and alloy, the waste time per batch may be assumed to be 7 minutes, and the corresponding productivity can be estimated by equation 4.46.

It is important to remark that the productivity tends to increase as the size of the press increases [26], [53], because the greater weight per unit length extruded in larger presses offsets the longer dead cycle time in them. The alloy and the geometry of the cross section also play an important role in productivity, as the extrusion speed is dependent on both of them. Moreover, the batch size and the scrap losses also have an impact on productivity, as they

[9] Productivity is defined as the quantity of good extrusion produced per unit of time, expressed in kg/hr (or lb/hr) [22].

affect the cycle time and the net mass per batch. Therefore, the benchmark productivity used to calibrate the cost model (6000 lb/hr, or 2721 kg/hr) is not expected to hold for different cross sections and alloys, or for different batch sizes.

Finally, the waste time is translated to an additional direct cost, called "Waste Time Cost" in this thesis. The waste time cost per part can be calculated by:

$$W_{cost} = t_{wast\,e_{part}} \left(n_{operators}\, L_{rate} + OH_{rate}\right) \quad (4.47)$$

where $t_{waste\_part}$ is the setup time per part, calculated as:

$$t_{wast\,e_{part}} = \frac{t_{wast\,e_{batc\,h}}}{N_{part\,s_{batc\,h}}} \quad (4.48)$$

where $t_{waste\_batch}$ is the waste time per batch, which may be assumed to be ~7 minutes, as discussed above.

## 4.6 Piece Part Cost

Once all the recurrent costs described in the previous sections have been estimated, the piece part cost can be readily calculated as:

$$Piece\ Part\ Cost = M_{cost} + L_{cost} + OH_{cost} + S_{cost} + W_{cost} \quad (4.49)$$

which is simply the sum of Material, Labor, Overhead, Setup and Waste Time Costs per part. It is common practice in the extrusion industry to also estimate the piece part cost in a per unit mass or per unit length basis. To do so, the piece part cost is simply divided by the mass of the part (to give a $/kg, or $/lb cost) or by the length of the part (to give a $/m, or $/ft cost), respectively. The piece part cost per unit mass is particularly useful in comparing the relative costs of different designs having different weights, as it is a normalized piece part cost.

# CHAPTER 5: EXTRUSION NON-RECURRING COSTS ESTIMATION

## 5.1 Extrusion Tooling Background

In the Aluminum Extrusion Industry, the only non-recurring cost that is usually considered when a design is quoted is the Tooling Cost [25]. Before getting into details on cost estimation procedures, it is imperative to introduce important background information on hot extrusion tooling. The information presented in the following subsections constitutes the basis for the Tooling Cost Model presented later in this chapter.

### *5.1.1 Classification of Shapes*

The aluminum extrusion technology provides a wide range of shapes that can be successfully manufactured. In an effort to classify the large variety of shapes into groups according to complexity, the Aluminum Extrusion Industry has widely adopted a standard division of shapes into three broad groups [24], [25], [6]: Solid Shapes, Hollow Shapes, and Semihollow Shapes, the latter being an intermediate group between the first two types, as depicted in Figure 5.1.

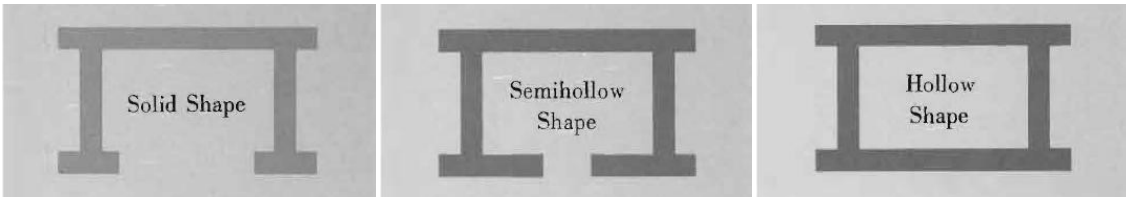


**Figure 5.1** Shape Groups [24]

In addition, the Hollow and Semihollow shapes are further divided into different classes, according to the criteria listed in Table 5.1, defined by the Aluminum Association Standards and Data [55] and also published in [6] and [8]. The sketches in Figure 5.2 provide an illustration of the differences between each class of Hollow and Semihollow shapes.

**Table 5.1** Hollow and Semihollow Class Criteria [55], [6].

| Class | Description |
|---|---|
| **Hollow profiles** | |
| Class 1 | A hollow extruded shape whose void is round and 1 inch (25.4 mm) or more in diameter, and whose weight is equally distributed on opposite sides of two or more equally spaced axes. |
| Class 2 | Any hollow extruded shape other than Class 1, which does not exceed a 5-inch (127 mm) diameter circumscribing circle and has a single void of not less than 0.375-inch (9.53 mm) diameter or 0.110 $in^2$ (71 $mm^2$) area. |
| Class 3 | Any hollow extruded shape other than Class 1 or Class 2 (Class 3 Hollow would include multi-void hollow profiles). |
| **Semihollow profiles** | |
| Class 1 | A semihollow extruded shape of two or less partially enclosed voids in which the area of the voids and the surrounding metal thickness is symmetrical about the centerline of the gap. |
| Class 2 | Any semihollow profile other than Class 1 Semihollow. Class 2 Semihollow would include nonsymmetrical void surrounded by symmetrical wall thickness, or symmetrical void surrounded by nonsymmetrical wall thickness. |

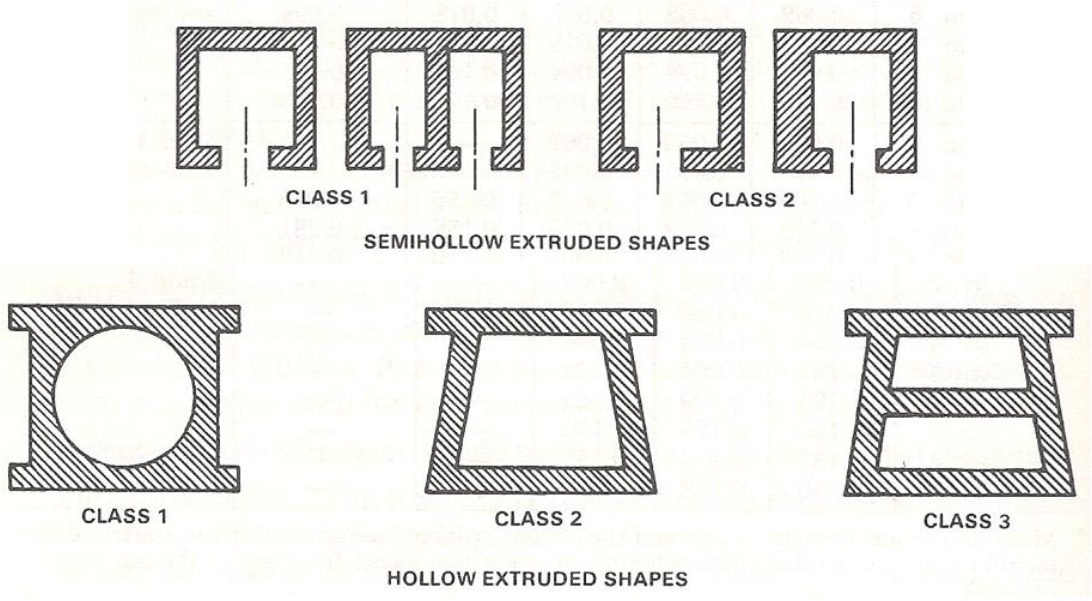


**Figure 5.2** Examples of Hollow and Semihollow Shapes of different Class [8].

In order to differentiate between a Solid and a Semihollow Profile, the ratio of the area of the partially enclosed void to the square of the gap width must be calculated [25]. Such ratio is called the "Tongue Ratio" and if it exceeds the values tabulated in Table 5.2, the shape is then classified as a Semihollow; otherwise the shape is considered a Solid.

**Table 5.2** Tongue Ratio Criteria to differentiate between Semihollows and Solid Shapes [6], [25].

| Gap Width, in. | Tongue Ratio[(a)] | | | |
|---|---|---|---|---|
| | Class 1[(b)] | | Class 2[(b)] | |
| | Alloy Group A | Alloy Group B | Alloy Group A | Alloy Group B |
| 0.040–0.062 | 2.0 | 1.5 | 2.0 | 1.0 |
| 0.063–0.124 | 3.0 | 2.0 | 2.5 | 1.5 |
| 0.125–0.249 | 3.5 | 2.5 | 3.0 | 2.0 |
| 0.250–0.499 | 4.0 | 3.0 | 3.5 | 2.5 |
| 0.500–0.999 | 4.0 | 3.5 | 3.5 | 2.5 |
| 1.000–1.999 | 3.5 | 3.0 | 3.0 | 2.0 |
| ≥2.000 | 3.0 | 2.5 | 3.0 | 2.0 |

(a) Tongue Ratio=Void Area/(Gap Width)$^2$. To calculate the Tongue Ratio, use the void-gap combination that yields the largest calculated ratio, whether the innermost void and gap of the profile or the entire void and gap features.
(b) Alloy Group A: 6061, 6063, 5454, 3003, 1100, 1060; Alloy Group B: 7079, 7178, 7075, 7001, 6066, 5066, 5456, 5086, 5083, 2024, 2014, 2011.

The shape classifications introduced above are often used to assess the production and tooling costs of extrusions [6], [24], [25], [8]. The six shape categories can be sorted in increasing order of production and tooling costs as follows [8]:

- Solid
- Semihollow Class 1
- Semihollow Class 2
- Hollow Class 1
- Hollow Class 2
- Hollow Class 3

Thus, with all other geometric and non-geometric cost drivers being the same, the manufacturing costs (recurring and non-recurring) are lowest for the Solid shapes and highest for the Hollow Class 3 profiles [8].

### *5.1.2 Extrusion Die Types*

The extrusion dies used in the industry can be classified into three basic categories in accordance with the type of shape they produce: Solid Dies, Semihollow Dies and Hollow Dies

[25]. Additionally, within each of these categories, there are different die configurations. The Solid Dies are the simplest ones in that they are machined from one piece of steel [6], as opposed to Hollow and Semihollow Dies, which are two-piece dies, as it will be shown later in this section.

Solid Dies can be of the "Flat-face" or "Shaped" type design, as shown in Figure 5.3. Flat-face Dies (also called shear dies or square dies) are characterized by a bearing surface that is perpendicular to the face of the die, as depicted in Figure 5.3, and they are generally used for the most common aluminum extrusion alloys (i.e. soft alloys) [6]. Shaped Dies (also called converging or streamlined dies) often have a conical entry opening with a circular cross section that changes progressively to the final extruded shape required. This attribute is shown in Figure 5.3 as a choke. Shaped Dies are more difficult and costly to design and manufacture than Flat-face Dies, and they are generally used for the hot extrusion of high-strength aluminum alloys (such as 2xxx and 7xxx alloys), as well as steels, titanium alloys, and other metals [6].

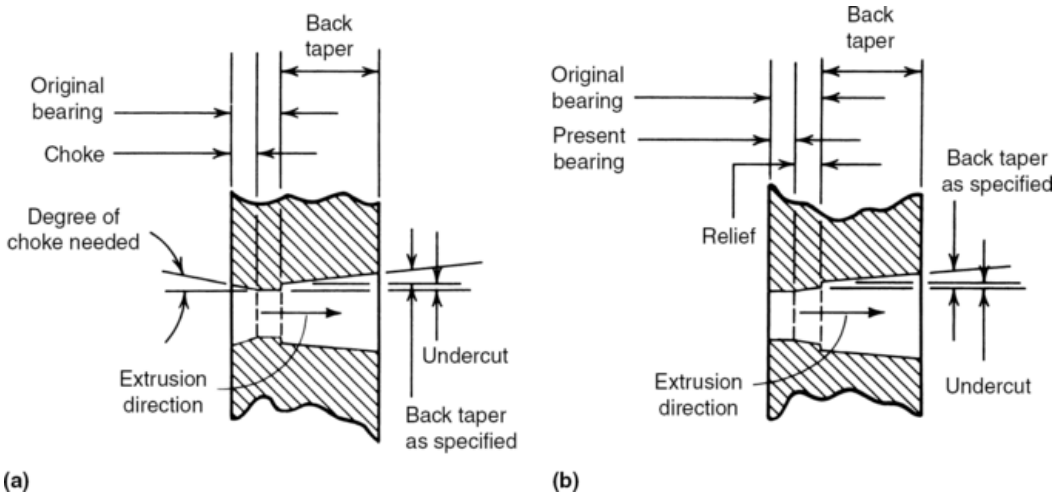


**Figure 5.3** Cross-sections showing the types of Solid Dies: a) Shaped Dies, b) Flat-face Dies [6].

Moreover, in order to have a billet-on-billet extrusion process (as previously defined in Section 3.3), Solid Dies are usually accompanied by a welding or feeder plate attached to the front of the die, as shown in Figure 5.4 and Figure 5.5. Another alternative is to use a recessed

die, which contains a pocket slightly larger than the profile itself, as illustrated in Figure 5.4 and Figure 5.6. The pocket helps to control the metal flow and serves as the welding chamber for the billet-on-billet extrusion [25].

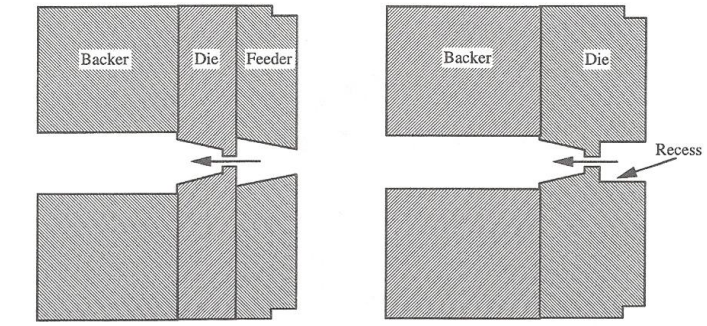


**Figure 5.4** Configurations used for billet-on-billet extrusion on Solid Dies [22].

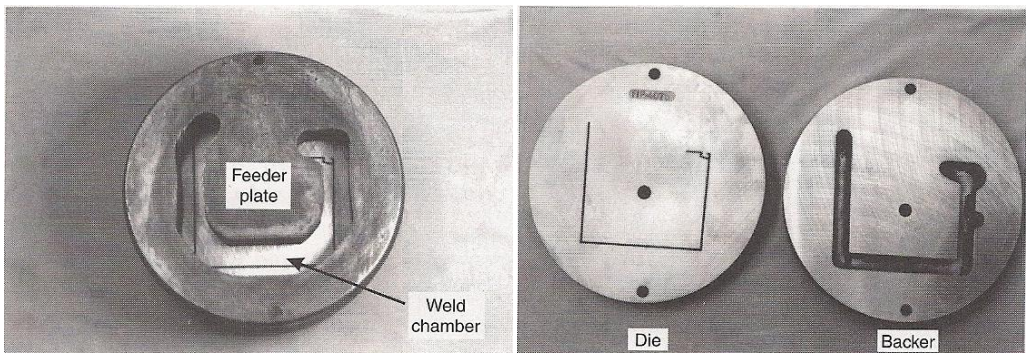


**Figure 5.5** Example of Solid Die with Feeder Plate [22].

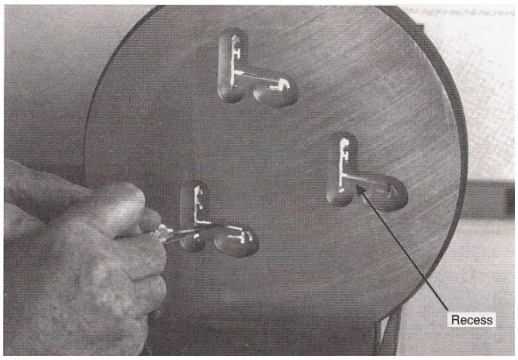


**Figure 5.6** Example of a Recessed Solid Die [22].

Hollow Dies are much more complex than Solid Dies, as they need a mandrel to form the inner features of the voids and a die cap (or die insert) to form the outer features of the profile. Thus, hollow dies are made of two pieces. The three basic types of hollow dies are shown in Figure 5.7, and they are: Bridge Die, Spider Die and Porthole Die [26]. All of them operate under the same principle: the hot metal is forced to flow around the bridge/spider (or through the ports in a porthole die), dividing into strands; then, a solid-state weld is formed where the aluminum flows back together at the downstream side of the bridge/spider/port. This location is referred to as the "welding chamber" of the die. If properly done, the solid-state weld is undetectable in either appearance or performance [6]. Once the solid-state weld is formed, the metal flows from the weld chamber to the gap between the mandrel and the die cap to form the desired hollow shape. It is important to remark that hollow sections in a variety of shapes and sizes are reserved for Aluminum Alloys, apart from the simple hollow sections that can be produced in the heavy metals or steel with a classical mandrel [26].

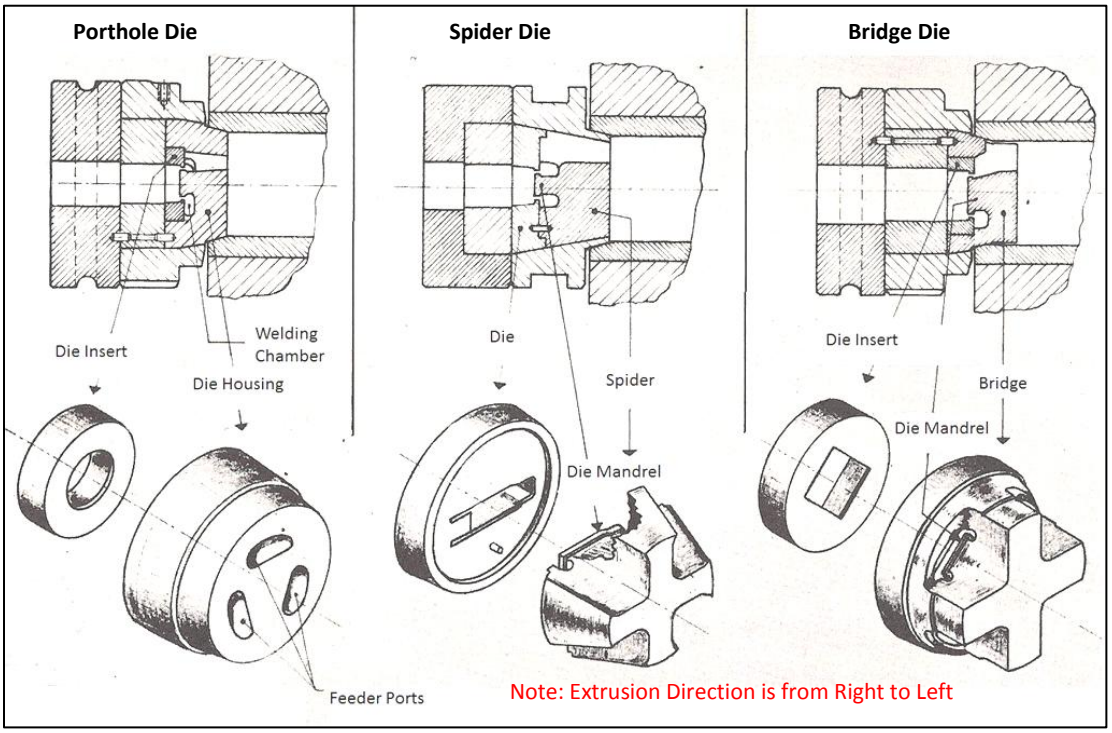


**Figure 5.7** The three basic types of Hollow Dies [26].

Of the three types of hollow dies, Porthole Dies are recognized as the best and the most suitable for modern requirements [26]; hence, they are the most commonly used in the industry [25]. Figure 5.8 shows two examples of Porthole Dies designed to extrude complex hollow profiles. Furthermore, Porthole Dies are suitable for multi-hole die construction, as shown in Figure 5.9, and they are the only ones capable of extruding very difficult sections with large variations in thickness or many openings [26]. Thus, Bridge Dies and Spider Dies are rarely used today because of their limitations [42] and higher machining costs [26].

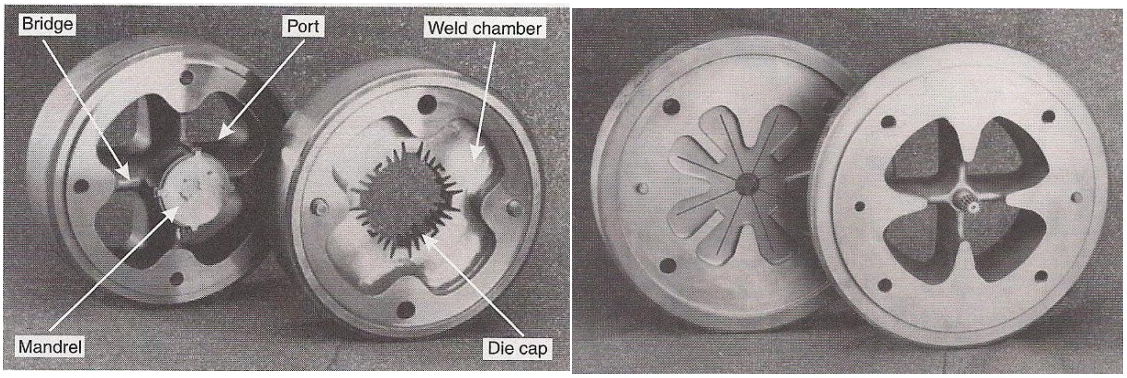


**Figure 5.8** Examples of Porthole Dies [22]

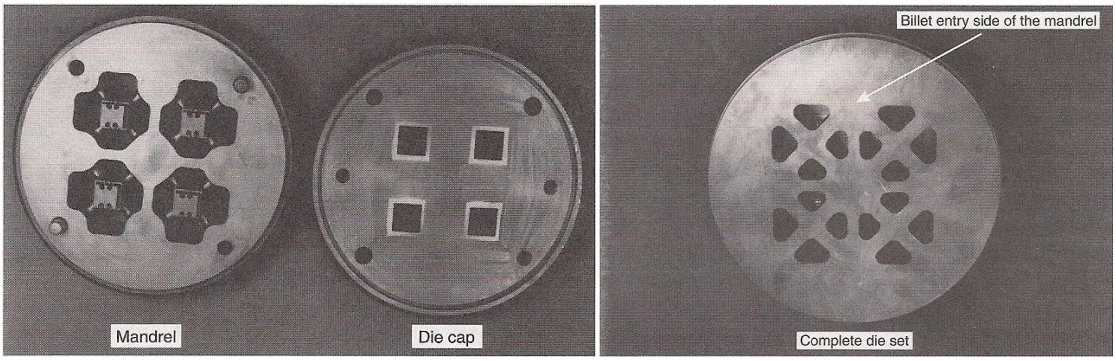


**Figure 5.9** Example of Multi-hole Porthole Die [22]

Finally, Semihollow Dies can be designed as Flat-face, Recessed-pocket, Weld-plate or Porthole Dies, depending on the Tongue Ratio [25]. However, in most of the cases, Semihollow Dies are designed in a Porthole configuration [6], [26], [25]; therefore, the term “Hollow Die” is

commonly used in the literature to refer to both Semihollow and Hollow Dies. The same thing will be done in this thesis.

### *5.1.3 Tooling Set*

In a typical extrusion operation, the die will be placed in the press along with several supporting tools, as shown in Figure 5.10. Both Solid and Hollow Dies are accompanied by the same tool stack, except for the backer, which may or may not be used in the case of Hollow Dies [25]. Technically, the main tooling for hot extrusion includes all the components shown in Figure 5.10, that is the container, liners, stem, dummy block, die, die holder, backer, bolster and the die carrier (or die slide) [6], as well as other elements not shown in Figure 5.10, like the pressure ring and feeder plate [26]. The functions of each of the individual tools are described in Table 5.3.

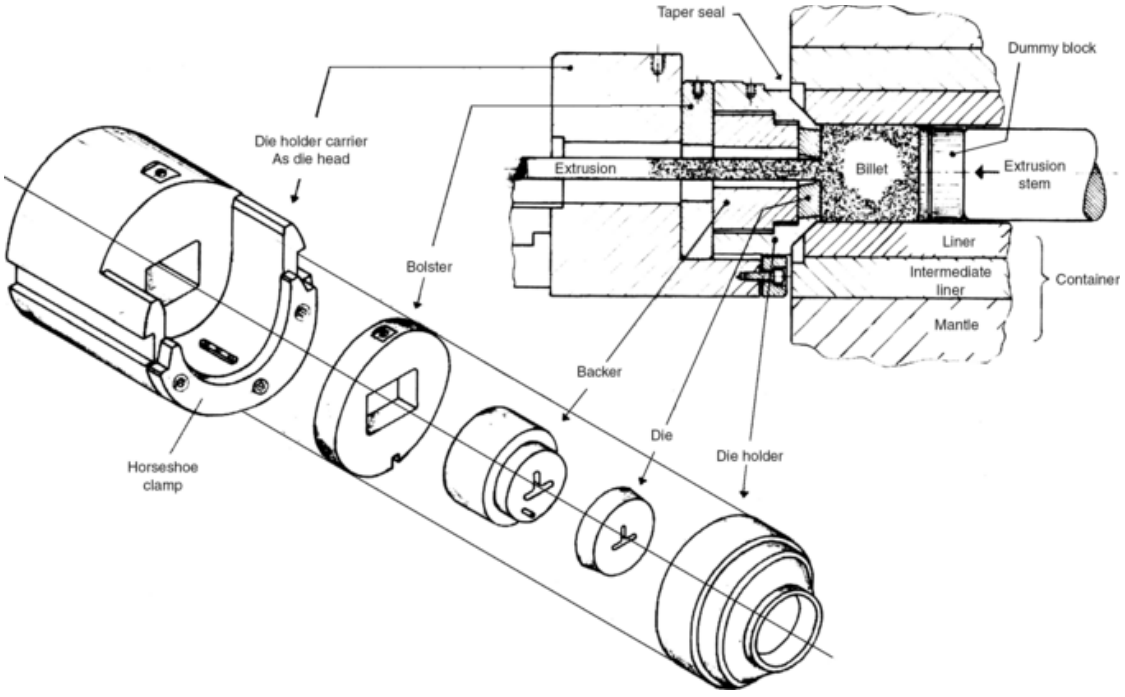


**Figure 5.10** Schematic of Hot Extrusion Tooling Arrangement [26]

**Table 5.3** Functions of the Individual Tools used in Hot Extrusion [22], [26].

| Tool | Function |
|---|---|
| Die | Makes the shape of the extrusion. |
| Die Holder/Ring | Holds the die with feeder plate and backer. |
| Backer | Supports the die to prevent die collapse or fracture. |
| Bolster | Transmits the extrusion load from the die to the pressure ring. |
| Pressure Ring | Transmits the extrusion load from the bolster to the press platen, prevents bolster deflection and extends the length of the die set to the dimensions of the die carrier. |
| Die Carrier/Slide | Holds the complete die set (die holder and bolster) in the press. |
| Feeder Plate | Sits in front of the die to balance the metal flow and also to make a continuous extrusion. |
| Liner | Protects the life of an expensive and huge container from thermal and mechanical stresses. |
| Stem | Transmits the extrusion load through the dummy block to the billet. |
| Dummy Block | Protects the life of the expensive stem and is fixed or floating in front of the stem. |

Containers are the most expensive of all extrusion tooling because of the large volume of hot working alloy steel needed [26]. However, they are not actually considered part of the tooling in practice, as they are part of the press and are not custom for a specific shape [26], [25]. The same applies for other tools like the stem, dummy block, liners and the die carrier [26]. Hence, for the sake of FBC, the Tooling Set includes only the following components: die, die holder, feeder plate, backer, bolster and pressure ring.

Finally, if the shape to be extruded is relatively simple (i.e. it has standard dimensional tolerances, acceptable wall thicknesses and low die tongue ratios that do not require much support), then the use of standard support tooling (i.e. backers and bolsters without custom apertures) is acceptable [25]. If that is not the case, then a custom backer with an aperture almost identical to that of the die is necessary [42]. Moreover, if the section is very critical and additional support of the backer is needed, then the usual practice is not to make a custom full size bolster, but to use an “Insert Bolster” designed to match closely the aperture in the die backer and held in place by an insert bolster holder [42].

### *5.1.4 Tooling Sizing*

This section presents a set of design rules published in [26] and used in the industry as a guideline to size the extrusion tooling set. They are reported here with the purpose of providing insight into the drivers of the material costs of the tooling itself (i.e. the amount of steel required for the tooling).

The recommended Die Diameter depends on the CCD, the complexity of the shape and the alloy [26]. According to practical experience, the following guidelines are used:

$$D_{die} = (1.25\ to\ 1.45)CCD \quad for\ Simple\ Shapes \qquad (5.1a)$$

$$D_{die} = (1.45\ to\ 1.6)CCD \quad for\ Complicated\ Shapes^{*} \qquad (5.1b)$$

*including those with thin walls or those made with alloys difficult to extrude.

The recommended Die Thickness, as used by press manufacturers [26] is:

$$THK_{die} = (0.12\ to\ 0.22)D_{1000} \qquad (5.2)$$

where $D_{1000}$ is a reference parameter used for many calculations and is defined as "the inside diameter of the container for a specific pressure of 1000 MPa" [26]. Based on this definition, and after some algebraic simplification, the parameter $D_{1000}$ can be expressed mathematically as:

$$D_{1000} = D_o\sqrt{\frac{p}{1000\ MPa}} \qquad (5.3)$$

where $D_o$ is the Billet Diameter (or Container Inner Diameter) and $p$ is the actual specific pressure acting on the billet, as defined previously in Section 4.1.1 and rewritten here by the combination of equations 4.1-4.9 as:

$$p = 1.67\left[0.95 + 0.05\left(\frac{P_{ext}}{2\sqrt{\pi A_f}}\right)^{1.5}\right]\left[C\left(\frac{6v_o \ln R}{D_o}\right)^{m}\left(\ln(R) + \frac{2L_o}{D_o}\right)\right] \qquad (5.4)$$

The recommended External Diameter of the die set (i.e. the Outer Diameter of the Bolster and the Die Holder) is given by:

$$D_{die\ set} = 2.65 D_{1000} \quad (5.5)$$

The recommended total depth of the tool set (i.e. the sum of the thicknesses of all components in the tool stack) is:

$$L_{die\ set} = 2.8 D_{1000} \quad (5.6)$$

As a final reference, the backer is usually of the same outer diameter than the die, but two or three times thicker [25]. Likewise, the bolster disk is normally the same diameter as the die holder and thicker than the backer [25].

### *5.1.5 Materials and Heat Treatment for Tooling*

Extrusion dies are typically made of the well-established AISI H13 Tool Steel, heat treated to the desired condition [25], [22]. Some die manufacturers use AISI H11 and H12 Tool Steels as an alternative to H13 [6], [26]. All these materials are Hot-Work Steels (H series) alloyed with a Chromium Base. They are designed for use at elevated temperatures, and have a high toughness and high resistance to wear and cracking [1]. The support tooling (backers, bolsters and die holders) is also generally made from H11, H12 or H13 Tool Steel [6].

The heat treatment applied to extrusion tooling starts with a Thermal Stress Relief performed after the initial rough machining, usually at 550-650 °C for several hours, with furnace cooling at controlled rate [26]. After the machining is completed, the tooling is subjected to a Hardening Treatment (Heating and Quenching) followed by Tempering [26]. Finally, once all the finishing operations have been completed, a Nitrogen Diffusion Hardening Treatment (a.k.a. Nitriding) is typically carried out in the temperature range of 400-550 °C, as a surface treatment for the bearing surface of the die [26], [25]. This treatment greatly increases the surface hardness and the resistance to wear of the bearing; consequently, it prolongs the service life of the dies by three to six times that of un-nitrided ones [26], as well as improving

the surface quality of the product. Furthermore, if properly monitored, Nitriding can be repeated several times before a new die needs to be made [25].

### *5.1.6 Die Manufacturing Process*

The die making process has been improved significantly over the last couple of decades as die manufacturers have made full use of the latest technologies in CAD/CAM and Numerical Computer Simulations (i.e. FEA) [6]. Multi-axis Computer Numerical Control (CNC) Machining Centers and CNC Electrical Discharge Machining (EDM) have practically eliminated the time-consuming manual work and have greatly improved precision and decreased lead times [6]. The typical die manufacturing process map is depicted in Figure 5.11. It is important to note that Wire EDM (a process similar to cutting with a band saw) is performed after the heat treatment and grinding steps, as a final machining to refine the profile cut on the die.

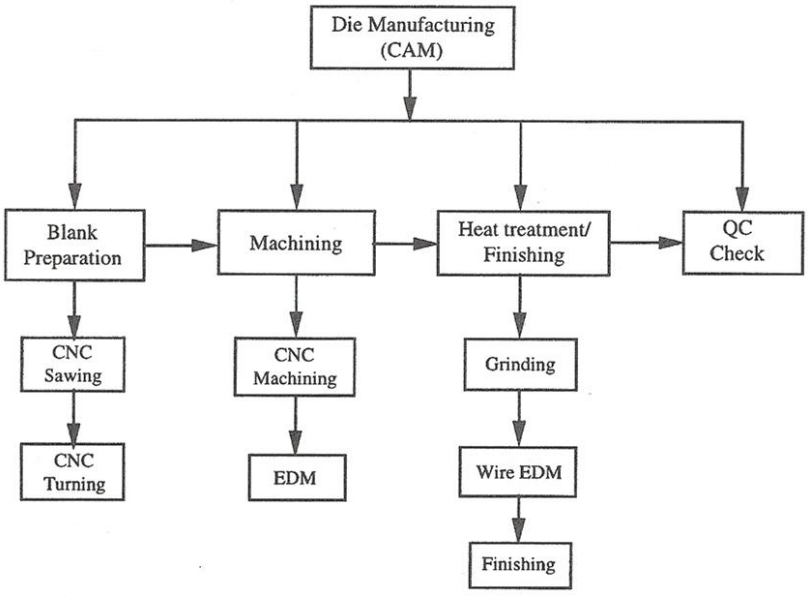


**Figure 5.11** Typical Die Manufacturing Process Map [22].

Additionally, within the traditional die manufacturing method, there are two choices for doing the rough machining part of the process: one option is to do it all by CNC milling, and the

other is to combine CNC milling with EDM [22]. Moreover, a state-of-the-art manufacturing method has significantly reduced the number of steps in the process, by starting with hardened blanks (i.e. heat treated) instead of soft blanks, and replacing CNC milling with Wire EDM, as shown in Figure 5.12 [22].

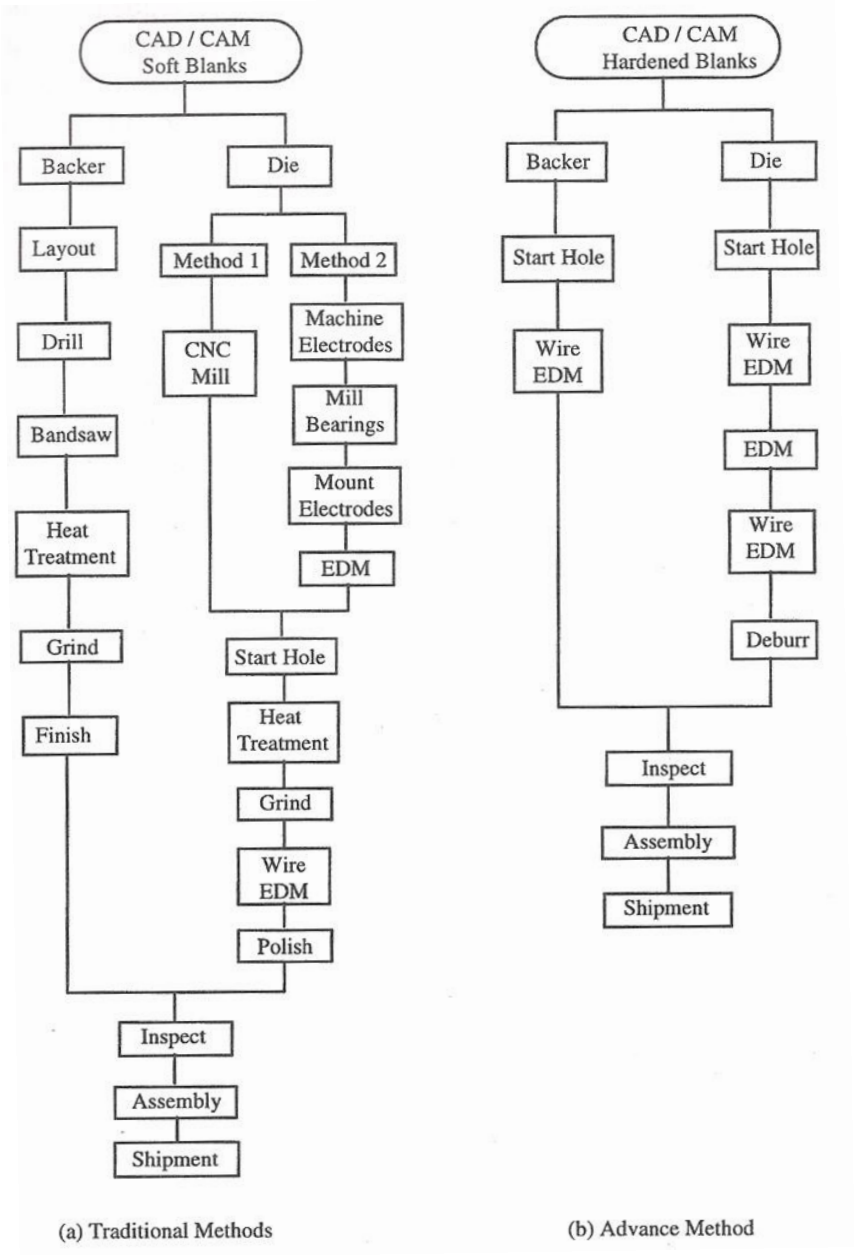


**Figure 5.12** Traditional vs. Advanced Methods for Manufacturing Dies and Backer [22].

## 5.2 Tooling Cost Estimation Approach

In defining a suitable model for predicting the Tooling Cost, the ideal method would be to consider detailed estimates of the typical elements that form the manufacturing cost of the tooling itself, that is, the material, labor, overhead, fixtures and jigs, programming, and all other costs incurred by the tooling manufacturer. Indeed, many modern shops calculate the tooling cost in that way [21]. Nevertheless, creating a Tooling Cost Model with such approach would be time-consuming and complicated, and is out of the scope of this thesis, as it would be like doing a new FBC Model of a CNC milled and electro-discharge machined part.

An alternative simpler approach is to create an empirical model, by requesting quotes to extruders for a series of shapes, judiciously designed to cover a wide enough design space, and then fit an equation (a.k.a. "Transfer Function") that predicts the Tooling Cost (a.k.a. the "Y" or dependent variable) as a function of the main geometric and non-geometric tooling cost drivers (a.k.a. the "Vital Xs" or independent variables). This approach can be carried out either by Design of Experiments (DOE) or by Multivariate Regression Analysis. The former represents a more structured method to obtain a robust transfer function that is valid within a certain design space; however, it has the disadvantage of requiring a large number of "experiments" (i.e. quotes) to obtain the transfer function, which by the way is limited to a polynomial of first or second order only. Conversely, a Multivariate Regression Analysis is less methodical than a DOE, so it is more prone to yield a transfer function that is not accurate enough throughout the entire design space; however, it usually requires less experimental data points (i.e. quotes) to do the curve fitting and it offers an unlimited variety of regression model types, giving the analyst high flexibility in choosing the form of the transfer function.

Given the relative difficulty in obtaining quotes from extruders, the Multivariate Regression Analysis Approach will be adopted in this thesis, using the software "*Data Fit*", developed by *Oakdale Engineering* [56]. Furthermore, in order to obtain a robust transfer function, a structured methodology to distribute the experiments throughout an appropriate design space will be followed, resembling the DOE technique. The aim is then to obtain the "best of both worlds".

## 5.3 Vital Xs Screening and Selection

### *5.3.1 Potential Vital Xs*

The first step in the creation of the empirical model for Tooling Cost is to identify the independent variables -the Vital Xs- that drive the Y. In order to do so, a list of "Potential Vital Xs" with the corresponding rationale is presented below, based on the insight gained from the literature review covered in Section 5.1:

1) ***CCD***: The larger the CCD, the larger the die diameter (per equation 5.1). Also, a larger CCD implies a larger billet diameter ($D_o$), which raises the value of the $D_{1000}$ parameter (per equation 5.3). This increases the required thickness of the die (per equation 5.2), as well as the diameter and length of the tooling set (per equations 5.5 and 5.6). All these effects represent a higher Material Cost of the Tooling, and longer machining times (i.e. higher Labor and Overhead Costs) due to the larger volume of steel to be removed from a thick tooling set.
2) ***Alloy***: Difficult to extrude alloys (i.e. Hard Alloys) require a larger die diameter than soft alloys, as indicated by equations 5.1a and 5.1b. Moreover, hard alloys generally imply higher specific pressures (due to their higher flow stress), which raises the value of the $D_{1000}$ parameter (per equation 5.3). This increases the required thickness of the die (per equation 5.2), as well as the diameter and length of the tooling set (per equations 5.5 and 5.6). Furthermore, hard alloys typically require Shaped Dies, which are more expensive than Flat-face Dies used for soft alloys. All these effects represent a higher Material Cost of the Tooling, and longer machining times (i.e. higher Labor and Overhead Costs).
3) ***External Perimeter ($P_{ext}$):*** The larger the external perimeter of the shape, the higher the specific pressure (per equation 5.4), which raises the value of the $D_{1000}$ parameter (per equation 5.3). This increases the required thickness of the die (per equation 5.2), as well as the diameter and length of the tooling set (per equations 5.5 and 5.6). These effects represent a higher Material Cost of the Tooling. Moreover, a larger perimeter

may have an impact on the machining time (i.e. Labor and Overhead Costs), as traverse time may be affected.

4) ***Cross-Sectional Area ($A_f$)***: The larger $A_f$ is, the lower the extrusion ratio $R$ and the shape complexity index $K_{shape}$ will be. This would decrease the specific pressure (per equation 5.4) and the $D_{1000}$ parameter (per equation 5.3). Ultimately, this would reduce the required thickness of the die (per equation 5.2), as well as the diameter and length of the tooling set (per equations 5.5 and 5.6). These effects would represent a lower Material Cost of the Tooling. As far as machining time, the net effect of $A_f$ is not obvious, as on the one hand, a larger cross sectional area increases the volume of material to be removed, but on the other hand, the thinner tooling decreases the volume of steel to be machined.
5) ***Shape Type:*** As it was discussed in Section 5.1.1, the shape type (e.g. Solid, Semihollow Class 1, Semihollow Class 2, etc.) has a direct impact on the tooling cost. The more complex the shape type (Hollow Class 3 being the most complex, Solid being the simplest) the more expensive the tooling.
6) ***Thickness Variation (ΔTHK):*** The larger the thickness variation in the section, the more difficult it is to balance the metal flow [26], [22], so the more time it is required for die correction of the bearing lengths. This increases the Labor and Overhead Costs of die making.
7) ***Minimum Thickness ($THK_{min}$):*** The thinner the walls of the shape, the more difficult it is to do the die correction [26], [22], increasing the Labor and Overhead Costs of die making. Also, sections with thin walls require a larger diameter of the die (per equations 5.1a and 5.1b), which then increases the Material Cost of the Die.
8) ***Number of Voids ($N_{voids}$):*** The more voids a Hollow Section Class 3 has, the larger the number of mandrels required in the Porthole Die, and the more complicated the machining will be. This adversely affects the machining time (Labor and Overhead Costs) as well as the Programming Time for CNC machining.
9) ***Tongue Depth ($a_t$):*** The larger the Tongue Depth "$a_t$" (as depicted in the sketch in Figure 5.13), the higher the bending and shear stresses on the narrowest part of the die

tongue [26], as a larger "$a_t$" would increase both the force and lever arm from the centroid to the "cantilevered" end of the tongue. Furthermore, increasing "$a_t$" increases "$L_c$", which has an adverse impact on the stiffness of the tongue, a requirement that is critical to limit the die deflection and consequently to meet the tolerance requirements [26]. Hence, a larger Tongue Depth in a Shape requires a thicker die and backer to maintain the effective stresses and deflection of the die tongue within allowable levels. This implies higher Material Costs of the Tooling, as well as longer machining time to remove the extra volume of steel, increasing Labor and Overhead Costs.

10) ***Tongue Width ($b_t$):*** The larger the Tongue Width "$b_t$" (as depicted in Figure 5.13), the higher the bending and shear stresses on the narrowest part of the die tongue, as a larger "$b_t$" would increase the force acting on the tongue. This would require a thicker die and backer; thus, the Material Costs and the Labor and Overhead Costs of the Tooling would be higher, as explained before.

11) ***Tongue Gap ($b_{gap}$):*** The smaller the Tongue Gap "$b_{gap}$" is (as depicted in Figure 5.13), the higher the bending and shear stresses will be on the narrowest part of the die tongue. This implies a thicker die and backer, increasing the Material Costs as well as the Labor and Overhead Costs of the Tooling, as described before.

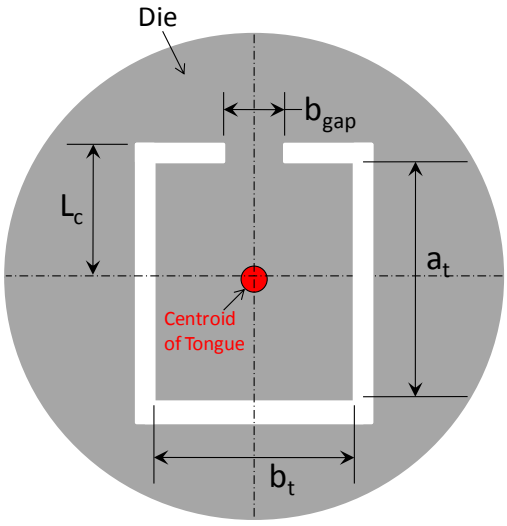


**Figure 5.13** Schematic of Tongue Dimensions in a Solid or Semihollow Die.

### *5.3.2 Selection of Vital Xs*

Even though all the 11 variables listed above represent Potential Vital Xs, it would be unfeasible to include them all in the empirical model for Tooling Cost, as the number of quotes required would be tremendously large. Just to provide an idea on the number of data points needed, an example can be illustrated for a relatively simple regression model consisting of a second order polynomial of the form:

$$y(x_1, x_2) = ax_1^2 + bx_2^2 + cx_1x_2 + dx_1 + ex_2 + f$$

where only 2 Xs have been considered, resulting in 6 unknown coefficients (*a, b, c,..f*). A regression analysis needs at least one more data point than the number of unknown coefficients in the proposed model; so, for the case considered above, 7 data points (i.e. quotes) would be required to run the regression analysis. As the number of Xs in the transfer function increases, so does the number of unknown coefficients, in a non-linear fashion. For a second order polynomial, considering all the quadratic and interaction terms, it can be mathematically shown that the number of terms (or unknown coefficients) in the transfer function is given by the following expression:

$$N_{terms} = 2n + 1 + \frac{n!}{2!\,(n-2)!};\ n \geq 2 \quad (5.7)$$

where $N_{terms}$ is the number of terms in the transfer function and $n$ is the number of Xs. So, for a transfer function with 3 Xs ($n$=3), the number of terms, $N_{terms}$ is 10; for 4 Xs, $N_{terms}$=15; for 5 Xs, $N_{terms}$=21, and so on. If the 11 Potential Vital Xs described before were desired in the transfer function, the number of terms in the model would be $N_{terms}$=78, requiring at least 79 quotes to run the regression analysis!

In order to keep the quotes required within a feasible number, the author of this thesis decided to limit the transfer function to 3 Vital Xs, which would imply having 10 terms in a full-quadratic regression model, requiring at least 11 different designs to be quoted. Based on the screening of Potential Vital Xs presented in Section 5.3.1 and the guidelines mentioned in the literature [6], [22], [24], [25], [26], [8], the first five variables in the list of Potential Vital Xs (*CCD,*

*Alloy*, $P_{ext}$, $A_f$, and *Shape Type*) appear to be the ones with the highest impact on Tooling Cost. This reduces the list of Vital Xs to 5, so two variables still need to be removed.

The variable "*Alloy*" is a discrete one, with only two possible values: Soft Alloy or Hard Alloy. Since the majority of the extruded products in the market are made of soft alloys, (with 6xxx aluminum alloys covering about 80% of the commercial volume [23]), and given the limited number of extruders capable of producing complex shapes made of hard alloys (i.e. making it more difficult to obtain quotes), the variable *Alloy* will be eliminated from the Vital Xs. This will limit the validity of the empirical model to soft alloys only. However, even though hard alloys have a higher flow stress than soft alloys, a comparison of the specific pressure required to extrude a shape (calculated using equation 5.4) against the specific pressure capacity of several presses in the market (data in APPENDIX B: EXTRUSION PRESS DATABASE) suggests that the press capacity is usually the limiting factor for the specific pressure, so the billet length ($L_o$) must be reduced accordingly to make the extrusion possible. Hence, at the end of the day, the value of $p$ (the specific pressure) does not vary as much as expected from alloy to alloy. Indeed, the maximum specific pressure for heavy metals and aluminum alloys is usually in the range of 1000 to 1250 MPa [26]. Based on the argument presented above, it may be adequate to assume that the empirical model to be obtained for the Tooling Cost of extrusions made of soft alloys could be adapted in the future for hard alloys, by simply including an additional factor (obtained by experience) to account for the fact that hard alloy extrusions require Shaped Dies, as opposed to Flat-face dies used for soft alloy extrusions.

Finally, to further reduce the list of Vital Xs from 4 to 3, the variables $A_f$ and $P_{ext}$ can be combined into a single one, in the form of a ratio. This is consistent with the practice in the extrusion industry, where the "Shape Factor" (the ratio of $P_{ext}/\rho A_f$) is often used as a measure of complexity of the shape [1], [6], [24], [26], [8]. Another common measure of shape complexity combining the variables $A_f$ and $P_{ext}$ is the "Perimeter Ratio" or "Circumferential Ratio", which is the ratio of the external perimeter of the shape to the perimeter of an equivalent solid round section with the same cross sectional area ($A_f$) as the actual shape [26], [34], [39]. This ratio was introduced previously, as part of the definition of the "shape

complexity factor", $K_{shape}$, in Section 4.1.1. The mathematical definition of the Perimeter Ratio (PR) is:

$$PR = \frac{P_{ext}}{2\sqrt{\pi A_f}} \quad (5.8)$$

Both the Shape Factor and the Perimeter Ratio are adequate ways of combining the variables $A_f$ and $P_{ext}$ into a single one. In this thesis, the Perimeter Ratio will be used, as it represents an adimensional parameter and it is consistent with the model chosen before for predicting the specific pressure. Thus, the reduced list of Vital Xs is:

1) CCD
2) Perimeter Ratio (PR)
3) Shape Type

Although the empirical model obtained with these 3 Vital Xs is not expected to be 100% accurate, it should be able to explain a fairly high percentage of the Tooling Cost variation from one design to the other. This will be verified later in this chapter when the regression model is evaluated.

## 5.4 Experiments Planning and Results

In order to improve the robustness of the transfer function to be obtained, the settings for the Vital Xs in the experiments (i.e. the designs to be quoted) were carefully selected to cover a significant amount of the design space. The target for the number of required quotes was set to 11, based on the analysis presented in Section 5.3.2. The quotes were obtained in two steps, as the first four data points were already available from quotes previously gathered to validate the Recurring Costs Model. The remaining seven data points were distributed throughout the design space, as shown in Table 5.4, covering a CCD range from 5" to 10", a Perimeter Ratio range from 2.2 to 6.3, and Shape Types ranging from Solid to Hollow Class 3.

As it can be noticed from Table 5.4, the experiments included designs with "intermediate values" for the 3 Vital Xs, so that non-linear variations of the Y can be adequately assessed.

For simplicity purposes, the variable X3 (Shape Type) was designated as a four-level discrete variable, instead of a six-level discrete variable. Solid Sections were grouped in the first category (X3=1), Semihollows (Class 1 and 2) in the second (X3=2), Hollows Class 1 and 2 were classified in the third category (X3=3), and Hollows Class 3 formed the fourth category (X3=4). As it will be shown later in this chapter, the numerical values designated for each of the four levels in X3 were modified during the regression analysis to improve the accuracy of the model, but the grouping of shapes in the four categories aforementioned remained.

**Table 5.4** Settings for Vital Xs in Experiments.

| Design # | X1= CCD (in) | X2= PR | Shape Type | X3 |
|---|---|---|---|---|
| 1 | 6.96 | 4.6 | Solid | 1 |
| 2 | 6.10 | 4.1 | Semihollow Class 1 | 2 |
| 3 | 5.00 | 3.6 | Hollow Class 2 | 3 |
| 4 | 8.00 | 2.2 | Hollow Class 3 | 4 |
| 5 | 10.00 | 6.3 | Solid | 1 |
| 6 | 5.00 | 2.3 | Solid | 1 |
| 7 | 7.50 | 2.9 | Semihollow Class 1 | 2 |
| 8 | 9.00 | 6.0 | Semihollow Class 2 | 2 |
| 9 | 8.08 | 6.2 | Hollow Class 1 | 3 |
| 10 | 10.00 | 5.8 | Hollow Class 3 | 4 |
| 11 | 5.00 | 3.7 | Hollow Class 3 | 4 |

It is important to remark that, even though the initial intend was to resemble the DOE technique in the distribution of experiments, practical limitations and producibility constraints encountered during the Request for Quotation (RFQ) Process affected the initial plans and therefore, the Vital Xs settings shown in Table 5.4 do not strictly correspond to the ones in a formal DOE. However, the flexibility offered by regression analysis techniques made that a minor issue.

The eleven designs listed in Table 5.4 are drawn to scale in Figure 5.14, where the variety of sizing and shapes can be readily visualized. Detailed Drawings for all designs are

attached in APPENDIX D: DETAILED DRAWINGS OF EXTRUDED SHAPES QUOTED; such drawings were used to request the quotes to vendors. All designs are made of Al 6063-T6, with a Mill Finish (i.e. as Extruded) on all surfaces. Standard tolerances per Aluminum Association Standards [55] were specified for all geometrical and metallurgical characteristics. Order quantities were indicated as appropriate to meet the minimum order requirements of the various suppliers. However, for the sake of Tooling Costs Quoting, order quantity is irrelevant[10], as the former are independent of the latter; this was confirmed by the extruders who provided quotes. Indeed, Tooling Maintenance Costs are considered part of the Production Costs of the extruded parts (i.e. Overhead Costs) [23].

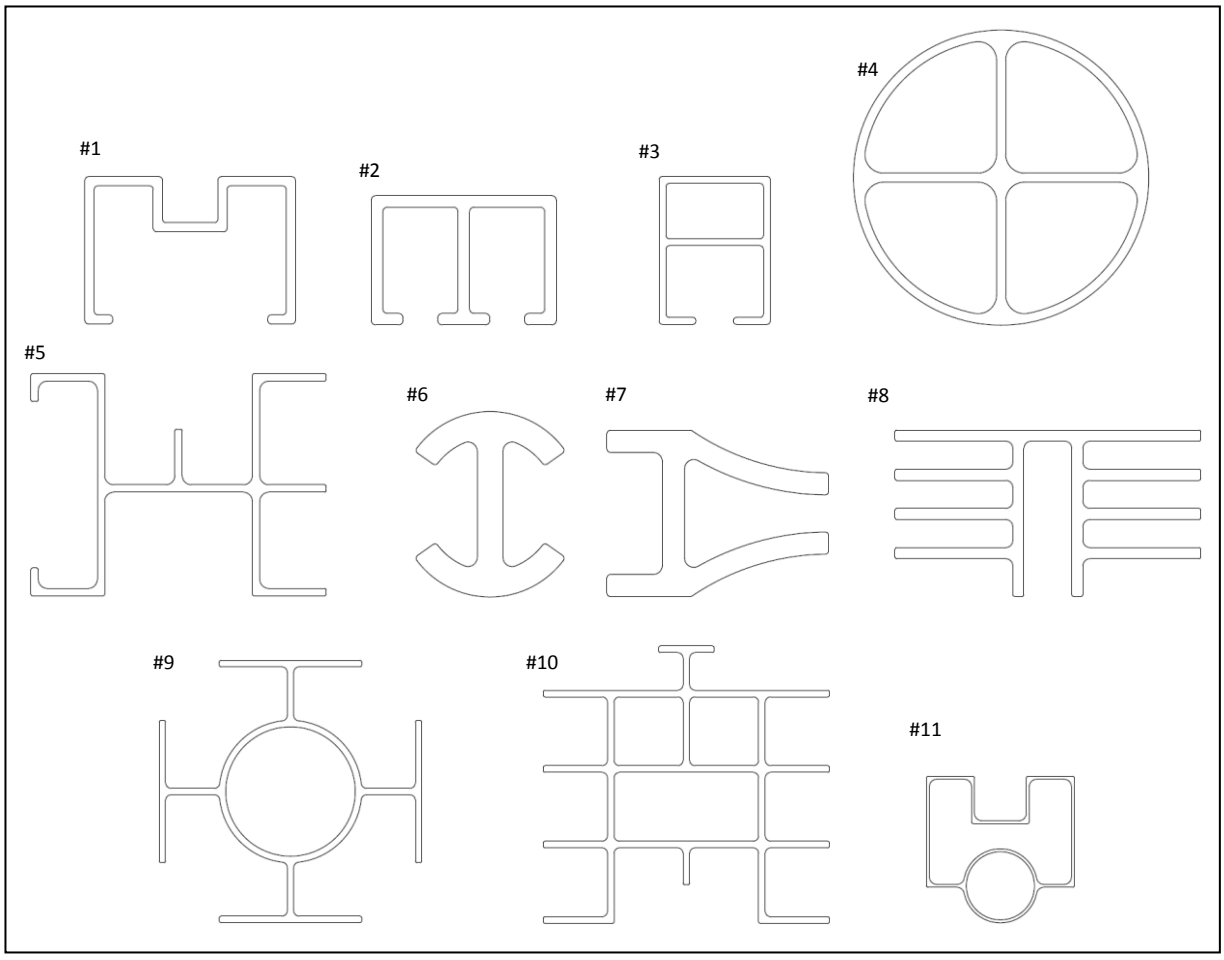


**Figure 5.14** Design Shapes Quoted (all drawn to same scale).

[10] Order quantity may be relevant though, in deciding if a Multi-hole Die should be used to extrude the part. Multi-hole Dies are usually disqualified for low-volume production.

Quotes were requested from eight different extruders in the US who had the technical capabilities to produce the designs. Nevertheless, only two companies provided quotes. Such companies will be denoted here as "*Company A"* and "*Company B"*, to prevent misuse of their pricing information. *Company A* quoted all designs except for design #2, whereas *Company B* quoted only designs #1, #2 and #4. Fortunately, *Company A* quoted cheaper than *Company B* in both designs they had in common (designs #1 and #4, quoted 1% and 36% cheaper, respectively), which suggests that the Tooling Costs obtained from *Company A* are closer to the real costs. The Tooling Costs for all designs are reported in Table 5.5 along with relevant geometric parameters. Such costs correspond to the quotes received from *Company A* (cheaper), except for design #2, which was only quoted by *Company B*. The Tooling Quotes for the 11 shapes range from $2270 to $7725, which is in the ballpark of typical figures for Hot Extrusion Tooling Costs ($500-$5000), as reported by the Aluminum Extruders Council [25]. With this data, all the necessary input for running the regression analysis is ready.

**Table 5.5** Tooling Costs Quotes.

| Design # | X1= CCD (in) | THK (in) | $P_{ext}$ (in) | $A_f$ ($in^2$) | X2= PR | Shape Type | X3 | Y = Tooling Cost ($) |
|---|---|---|---|---|---|---|---|---|
| 1 | 6.96 | 0.250 | 33.04 | 4.166 | 4.57 | Solid | 1 | $2,270.00 |
| 2 | 6.10 | 0.313 | 33.06 | 5.222 | 4.08 | Semihollow Class 1 | 2 | $3,600.00 |
| 3 | 5.00 | 0.188 | 21.02 | 2.789 | 3.55 | Hollow Class 2 | 3 | $2,449.00 |
| 4 | 8.00 | 0.250 | 25.13 | 10.576 | 2.18 | Hollow Class 3 | 4 | $7,725.00 |
| 5 | 10.00 | 0.200 | 53.71 | 5.698 | 6.35 | Solid | 1 | $5,000.00 |
| 6 | 5.00 | 0.700 | 23.79 | 8.377 | 2.32 | Solid | 1 | $2,865.00 |
| 7 | 7.50 | 0.600 | 31.43 | 9.547 | 2.88 | Semihollow Class 1 | 2 | $3,285.00 |
| 8 | 9.00 | 0.300 | 70.60 | 10.897 | 6.03 | Semihollow Class 2 | 2 | $5,000.00 |
| 9 | 8.08 | 0.175 | 53.23 | 5.792 | 6.24 | Hollow Class 1 | 3 | $4,208.00 |
| 10 | 10.00 | 0.180 | 58.33 | 8.003 | 5.82 | Hollow Class 3 | 4 | $5,974.00 |
| 11 | 5.00 | 0.080 | 17.03 | 1.697 | 3.69 | Hollow Class 3 | 4 | $2,911.00 |

## 5.5 Regression Analysis

The multivariate regression analysis was run in *DataFit* Software, which has the capability of curve fitting data to any user-defined model. A variety of regression models were defined in *DataFit* including polynomials (quadratic, linear, linear + interactions, and all possible

combinations), power-law models (with or without interaction terms), logarithmic, exponential and transformed variations (e.g. square root of Xs) of all of the previous ones.

### *5.5.1 Refinement of Vital Xs Definitions*

The regression analysis was an iterative process, as preliminary results lacked statistical significance and/or physical coherence. For instance, according to the qualitative analysis of the 3 Vital Xs effects on the Y (presented in Section 5.3.1), all of them have a positive correlation with the Tooling Cost (i.e. an increase on X1, X2 or X3 would cause an increase on Y); however, in many cases the regression analysis resulted in negative slopes for some terms of the models, which did not make physical sense.

As a first check, a "scatter plot" of the Actual Tooling Costs (Y) vs. the Vital Xs was verified, as shown in Figure 5.15. This plot reveals a very critical inconsistency: the first point in the curve for Y vs. X2 (blue curve with square markers) is the one with the lowest PR, yet it has the highest Tooling Cost. This data point corresponds to Design #4, which has a relatively small external perimeter (i.e. it is circular) in relation with its size. This suggested that the Perimeter Ratio definition for X2 needed to be adjusted, to include the Internal Perimeter (of the voids) as well. So, the revised version of PR became:

$$PR' = \frac{P_{tot}}{2\sqrt{\pi A_f}} \quad (5.9)$$

where $P_{tot}$ is the Total Perimeter of the Shape (i.e. External + Internal Perimeter). Furthermore, an inspection of the Tooling Costs for Hollow Class 3 Shapes in Table 5.5 suggests that the number of voids in hollow shapes (a Potential Vital X discarded before) has a significant effect on the Y. In order to incorporate such effect in the model, a variable for the number of voids ($N_{voids}$) was introduced in X3 along with the previous four-level discrete values designation. The new definition for X3 became:

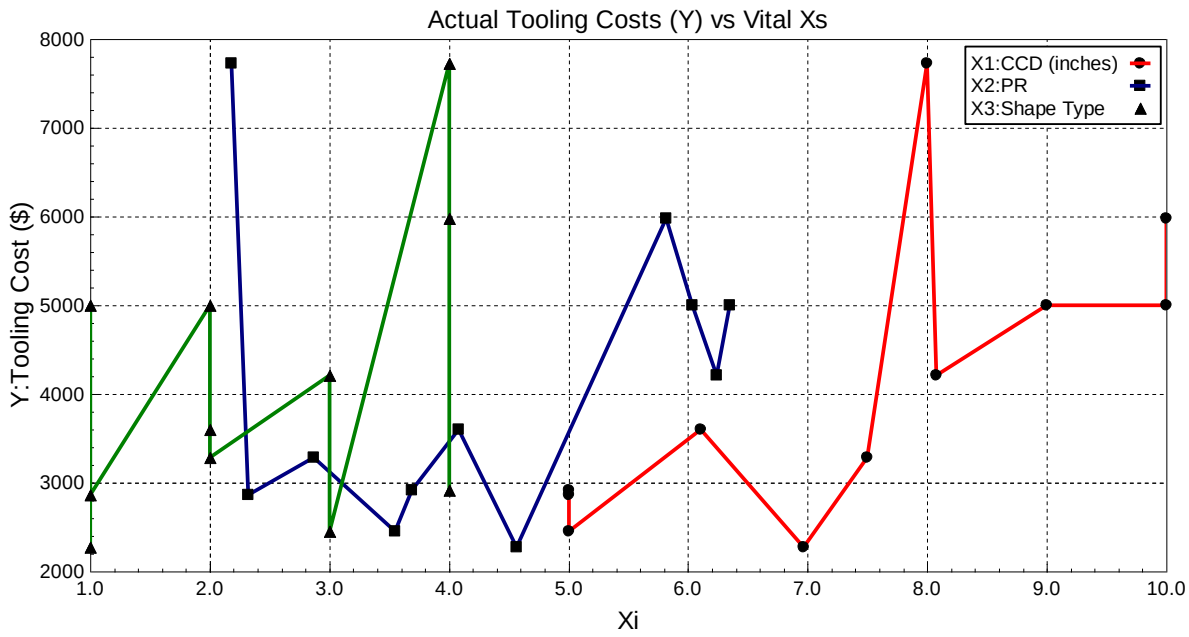


**Figure 5.15** Scatter Plot of Tooling Costs vs. Vital Xs (Initial Definition).

$$X3 = \begin{cases} 1.0, & \text{for Solids} \\ 1.5, & \text{for Semihollows} \\ 2.0, & \text{for Hollows Class 1 or 2} \\ 1 + N_{voids}, & \text{for Hollows Class 3} \end{cases} \qquad (5.10)$$

where the values of X3 for Hollow Class 3 Shapes start from 2.0 (if $N_{voids}$=1, resulting in a shape that is similar to a Hollow Class 1 or Class 2) and increase to larger integers as the number of voids goes up (e.g. X3=3 if $N_{voids}$=2, X3=4 if $N_{voids}$=3, and so on). Also, it must be noted that the discrete value of X3 for Semihollow Shapes was changed from 2.0 to 1.5, as it resulted in improved regression accuracy (after a number of run trials with different values). The same thing applies to the value of X3 for Hollows Class 1 or 2, which was reduced from 3.0 to 2.0.

The changes aforementioned for X2 (with the revised definition of PR) and X3 resulted in a significant improvement in the regression accuracy. A scatter plot of the Actual Tooling Costs (Y) vs. the revised Vital Xs is shown in Figure 5.16, where the trends of Y vs. Xi are now much clearer than before. However, negative terms were still obtained in the regression models, particularly in the terms involving X2. Hence, a closer review at the Vital Xs selection and definition was deemed appropriate.

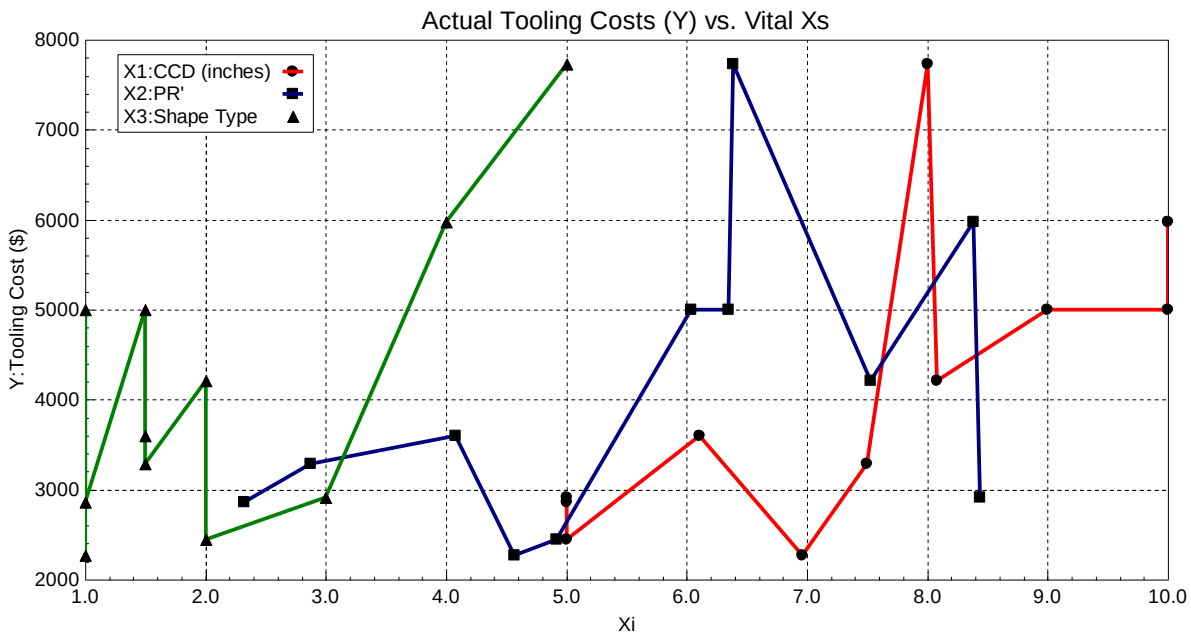


**Figure 5.16** Scatter Plot of Tooling Costs vs. Vital Xs (Revised Definition).

In order to check the significance of the Vital Xs selected, a "Variable Selection Analysis" was performed in *DataFit*. In this type of assessment, a Correlation Matrix like the one shown in Table 5.6 is obtained. Note that five Potential Vital Xs were considered, and the PR parameter was broken down into two separate Xs: $P_{tot}$ and $A_f$. The Correlation Matrix provides information on the degree of linear relationship between different pairs of variables [57]. The coefficients in the matrix lie between -1 and 1, where -1 indicates a perfect linear negative relationship between two variables, +1 indicates a perfect positive linear relationship, and 0 indicates lack of any linear relationship [57].

**Table 5.6** Correlation Matrix.

| VARIABLES | X1:CCD | X2:$P_{tot}$ | X3:$A_f$ | X4:THK | X5:Shape Type | Y:Tooling Cost |
|---|---|---|---|---|---|---|
| **X1:CCD** | 1 | 0.80 | 0.51 | -0.23 | 0.19 | 0.69 |
| **X2:$P_{tot}$** | 0.80 | 1 | 0.48 | -0.45 | 0.63 | 0.86 |
| **X3:$A_f$** | 0.51 | 0.48 | 1 | 0.52 | 0.21 | 0.63 |
| **X4:THK** | -0.23 | -0.45 | 0.52 | 1 | -0.40 | -0.23 |
| **X5:Shape Type** | 0.19 | 0.63 | 0.21 | -0.40 | 1 | 0.71 |
| **Y:Tooling Cost** | 0.69 | 0.86 | 0.63 | -0.23 | 0.71 | 1 |

An examination of the Correlation Matrix in Table 5.6 reveals several key facts. First of all, in comparing the correlations between each X and the Y, one can identify that the X with the strongest correlation to the Y is the Total Perimeter ($P_{tot}$), with a correlation coefficient of 0.86. The second strongest correlation to the Y is found in the Shape Type variable, with a correlation coefficient of 0.71. Finally, the third strongest correlation to the Y is observed in the CCD, with a correlation coefficient of 0.69. These three Xs have a strong, positive correlation to the Tooling Cost, as expected from the previous qualitative analysis presented in Section 5.3.1. On the other hand, the wall thickness (THK) has a weak negative correlation to the Y (with a coefficient of -0.23) which confirms the fact that this X may be removed from the model without compromising its accuracy.

A fundamental inconsistency was found when the correlation between the cross sectional area ($A_f$) and the Y was inspected. Those variables were expected to hold a strong negative correlation according to the analysis presented in Section 5.3.1; however, in the Correlation Matrix they showed a positive correlation (with a coefficient of 0.63), which is not physically logic at all. As it was mentioned before, it is well documented in the literature and known by extruders that a higher Shape Factor or Perimeter Ratio increases the production and tooling costs of an extruded part. Both Shape Factor and Perimeter Ratio equations contain the cross sectional area of the part ($A_f$) in the denominator, meaning they would decrease as $A_f$ is increased, and so would the production and tooling costs. The positive correlation coefficient obtained in the matrix above may be the result of statistical error due to the relatively small sample of shapes quoted. Therefore, the author of this thesis decided to leave the cross-sectional area ($A_f$) out of the tooling cost model. Indeed, it is very likely that the previously mentioned regression results issues on negative coefficients for PR were due to the inclusion of $A_f$ in the model.

Based on the arguments presented above, the **revised list of 3 Vital Xs** to be included in the transfer function for the Tooling Cost is the following:

- X1= CCD (inches)
- X2= $P_{tot}$ (inches)
- X3= Shape Type (per Equation 5.10)

Finally, when building regression models, it is always a good practice to check correlation between the Xs. If two Xs show a strong correlation, they should not be included in the regression model together [58]. In the Correlation Matrix presented in Table 5.6, the Xs for $P_{tot}$ and CCD appear to have a strong positive correlation, with a coefficient of 0.80. Nevertheless, engineering judgment proves this wrong, as depicted in Figure 5.17. The same thing applies to the correlation between $P_{tot}$ and Shape Type, which despite having a coefficient of 0.63 in the matrix, are not physically correlated, as demonstrated in Figure 5.17. Hence, the 3 Vital Xs are not correlated with each other; they can be included together in the model.

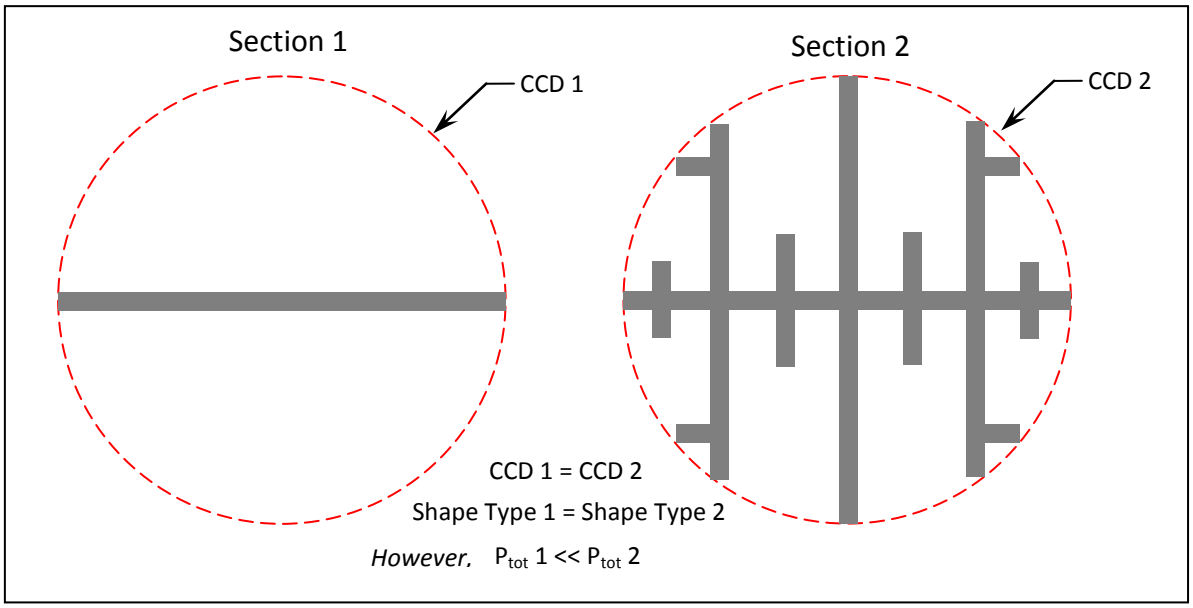


**Figure 5.17** A simple proof that $P_{tot}$ is not correlated to either CCD or Shape Type.

An updated version of Table 5.5, reflecting the changes in Vital Xs definitions for X2 and X3, is shown in Table 5.7 for reference. Likewise, an updated scatter plot of the Actual Tooling Costs vs. the finalized definition of Vital Xs is shown in Figure 5.18, where it can be seen that the trends of Y vs. the 3 Xs look clearer than the previous versions, and positively correlated, as expected. Regression results were improved significantly with the refined definition of Vital Xs described above. The next subsection covers those results in detail.

**Table 5.7** Tooling Costs for Designs Quoted (Updated Vital Xs)

| Design # | X1= CCD (in) | $P_{ext}$ (in) | $P_{int}$ (in) | X2= $P_{tot}$ (in) | Shape Type | X3 | Y = Tooling Cost ($) |
|---|---|---|---|---|---|---|---|
| 1 | 6.96 | 33.04 | 0 | 33.04 | Solid | 1 | $2,270.00 |
| 2 | 6.10 | 33.06 | 0 | 33.06 | Semihollow Class 1 | 1.5 | $3,600.00 |
| 3 | 5.00 | 21.02 | 8.09 | 29.11 | Hollow Class 2 | 2 | $2,449.00 |
| 4 | 8.00 | 25.13 | 48.47 | 73.60 | Hollow Class 3 | 5 | $7,725.00 |
| 5 | 10.00 | 53.71 | 0 | 53.71 | Solid | 1 | $5,000.00 |
| 6 | 5.00 | 23.79 | 0 | 23.79 | Solid | 1 | $2,865.00 |
| 7 | 7.50 | 31.43 | 0 | 31.43 | Semihollow Class 1 | 1.5 | $3,285.00 |
| 8 | 9.00 | 70.60 | 0 | 70.60 | Semihollow Class 2 | 1.5 | $5,000.00 |
| 9 | 8.08 | 53.23 | 11.00 | 64.22 | Hollow Class 1 | 2 | $4,208.00 |
| 10 | 10.00 | 58.33 | 25.72 | 84.05 | Hollow Class 3 | 4 | $5,974.00 |
| 11 | 5.00 | 17.03 | 21.92 | 38.95 | Hollow Class 3 | 3 | $2,911.00 |

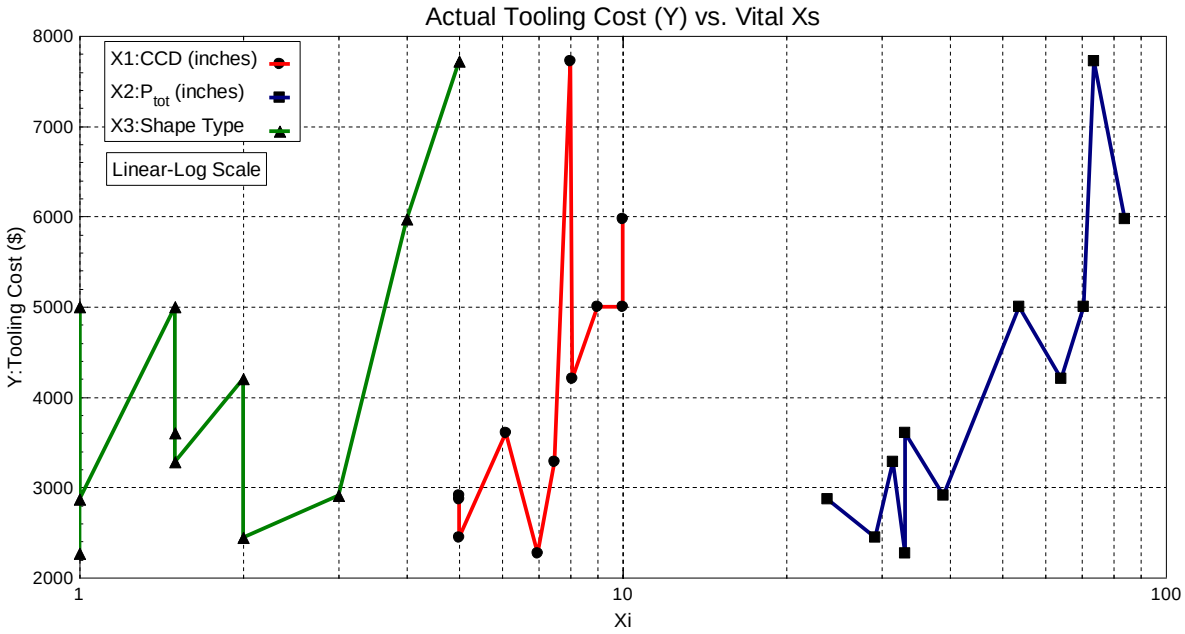


**Figure 5.18** Scatter Plot of Tooling Costs vs. Vital Xs (Finalized Definition).

### *5.5.2 Regression Results*

As it was mentioned before, a variety of mathematical functions were tried in the regression analysis, including polynomial, power-law, logarithmic, exponential and transformed versions of all of the above. Several statistical criteria were considered in evaluating the quality

of the different models obtained. Moreover, the physical coherence of the results was consistently assessed. After careful examination of multiple models, the best results were obtained with a relatively simple function, consisting of a linear term added to an interaction term, as follows:

$$Y(X_1, X_2, X_3) = aX_1 + bX_2X_3 \quad (5.11)$$

where *a* and *b* are the coefficients obtained by the regression analysis, and they are reported in Table 5.8. Substitution of those values into equation 5.11 yields the empirical model to predict the Tooling Cost of an extruded part:

$$Y(X_1, X_2, X_3) = 407.028X_1 + 9.219X_2X_3 \quad (5.12)$$

where *Y* is the Tooling Cost (in USD), $X_1$ is the CCD (in inches), $X_2$ is the Total Perimeter $P_{tot}$ (in inches) and $X_3$ is the Shape Type discrete variable, defined by Equation 5.10.

**Table 5.8** Regression Variable Results for Model Selected.

| REGRESSION RESULTS FOR Y=a*X1+b*X2*X3 | | | |
|---|---|---|---|
| **Variable** | **Value** | **95% Confidence Interval[11] (+/-)** | **p-value** |
| **a** | 407.028 | 103.149 | 0.00001 |
| **b** | 9.219 | 4.697 | 0.00162 |

As it can be noticed from the data in Table 5.8, the two terms in the regression model are statistically significant as they both have a p-value that is smaller than 0.05 (a typical criterion used in Hypothesis Testing) [59]. Indeed, the maximum p-value obtained is 0.00162, for coefficient *b*, which means that there is only a 0.16% probability that the actual value of *b* is zero [58]. In addition, the fact that both terms in the regression model are positive makes perfect physical sense according to the qualitative analysis discussed before and the trends observed in Figure 5.18. Moreover, the 95% Confidence Intervals obtained for both coefficients

[11] This does not mean that there is a 95% probability that the actual values of *a* and *b* lie within the calculated intervals. Instead, it means that if an experiment is performed many times (i.e. data is sampled again, followed by regression analysis), in 95% of the cases the resulting values of *a* and *b* will lie within the computed intervals [58].

are relatively narrow (which is good), especially considering the small sample of designs quoted.

Regarding the overall performance and statistical behavior of the regression model, a summary of important metrics is reported in Table 5.9. First of all, it must be noted that the overall statistical significance of the model complies with the minimum p-value requirement of 0.05, as the reported value of Prob(F) –which is the p-value for an hypothesis test of the overall significance of the model- is 0.00008. This means there is only a 0.008% chance that all of the actual parameters in the regression model (i.e. *a* and *b*) are zero [58]. Secondly, the value of $R^2$ (Coefficient of Multiple Determination) is 0.836, which means that the regression model explains 83.6% of the variance observed in the experimental data for Tooling Cost. This is a fairly good percentage of variance explained, considering that only 3 Vital Xs were included in the model out of a list of 11 Potential Vital Xs identified before in Section 5.3.1. Furthermore, the value of $R_a^2$ (Adjusted Coefficient of Multiple Determination) is 0.817, which is very close to the value of $R^2$, a very desirable characteristic meaning that this is a good, parsimonious model (i.e. with not too many Xs, and not too many terms) [58]. As a reference, an $R_a^2$ value that is greater than 0.8 is often used as a good indication that the regression model provides an adequate fit for the data [59].

**Table 5.9** Regression Model Overall Statistics.

| REGRESSION MODEL STATISTICS | |
|---|---|
| Prob(F) | 0.00008 |
| Sum of Residuals | 286 |
| Average Residual | 26 |
| Residual Sum of Squares | 4634065 |
| Standard Error of the Estimate | 718 |
| $R^2$ | 0.836 |
| $R_a^2$ | 0.817 |

A comparison of the model predictions against the actual data points obtained from the quotes is included in Table 5.10 (in a tabular form) and in Figure 5.19 (in a graphical format). It can be seen that most of the regression predictions correlate to the quotes within 20%, which is not bad for a ballpark Tooling Cost estimate. In fact, the average absolute error obtained is

14%, and the average absolute residual is only $545, with a standard deviation of $370. Those small errors are very likely to be wiped out as production quantity is increased and the Tooling Costs are amortized over the entire production volume.

**Table 5.10** Actual Tooling Costs vs. Predicted Costs by Regression Model.

| Design # | Y: Tooling Cost ($) | Calculated Y ($) | Residual ($) | % Error | Abs (% Error) | Abs Residual ($) |
|---|---|---|---|---|---|---|
| 1 | 2270 | 3139 | -869 | -38% | 38% | 869 |
| 2 | 3600 | 2941 | 659 | 18% | 18% | 659 |
| 3 | 2449 | 2572 | -123 | -5% | 5% | 123 |
| 4 | 7725 | 6649 | 1076 | 14% | 14% | 1076 |
| 5 | 5000 | 4565 | 435 | 9% | 9% | 435 |
| 6 | 2865 | 2254 | 611 | 21% | 21% | 611 |
| 7 | 3285 | 3487 | -202 | -6% | 6% | 202 |
| 8 | 5000 | 4639 | 361 | 7% | 7% | 361 |
| 9 | 4208 | 4472 | -264 | -6% | 6% | 264 |
| 10 | 5974 | 7170 | -1196 | -20% | 20% | 1196 |
| 11 | 2911 | 3112 | -201 | -7% | 7% | 201 |
| MIN | 2270 | 2254 | -1196 | -38% | 5% | 123 |
| MAX | 7725 | 7170 | 1076 | 21% | 38% | 1196 |
| MEAN | 4117 | 4091 | 26 | -1% | 14% | 545 |
| STD DEV | 1680 | 1610 | 680 | 18% | 10% | 370 |

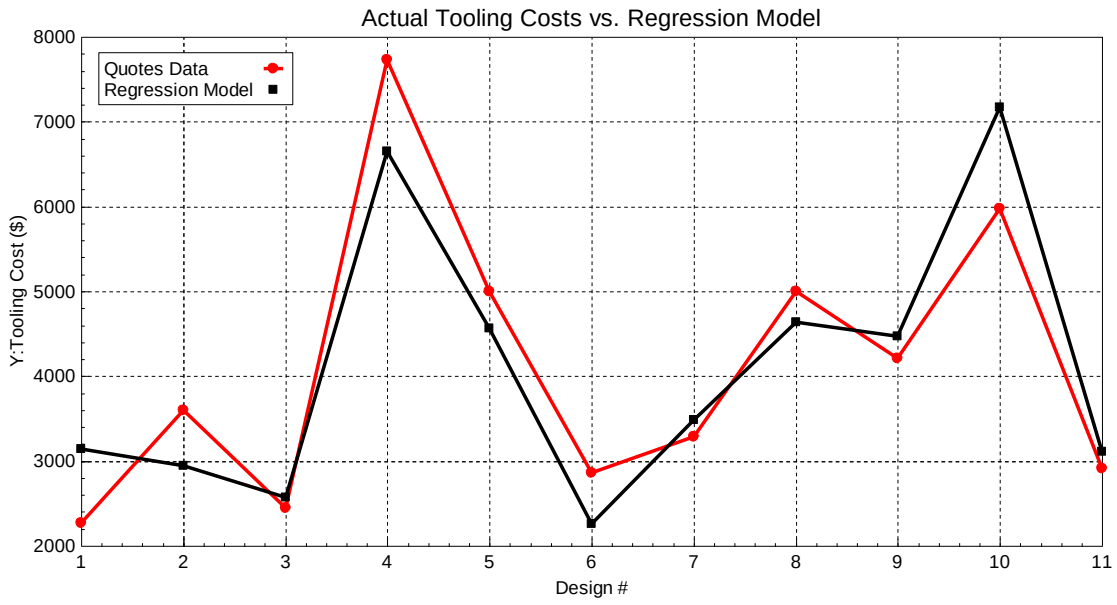


**Figure 5.19** Comparison of Actual Tooling Costs and Regression Model Predictions.

Another useful way to visualize the correlation between the Actual Tooling Costs (from quotes) and the Model predictions is depicted in the plots of Figure 5.20, Figure 5.21, and Figure 5.22, where the trends of Tooling Cost vs. each of the Vital Xs (CCD, Total Perimeter and Shape Type) are shown. The plots show that the Regression Model follows fairly well the trends observed in the Actual Tooling Costs obtained from the quotes.

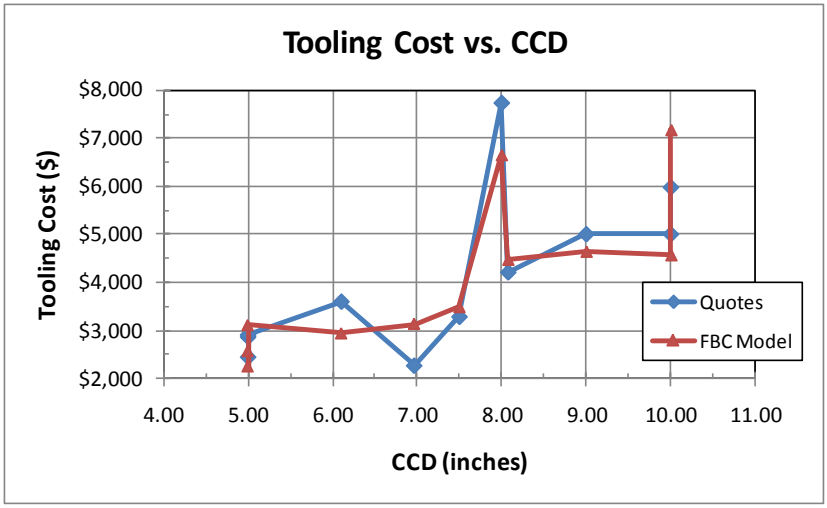


**Figure 5.20** Tooling Cost vs. CCD Trend.

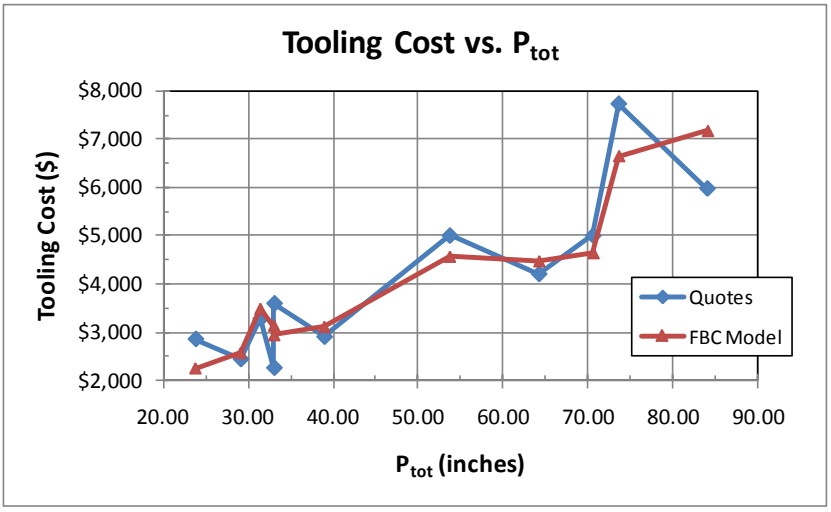


**Figure 5.21** Tooling Cost vs. Total Perimeter Trend.

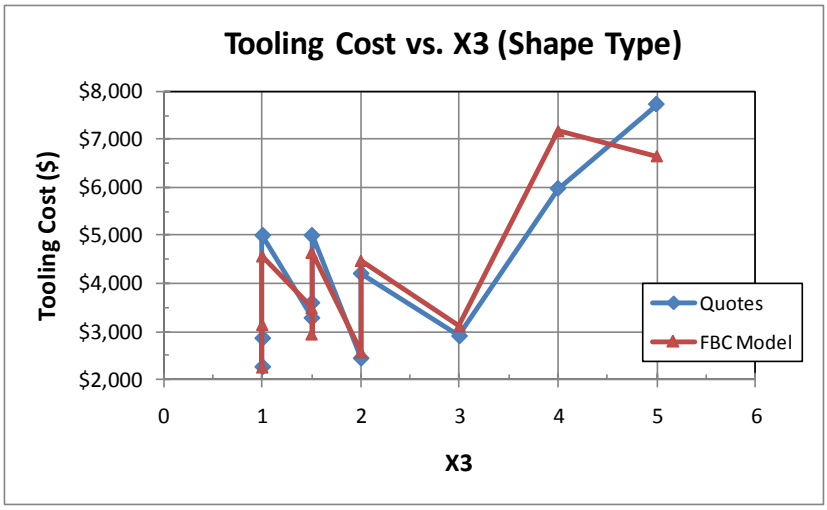


**Figure 5.22** Tooling Cost vs. X3 (Shape Type) Trend.

As a final check, residuals must be verified to make sure they are randomly scattered around zero, show no discernable pattern, and be normally distributed [58], [59]. A scatter plot of residuals is included in Figure 5.23, where no trends are visible, and the residuals seem to fluctuate fairly symmetrically around zero. Indeed, the statistics in Table 5.10 show that the mean of the residuals is $26, which is quite close to zero. Additionally, a Residual Normal Probability Plot provided by *DataFit* and included in Figure 5.24 shows that the normalized residuals are close to the Normal Reference Line, suggesting that they follow a normal distribution. The small departures from normality should not create any serious problems [59].

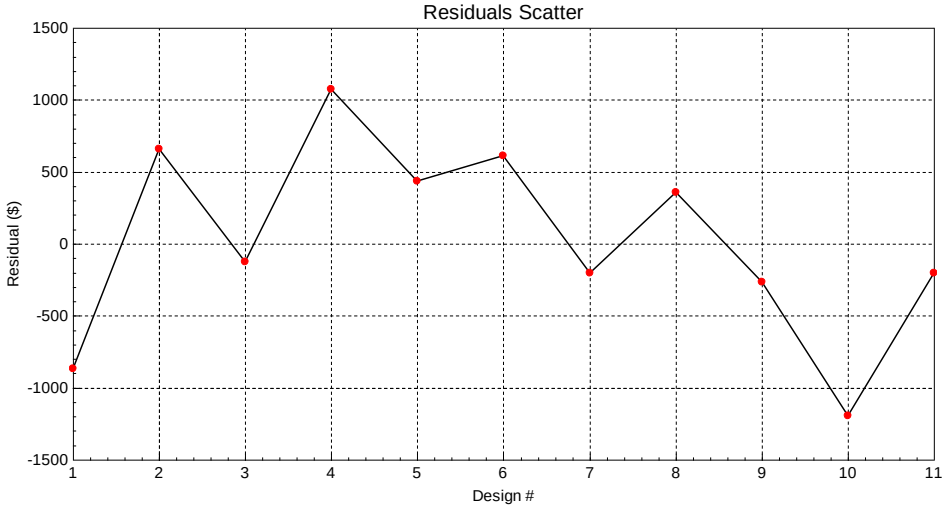


**Figure 5.23** Residuals Scatter Plot.

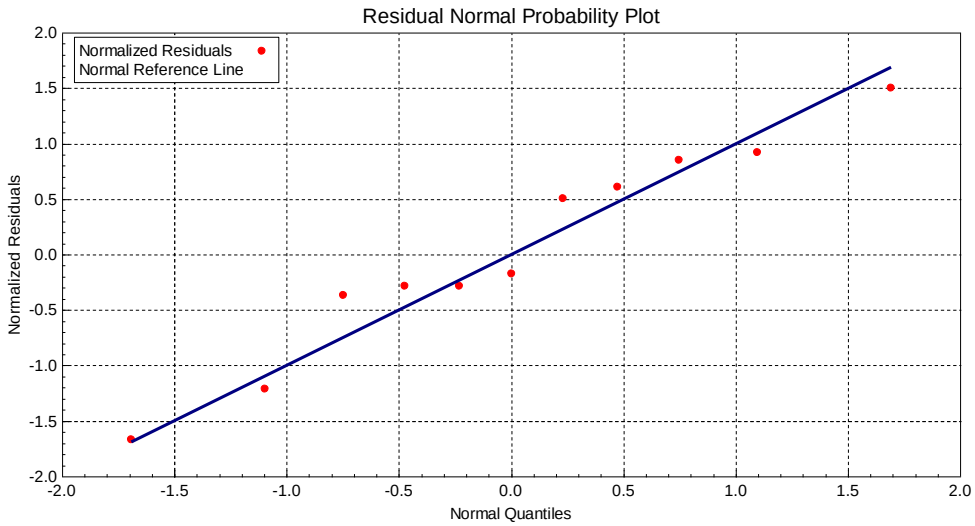


**Figure 5.24** Residual Normality Plot.

Finally, it is essential to remark that the transfer function obtained to predict the Tooling Cost (Equation 5.12) is, strictly speaking, valid only within the design space from which it was obtained. Such domain is the following:

$$5" \leq X_1 \leq 10"$$

$$23.79" \leq X_2 \leq 84.05"$$

$$1.0 \leq X_3 \leq 5.0$$

This domain covers a big portion of the design space typically found in the aluminum extrusion industry. While extrusions have been made with CCDs as small as 0.25 in (6.3 mm) [3] and as large as 29 in (737 mm) [46], the bulk of aluminum extrusion work, however, is done within a CCD range of 1-10 in (25-250 mm) [25], [3]. Moreover, if a design lies outside the domain mentioned above, the linear nature of the Tooling Cost Model provides with "stable" extrapolations. However, the latter should be carried out with caution and always using good engineering judgment.

# CHAPTER 6: COST MODEL VALIDATION

## 6.1 Cost Model Validation Approach

The last two chapters in this thesis described the FBC Model developed for predicting the Recurring and Non-Recurring Manufacturing Costs incurred in Hot Extrusion of Aluminum Alloys. The Non-Recurring Costs Model was already validated in Chapter 5, as part of the Regression Analysis Results documented in Section 5.5.2, where it was shown that Tooling Costs predicted by the Model for eleven different designs had a fairly good correlation with the corresponding quotes obtained from US extruders. The Recurring Costs Model, however, has not been validated yet. The approach to be followed for its validation is similar to the one used for the Non-Recurring Costs, since quotes from US extruders will also be used as a comparative reference. However, the validation strategy in this case will include a model calibration approach, summarized below and described in more detail in Section 6.2.

Recalling from Section 4.3, the Overhead Cost estimation (per equation 4.30) requires an input for the so called "Overhead Upcharge" ($OH_{upcharge}$), an unknown charge, priced per unit mass (in USD/kg or USD/lb) that accounts for a series of costs that are incurred on a per unit mass basis (e.g. Press and Tooling Maintenance, Expendable Tooling, Consumables for Cleaning and Inspection [23], [25]). In order to have a reasonable estimate for this charge, the quotes received from US extruders will be used to calibrate the value of $OH_{upcharge}$. After that, the accuracy of the model will be assessed by comparing its cost predictions with quotes data.

## 6.2 Overhead Upcharge Calibration

### *6.2.1 Recurring Costs Quotes*

The eleven designs that were quoted for Tooling Costs (in Section 5.4) were also quoted for Recurring Costs by the extruders. Such designs are shown again here in Figure 6.1 for reference. The detailed drawings that were used for requesting the quotes are attached in

APPENDIX D: DETAILED DRAWINGS OF EXTRUDED SHAPES QUOTED. In short, all designs are made of Al 6063-T6, with a Mill Finish (i.e. as Extruded) on all surfaces. Standard tolerances per Aluminum Association Standards [55] were specified for all geometrical and metallurgical characteristics. Order quantities were indicated as appropriate to meet the minimum order requirements (in pounds of extrusion) of the various suppliers. All the parts were specified with a length of 40 inches (1016 mm) or greater, long enough to prevent additional charges for cutting in a secondary operation offline. In fact, the first four designs were also requested in a short length configuration, with a length of 10 inches (254 mm), with the sole purpose of having an idea of the secondary cut charge magnitude as compared to the baseline prices.

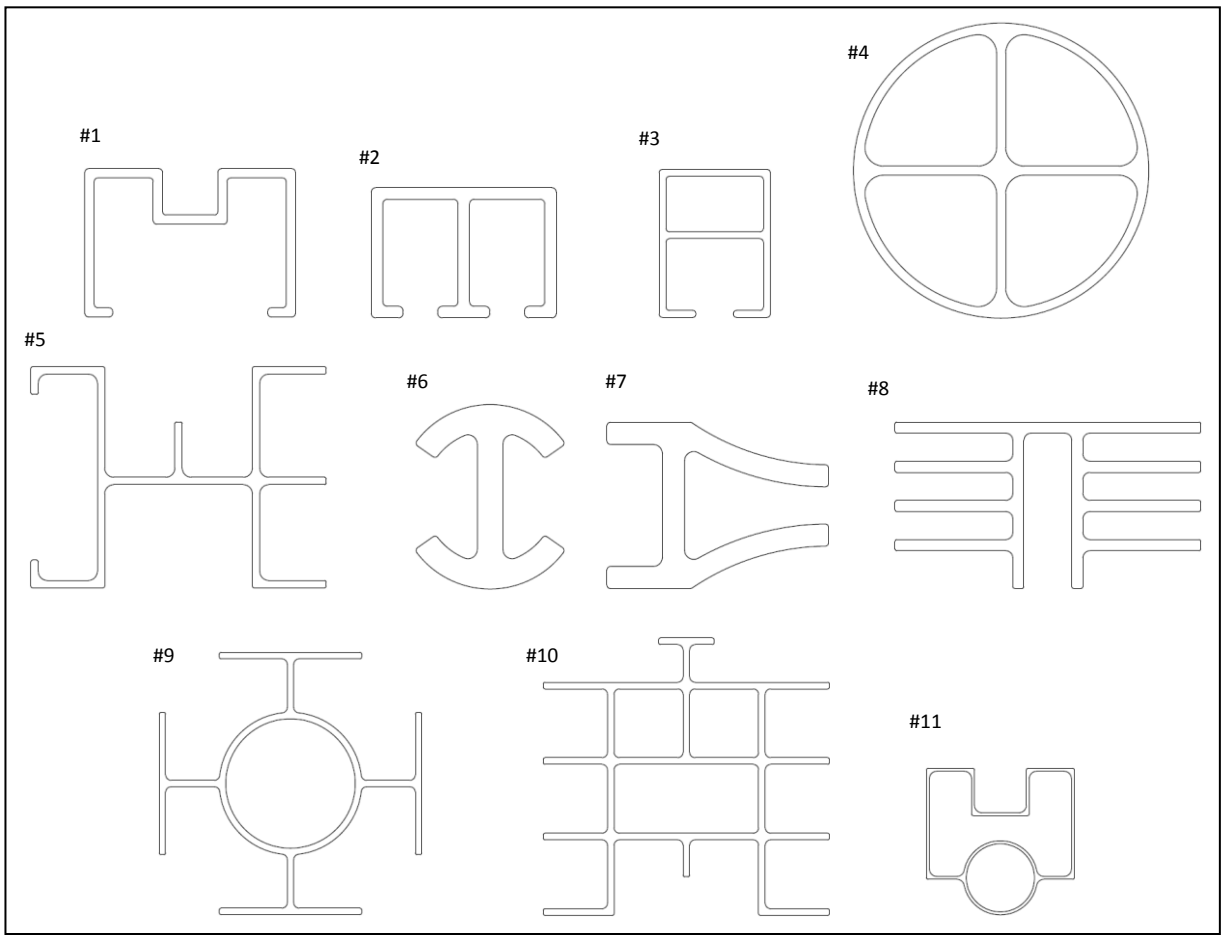


**Figure 6.1** Design Shapes Quoted (all drawn to same scale).

As it was mentioned before in Section 5.4, despite the fact that quotes were requested from eight different extruders in the US who had the technical capabilities to produce the

designs, only two companies provided quotes. Such companies will be denoted here again as "*Company A*" and "*Company B*", to prevent misuse of their pricing information. Before showing any of the quotes received for the eleven designs aforementioned, it is important to point out that US extruders usually quote Recurring Costs on a per unit mass basis (typically in $/lb). Moreover, they usually breakdown such costs into two components: 1) Metal Price, and 2) "Conversion Price". The former represents the Material Price ($M_{price}$), not the Material Cost ($M_{cost}$), and therefore it does not contain the cost of any scrap metal generated during the process (see definitions of $M_{price}$ and $M_{cost}$ in Section 4.4). The Conversion Price, on the other hand, accounts for the sum of Labor, Overhead, Scrap Metal and Other Direct Costs (e.g. Setup and Waste Time Costs).

Having said that, the Conversion Prices quoted by the extruders are reported in Table 6.1 along with relevant geometric parameters and order quantity, for reference. Note that *Company A* quoted all designs, except for design #2, whereas *Company B* only quoted designs #1, 2 and 4. Fortunately, *Company A* quoted cheaper than *Company B* in both designs they had in common (designs #1 and #4, 25% and 40% cheaper, respectively), which suggests that the Recurring Costs obtained from *Company A* are closer to the real costs. Thus, the quotes from *Company A* will be considered here as the "real costs" for calibration and validation purposes.

**Table 6.1** Conversion Prices Quotes.

| Design # | CCD (in) | $P_{ext}$ (in) | $A_f$ ($in^2$) | Length (in) | Qty | Shape Type | Conversion Price ($/lb), *Company A* | Conversion Price ($/lb), *Company B* |
|---|---|---|---|---|---|---|---|---|
| 1 | 6.96 | 33.04 | 4.166 | 200 | 200 | Solid | $0.490 | $0.65 |
| 2 | 6.10 | 33.06 | 5.222 | 200 | 21 | Semihollow Class 1 | N/A | $0.69 |
| 3 | 5.00 | 21.02 | 2.789 | 200 | 200 | Hollow Class 2 | $0.430 | N/A |
| 4 | 8.00 | 25.13 | 10.576 | 200 | 200 | Hollow Class 3 | $0.510 | $0.85 |
| 5 | 10.00 | 53.71 | 5.698 | 40 | 1000 | Solid | $0.510 | N/A |
| 6 | 5.00 | 23.79 | 8.377 | 40 | 500 | Solid | $0.510 | N/A |
| 7 | 7.50 | 31.43 | 9.547 | 40 | 400 | Semihollow Class 1 | $0.530 | N/A |
| 8 | 9.00 | 70.60 | 10.897 | 40 | 500 | Semihollow Class 2 | $0.550 | N/A |
| 9 | 8.08 | 53.23 | 5.792 | 100 | 400 | Hollow Class 1 | $0.530 | N/A |
| 10 | 10.00 | 58.33 | 8.003 | 100 | 400 | Hollow Class 3 | $0.530 | N/A |
| 11 | 5.00 | 17.03 | 1.697 | 50 | 2000 | Hollow Class 3 | $0.470 | N/A |

Regarding Metal Pricing, the quotes supplied by *Company A* and *Company B* differed slightly since they were quoted on a different month (i.e. market fluctuations caused a difference in pricing). The Metal Price quoted by *Company A* was $0.995/lb, corresponding to the month of September 2009, while the Metal Price quoted by *Company B* was $0.910/lb, corresponding to the month of June 2009. In order to be consistent with Conversion Prices, the Metal Price quoted by *Company A* ($0.995/lb) will be considered here for model validation purposes. Table 6.2 contains a summary of the Recurring Costs for the different designs, as quoted by *Company A*, where the Total Price (i.e. the sum of Conversion Price + Metal Price) is reported on a per unit mass basis ($/lb). The information in Table 6.2 will be the reference used for calibration and validation of the Recurring Costs Model.

**Table 6.2** Total Recurring Cost Quotes from *Company A*.

| Design # | CCD (in) | $P_{ext}$ (in) | $A_f$ ($in^2$) | Length (in) | Qty | Shape Type | Conversion Price ($/lb) | Metal Price ($/lb) | Total Price ($/lb) |
|---|---|---|---|---|---|---|---|---|---|
| 1 | 6.96 | 33.04 | 4.166 | 200 | 200 | Solid | $0.490 | $0.995 | $1.485 |
| 2 | 6.10 | 33.06 | 5.222 | 200 | 21 | Semihollow Class 1 | N/A | N/A | N/A |
| 3 | 5.00 | 21.02 | 2.789 | 200 | 200 | Hollow Class 2 | $0.430 | $0.995 | $1.425 |
| 4 | 8.00 | 25.13 | 10.576 | 200 | 200 | Hollow Class 3 | $0.510 | $0.995 | $1.505 |
| 5 | 10.00 | 53.71 | 5.698 | 40 | 1000 | Solid | $0.510 | $0.995 | $1.505 |
| 6 | 5.00 | 23.79 | 8.377 | 40 | 500 | Solid | $0.510 | $0.995 | $1.505 |
| 7 | 7.50 | 31.43 | 9.547 | 40 | 400 | Semihollow Class 1 | $0.530 | $0.995 | $1.525 |
| 8 | 9.00 | 70.60 | 10.897 | 40 | 500 | Semihollow Class 2 | $0.550 | $0.995 | $1.545 |
| 9 | 8.08 | 53.23 | 5.792 | 100 | 400 | Hollow Class 1 | $0.530 | $0.995 | $1.525 |
| 10 | 10.00 | 58.33 | 8.003 | 100 | 400 | Hollow Class 3 | $0.530 | $0.995 | $1.525 |
| 11 | 5.00 | 17.03 | 1.697 | 50 | 2000 | Hollow Class 3 | $0.470 | $0.995 | $1.465 |

As a reference only, the first four designs were also quoted in a short configuration, with a length of 10 inches (254 mm). The charge applied by each vendor for secondary cutting is somewhat different. While *Company A* Total Price quotes increase only by ~3-5% when the cut charge is included, *Company B* Total Price quotes increase by ~8-11% when such charge is included. Indeed, the basis for the cut charge applied by each vendor is different. *Company A* applies a fixed charge on a per piece basis of $0.20/piece, which becomes significant only if the

weight per unit length of the part is very low (which is unlikely, given the minimum thickness producibility limitations on Hot Extrusion [22], [24]) or if the cut length is very short (i.e. if $L_{part}$<3 inches, according to hand calculations). On the other hand, *Company B* applies a fixed charge in a per unit mass basis of $0.17/lb, which is relatively significant when compared with a typical Conversion Price of ~$0.5/lb, adding ~34% to the latter. Thus, whenever the length of the part is so that secondary cutting is likely to be required (i.e. $L_{part}$<3 ft, per Section 4.2), the cost estimates obtained from the model developed in this thesis should be used with caution. If necessary, a more accurate and consistent prediction of secondary cut-to-length costs should be obtained by means of another FBC Model for that process. Such task is beyond the scope of this thesis.

### *6.2.2 Overhead Upcharge Calibration Procedure*

The Manufacturing Cost Model developed in this thesis was implemented by the author in a computer spreadsheet, which includes the Recurring Costs Model described in Chapter 4, and the Non-Recurring Costs Model described in Chapter 5. The spreadsheet is included as a supplemental file for this thesis, as described in APPENDIX E: HOT EXTRUSION FBC SPREADSHEET. As it was mentioned before, the approach that was followed to calibrate the Recurring Costs Model consisted in calibrating the overhead upcharge ($OH_{upcharge}$) using the cost data from the quotes shown in Table 6.2. Since the spreadsheet follows the taxonomy described in Chapters 2 and 4, where Recurring Costs are broken down into Material, Labor, Overhead, Setup and Waste Time Costs, it was necessary to add to the spreadsheet the extruders' taxonomy as well, which divides the Recurring Costs into Conversion Price and Material Price. That was readily done using the following equation:

$$Conversion\ Price = \frac{Piece\ Part\ Cost}{m_{part}} - M_{price} \qquad (6.1)$$

where the Conversion Price units are US dollars per unit mass ($/kg or $/lb), the Piece Part Cost (calculated by equation 4.49) is in US dollars, $m_{part}$ is the mass of the part (in kg or lb), and $M_{price}$

is the Material Price (in $/kg or $/lb), estimated by equation 4.43. In order to be consistent with the quotes' time frame, the Material Price ($M_{price}$) was calculated using market data from September 2009. Such data was obtained from LME [51] and AMM [49], and is broken down as follows:

- LME HG Price= $1.834/kg ($0.832/lb)
- Midwest Premium= $0.119/kg ($0.054/lb)
- Billet Upcharge= $0.209/kg ($0.095/lb)
- Total Raw Material Price ($M_{price}$)= $2.162/kg ($0.981/lb)

Note that the Material Price calculated ($0.981/lb) is fairly close to the one quoted by *Company A* ($0.995/lb), with a difference of only 1.4%. Thus, the model for estimating the Material Price (by equation 4.43) seems adequate.

With all these proper taxonomy transformations in place, and assuming a Batch Size ($N_{parts\_batch}$) equal to the Order Quantity[12] (i.e. all the parts ordered for each design are produced in a single batch run), the Overhead Upcharge ($OH_{upcharge}$) was calibrated for every single design that was quoted (except for design #2, which was disregarded as it was not quoted by *Company A*). The calibration procedure was performed as follows: For each design, the value of $OH_{upcharge}$ was varied until the Conversion Price predicted by the Model was equal to the Conversion Price from the Quotes. This task was carried out easily in Excel 2007 by using the "Goal Seek" Function[13] within the "What-if-Analysis" Tool. The resulting values of $OH_{upcharge}$ for all designs are shown in Table 6.3, where it can be seen that they range from $0.34/kg ($0.15/lb) to $0.63/kg ($0.29/lb). The variation is significant, suggesting that this charge is dependent on some parameter(s) of each design.

[12] This was considered a reasonable assumption, as the resulting cycle time per batch predicted for all designs ranged from 0.62 to 2.60 hrs.

[13] The "Goal Seek" function in Excel finds the right input in one cell (e.g. $OH_{upcharge}$) when you know the result you want in another (e.g. Conversion Price).

**Table 6.3** Calibrated Values of OH Upcharge for all Designs Quoted.

| Design # | CCD (in) | $P_{ext}$ (in) | $A_f$ ($in^2$) | Length (in) | Qty | Billet Family (in) | Billet Diameter (mm) | OH Upcharge ($/kg) | OH Upcharge ($/lb) |
|---|---|---|---|---|---|---|---|---|---|
| 1 | 6.96 | 33.04 | 4.166 | 200 | 200 | 9 | 229 | $0.48 | $0.22 |
| 2 | 6.10 | 33.06 | 5.222 | 200 | 21 | N/A | N/A | N/A | N/A |
| 3 | 5.00 | 21.02 | 2.789 | 200 | 200 | 6 | 160 | $0.34 | $0.15 |
| 4 | 8.00 | 25.13 | 10.576 | 200 | 200 | 12 | 305 | $0.54 | $0.24 |
| 5 | 10.00 | 53.71 | 5.698 | 40 | 1000 | 13 | 330 | $0.55 | $0.25 |
| 6 | 5.00 | 23.79 | 8.377 | 40 | 500 | 11 | 279 | $0.53 | $0.24 |
| 7 | 7.50 | 31.43 | 9.547 | 40 | 400 | 13 | 330 | $0.50 | $0.23 |
| 8 | 9.00 | 70.60 | 10.897 | 40 | 500 | 13 | 330 | $0.63 | $0.29 |
| 9 | 8.08 | 53.23 | 5.792 | 100 | 400 | 10 | 254 | $0.58 | $0.26 |
| 10 | 10.00 | 58.33 | 8.003 | 100 | 400 | 13 | 330 | $0.58 | $0.26 |
| 11 | 5.00 | 17.03 | 1.697 | 50 | 2000 | 6 | 160 | $0.45 | $0.20 |

An inspection of the correlations observed between the Overhead Upcharge and the parameters of each design revealed that the Billet Diameter ($D_o$) is the main driver of such charge. The relationship between those variables is depicted in Figure 6.2, where it is shown that $OH_{upcharge}$ is directly proportional to $D_o$, which makes sense as larger presses tend to have a higher overhead cost. The curve fit shown in Figure 6.2 shows that a simple linear equation does a decent job in predicting a ballpark value for $OH_{upcharge}$ from $D_o$. Hence, in the absence of more specific data, the value of the Overhead Upcharge can be estimated by:

$$OH_{upcharge} \approx 0.001 D_o + 0.2606 \quad (6.2)$$

where $OH_{upcharge}$ is in $/kg and $D_o$ is in millimeters. Having obtained this empirical equation to predict the Overhead Upcharge, the entire Recurring Costs Model is now ready to be validated against Quotes Data.

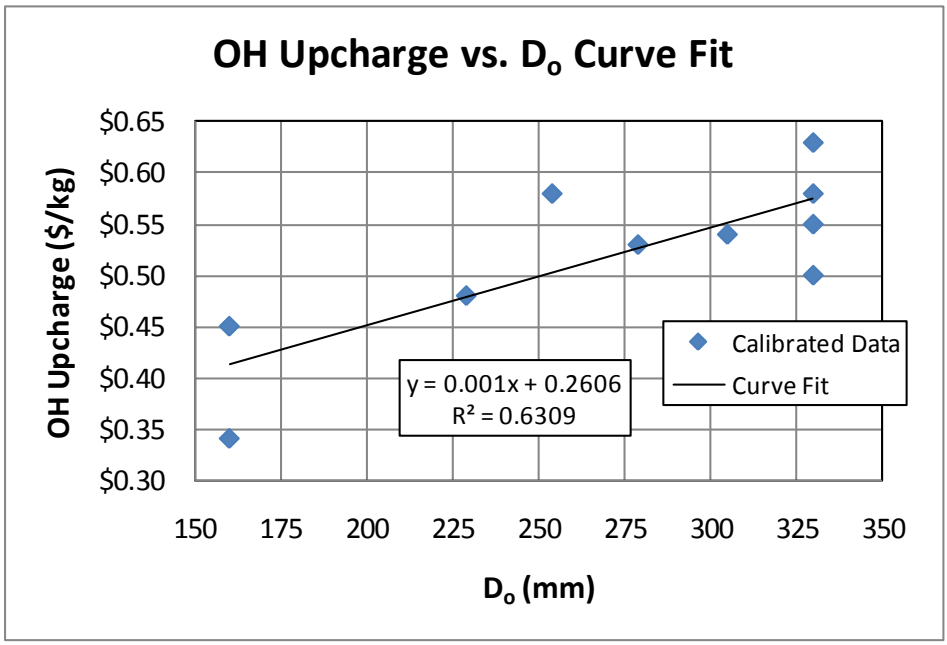


**Figure 6.2** Correlation between OH Upcharge and Billet Diameter.

## 6.3 Recurring Costs Model Validation

The spreadsheet containing the FBC Model (including equation 6.2 for $OH_{upcharge}$) was used to estimate the Manufacturing Cost of every single design that was quoted. The resulting Recurring Costs are compared here against quotes data, using the extruders' taxonomy (i.e. Total Price=Conversion Price + Material Price). As it was shown in the previous section, the Material Price estimated by the model was in excellent agreement with the one quoted by the extruders, with only 1.4% of difference. Regarding Conversion Prices, Table 6.4 shows a comparison between predicted values (by the model) and actual values (from quotes). Note that the percentage of error ranges from -8% to 7%, with the average of the absolute error being only 4%. Furthermore, the comparison of Total Prices (in Table 6.5) shows that the percentage of error ranges from -2% to 3%, with the average of the absolute error being only 1%. Thus, the model predictions are in excellent agreement with actual data (quotes).

**Table 6.4** Comparison of Actual (Quotes) vs. Predicted (Model) Conversion Prices.

| Design # | Conversion Price ($/lb), *Quotes* | Conversion Price ($/lb), *Model* | % Error | Abs (% Error) |
|---|---|---|---|---|
| 1 | $0.490 | $0.496 | -1% | 1% |
| 2 | N/A | N/A | N/A | N/A |
| 3 | $0.430 | $0.465 | -8% | 8% |
| 4 | $0.510 | $0.520 | -2% | 2% |
| 5 | $0.510 | $0.528 | -4% | 4% |
| 6 | $0.510 | $0.516 | -1% | 1% |
| 7 | $0.530 | $0.570 | -8% | 8% |
| 8 | $0.550 | $0.532 | 3% | 3% |
| 9 | $0.530 | $0.493 | 7% | 7% |
| 10 | $0.530 | $0.537 | -1% | 1% |
| 11 | $0.470 | $0.457 | 3% | 3% |
| **MIN** | $0.430 | $0.457 | -8% | 1% |
| **MAX** | $0.550 | $0.570 | 7% | 8% |
| **AVERAGE** | $0.506 | $0.511 | -1% | 4% |
| **STD DEV** | $0.035 | $0.034 | 5% | 3% |

**Table 6.5** Comparison of Actual (Quotes) vs. Predicted (Model) Total Prices.

| Design # | Total Price ($/lb), *Quotes* | Total Price ($/lb), *Model* | % Error | Abs (% Error) |
|---|---|---|---|---|
| 1 | $1.485 | $1.477 | 1% | 1% |
| 2 | N/A | N/A | N/A | N/A |
| 3 | $1.425 | $1.446 | -1% | 1% |
| 4 | $1.505 | $1.501 | 0.3% | 0.3% |
| 5 | $1.505 | $1.509 | -0.3% | 0.3% |
| 6 | $1.505 | $1.497 | 1% | 1% |
| 7 | $1.525 | $1.551 | -2% | 2% |
| 8 | $1.545 | $1.513 | 2% | 2% |
| 9 | $1.525 | $1.474 | 3% | 3% |
| 10 | $1.525 | $1.518 | 0.5% | 0.5% |
| 11 | $1.465 | $1.438 | 2% | 2% |
| **MIN** | $1.425 | $1.438 | -2% | 0.3% |
| **MAX** | $1.545 | $1.551 | 3% | 3% |
| **AVERAGE** | $1.501 | $1.492 | 1% | 1% |
| **STD DEV** | $0.035 | $0.034 | 2% | 1% |

The information in Table 6.5 can be presented in a graphical way to visualize the trends of the Total Price against some of the main Geometric Cost Drivers (GCDs). It is important to remind the reader that the Total Price is nothing else than the Piece Part Cost normalized by the mass of the part. It is convenient to plot the Piece Part Costs in a normalized format (in $/lb or $/kg), as this makes the comparisons easier between the relative cost of each design, regardless of its mass (or length). An inspection of the correlation between the Total Price and the GCDs of each part revealed that the CCD, the External Perimeter ($P_{ext}$) and the Cross Sectional Area ($A_f$) are the ones with the highest influence. The trends of Total Price (i.e. Normalized Piece Part Cost) vs. each of these GCDs are shown in Figure 6.3, Figure 6.4, and Figure 6.5, respectively, for both the FBC Model and the quotes. The plots show that, for the most part, the FBC Model follows fairly close the trends observed in the actual costs obtained from the quotes. The slight discrepancies observed in the trends are due to the fact that none of these GCDs alone is responsible for the Total Price of the part, as the latter is a function of other GCDs as well. Furthermore, for clarity purposes, the vertical axis scale in the plots has a very high resolution, so any minor discrepancies are greatly magnified.

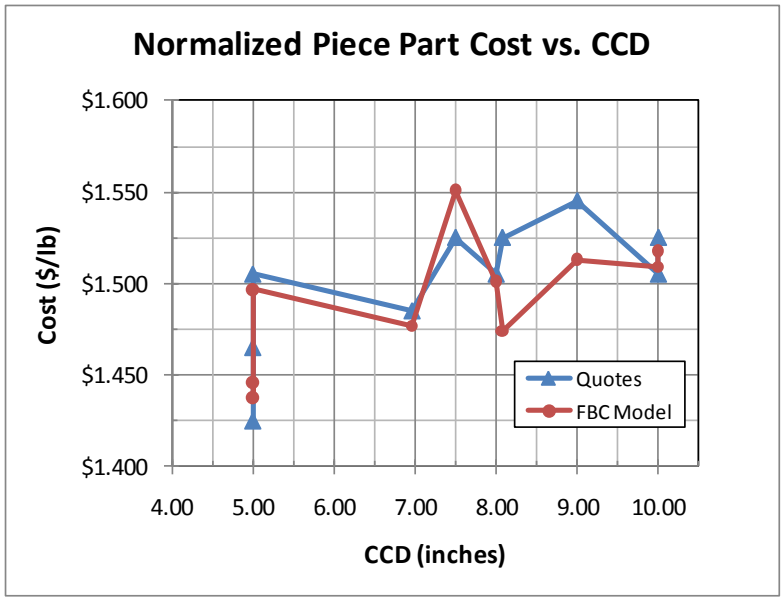


**Figure 6.3** Normalized Piece Part Cost vs. CCD Trend.

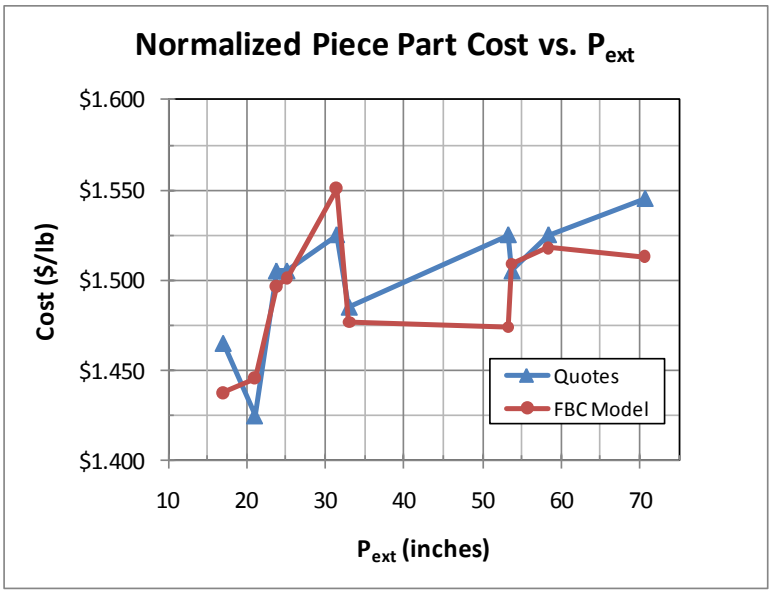


**Figure 6.4** Normalized Piece Part Cost vs. External Perimeter Trend.

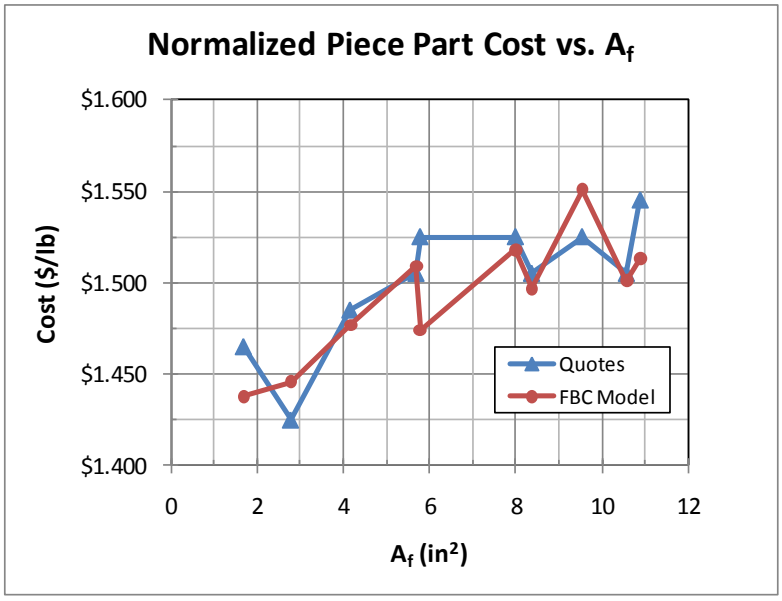


**Figure 6.5** Normalized Piece Part Cost vs. Cross Sectional Area Trend.

In order to make an assessment of the accuracy of the Total Manufacturing Cost Model (i.e. Recurring + Non-Recurring Costs[14]), the Piece Part Cost (in USD) and the Amortized

[14] Recall from Section 2.2.1 that Manufacturing Cost = Piece Part Cost + Amortized Investment.

Investment of each design are reported in Table 6.6, assuming a Total Production Volume of 2000 parts (arbitrarily defined) to amortize the Tooling Costs (which were reported in the previous chapter in Table 5.10). Note that the percentage of error of the Manufacturing Cost is within 3% for all designs quoted. Obviously, such percentage of error is dependent on the Total Production Volume (which was assumed to be 2000 in this case), as the Tooling Costs errors tend to be more significant with smaller volumes. However, even in the hypothetical (and unlikely) worst-case scenario of having only 1 part to amortize the Tooling Cost, the Manufacturing Cost error of the FBC Model would be practically the same as the error in the Tooling Cost Model, which would probably be within 20%, as shown before in Table 5.10. Thus, the lower bound for the Manufacturing Cost Model Accuracy is equal to the Tooling Cost Model Accuracy (i.e. error within 20%), while the upper bound is equal to the Piece Part Cost Model Accuracy (i.e. error within 3%).

**Table 6.6** Actual vs. Predicted Manufacturing Cost (Production Volume=2000).

| Design # | Part Mass (lb) | Piece Part Cost ($), *Quotes* | Piece Part Cost ($), *Model* | Amortized Investment ($), *Quotes* | Amortized Investment ($), *Model* | Manufacturing Cost ($), *Quotes* | Manufacturing Cost ($), *Model* | % Error |
|---|---|---|---|---|---|---|---|---|
| 1 | 81.28 | $120.71 | $120.06 | $1.14 | $1.57 | $121.84 | $121.63 | 0.2% |
| 2 | N/A | N/A | N/A | $1.80 | $1.47 | N/A | N/A | N/A |
| 3 | 54.41 | $77.53 | $78.68 | $1.22 | $1.29 | $78.76 | $79.96 | -2% |
| 4 | 206.33 | $310.52 | $309.70 | $3.86 | $3.32 | $314.39 | $313.02 | 0.4% |
| 5 | 22.22 | $33.44 | $33.53 | $2.50 | $2.28 | $35.94 | $35.82 | 0.4% |
| 6 | 32.69 | $49.20 | $48.94 | $1.43 | $1.13 | $50.64 | $50.07 | 1% |
| 7 | 37.26 | $56.82 | $57.79 | $1.64 | $1.74 | $58.46 | $59.53 | -2% |
| 8 | 42.50 | $65.67 | $64.31 | $2.50 | $2.32 | $68.17 | $66.63 | 2% |
| 9 | 56.50 | $86.17 | $83.29 | $2.10 | $2.24 | $88.27 | $85.52 | 3% |
| 10 | 78.06 | $119.05 | $118.50 | $2.99 | $3.58 | $122.04 | $122.09 | -0.04% |
| 11 | 8.27 | $12.11 | $11.89 | $1.46 | $1.56 | $13.57 | $13.44 | 1% |

The results presented in Table 6.6 are depicted in a graphical way in Figure 6.6 and Figure 6.7, for the Piece Part Cost and the Manufacturing Cost, respectively. Note in Figure 6.6 that the relationship between Piece Part Cost and Part Mass is fairly linear. This is mainly due to the fact that, in all designs evaluated, the Material Cost dominates the Recurring Costs, representing about 82% to 86% of the Piece Part Cost. The same is true for the Manufacturing

Costs depicted in Figure 6.7, since the Amortized Investment is not really significant in this case. It must be emphasized that that the linear trends aforementioned would not necessarily hold for a wider range of designs, such as parts made of other Aluminum Alloys, smaller Production Volumes, and different combinations of numerical values of the GCDs. Moreover, the highly fluctuating nature of Raw Material Prices in the market may definitely have an impact on the dominance of the Material Cost over the rest of the costs.

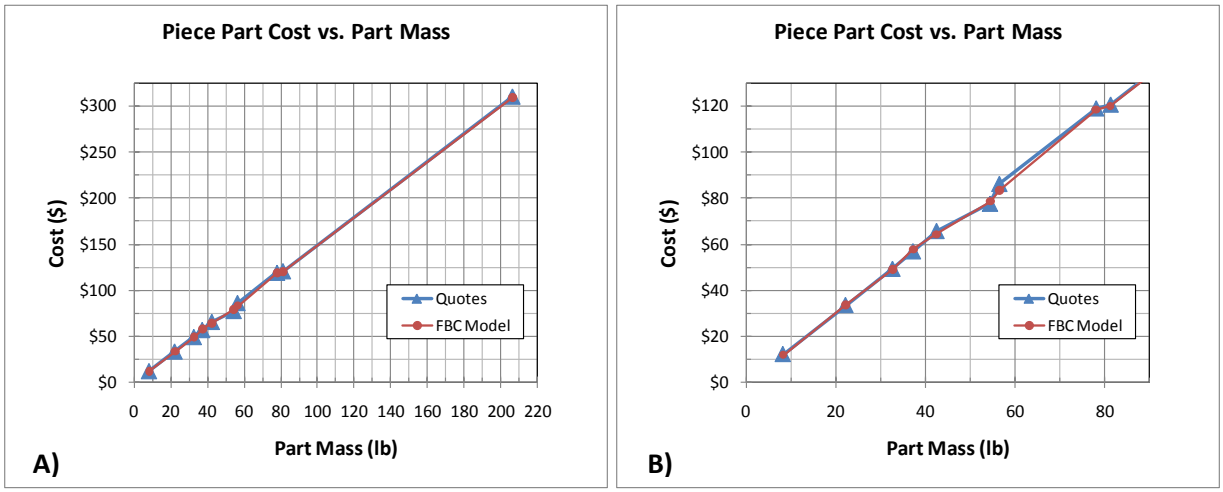


**Figure 6.6** Piece Part Cost vs. Part Mass. A) All quoted designs; B) Zoom in for clarity.

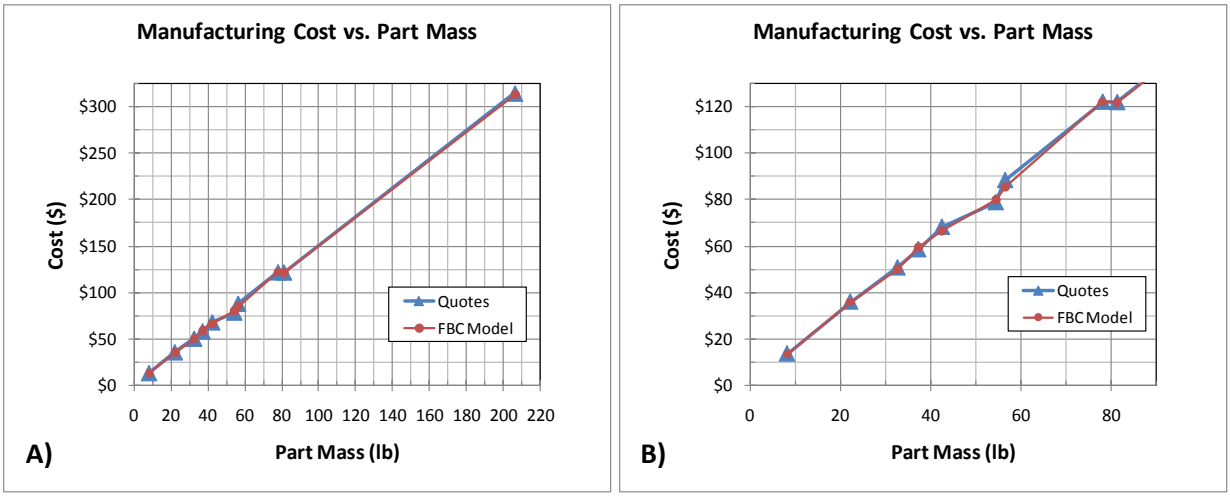


**Figure 6.7** Manufacturing Cost vs. Part Mass. A) All quoted designs; B) Zoom in for clarity.

A summary of the contributions of each of the Recurring and Non-Recurring Costs into the Manufacturing Cost on all designs evaluated is included in Table 6.7, as obtained from the FBC Model. Note that, as mentioned before, the Material Cost is the dominant factor in the Manufacturing Cost, representing about 76% to 84% of the Manufacturing Cost. The Direct Overhead Cost is the next most significant item, contributing with 12% to 17% of the Manufacturing Cost, and finally the Amortized Investment ranges from 1% to 12% of the Manufacturing Cost. In most of the designs evaluated, Labor Costs constitute less than 1% of the Manufacturing Cost, as the cycle times predicted were very short, ranging from 4.2 to 32.7 sec per part. This is remarkable, considering that the extrusion exit speed estimations made by the model seem to be conservative, as they ranged from 16 m/min to 35 m/min (as compared to the typical range of 35 m/min to 80 m/min in Al-6063 extrusions, per Table 4.1). Likewise, the other direct costs (i.e. Setup Cost and Waste Time Cost) represented less than 1% of the Manufacturing Cost.

**Table 6.7** Manufacturing Cost Breakdown in Designs Evaluated (Model Predictions).

| DESIGN # | CONTRIBUTION TO MANUFACTURING COST | | | | | |
|---|---|---|---|---|---|---|
| | Material (%) | Direct Overhead (%) | Labor (%) | Setup (%) | Waste Time (%) | Amortized Investment (%) |
| 1 | 84% | 15% | <1% | <1% | <1% | 1% |
| 2 | N/A | N/A | N/A | N/A | N/A | N/A |
| 3 | 84% | 13% | 1% | <1% | <1% | 2% |
| 4 | 82% | 17% | <1% | <1% | <1% | 1% |
| 5 | 77% | 17% | <1% | <1% | <1% | 6% |
| 6 | 82% | 16% | <1% | <1% | <1% | 2% |
| 7 | 80% | 17% | <1% | <1% | <1% | 3% |
| 8 | 79% | 17% | <1% | <1% | <1% | 4% |
| 9 | 81% | 16% | <1% | <1% | <1% | 3% |
| 10 | 80% | 17% | <1% | <1% | <1% | 3% |
| 11 | 76% | 12% | <1% | <1% | <1% | 12% |
| **MIN** | 76% | 12% | <1% | <1% | <1% | 1% |
| **MAX** | 84% | 17% | 1% | <1% | <1% | 12% |
| **MEAN** | 81% | 16% | <1% | <1% | <1% | 4% |
| **STD DEV** | 3% | 2% | N/A | N/A | N/A | 3% |

It must be noted that the significance reported above for the various cost items is based exclusively on the results observed for the sample of designs quoted, which were all made of Al-6063. In the case of more difficult-to-extrude alloys (e.g. hard alloys), the Overhead, Labor and Tooling Costs may become more significant in the Manufacturing Cost. Also, as the Total Production Volume is decreased from the one arbitrarily assumed in this case (2000 parts) the Amortized Investment becomes a bigger contributor to the Manufacturing Cost.

Finally, it is important to remark that the Piece Part Cost predicted by the FBC model developed in this thesis is somehow conservative, as it contains Extruder's Indirect Overhead and Profit implicit in the calibrated Overhead Upcharge that was obtained from quotes. However, according to FBC expert's opinion (Dr. Mike Philpott, Associate Professor, University of Illinois at Urbana-Champaign), it is common practice in the FBC community to assume that the user of the FBC Model will not make the part in-house, but rather buy it to an external supplier (i.e. an extruder). Hence, the "Product Price" quoted by extruders represents, in some way, a "Manufacturing Cost" for the buyer, especially if a Make vs. Buy Assessment is made.

# CHAPTER 7: CONCLUSIONS

## 7.1 Thesis Research Conclusions

The research work documented in this thesis accomplished the successful creation, implementation and validation of a Manufacturing Cost Model for Hot Extruded parts made of Aluminum Alloys, using Feature Based Costing (FBC) techniques. The Cost Model User Inputs consist of the following:

A. *Geometric Cost Drivers* (GCDs)
    1) Circumscribing Circle Diameter (*CCD*)
    2) Cross Sectional Area ($A_f$)
    3) External Perimeter ($P_{ext}$)
    4) Internal Perimeter ($P_{int}$)
    5) Maximum Wall Thickness ($THK_{max}$)
    6) Part Length ($L_{part}$)
    7) Shape Type (Solid, Semihollow Class 1, Semihollow Class 2, Hollow Class 1, etc.)
    8) Number of Voids ($N_{voids}$)

B. *Non-Geometric Cost Drivers* (NGCDs)
    1) Material (Aluminum Alloys Only)
    2) Batch Size ($N_{parts\_batch}$)
    3) Annual Production Volume ($N_{annual}$)
    4) Production Years ($P_{years}$)

Likewise, the main outputs of the Cost Model include the Piece Part Cost (broken down into its various recurring costs components), Amortized Investment and ultimately the Manufacturing Cost. In order to implement the FBC Model (in a computer spreadsheet), it was necessary to gather a considerable amount of information on material properties (of the most commonly extruded Aluminum Alloys) and technical specifications of modern presses in the

market (for Direct Extrusion of Aluminum Alloys). Such data is now stored in the form of Databases (a.k.a. Tables) in the FBC Spreadsheet attached as a supplemental file (see APPENDIX E: HOT EXTRUSION FBC SPREADSHEET).

The FBC Model estimations rely on prescribed (assumed) inputs for a number of variables that are necessary to calculate the various costs involved in Hot Extrusion. Such variables and their assumed values are:

- Billet Butt Discard Percentage (10%)
- Runout Table Length (35 m)
- Length of Scrapped Ends (after stretching) on each continuous extrusion (2 m)
- Quality Scrap Percentage (6%)
- Ram Acceleration Time per Billet (7 sec)
- Setup Time per Batch (1 min)
- Waste Time per Batch (7 min)
- Extrusion Line Crew Size (3 operators)
- Labor Rate (US $14.92/hr)
- Overhead Rate (US $45/hr)

It must be emphasized that the assumed values for all the variables above are based on state of the art data available in the literature and/or recommendations from recognized experts in the field. Yet, such prescribed values must be kept up to date with extrusion technology innovations in the future.

The research work performed in this thesis illustrated the difficulty involved in selecting the optimal combination of press and billet size to extrude a given shape with the maximum productivity at the lowest possible cost and without violating any of the producibility constraints. An algorithm to solve the optimization problem described above was proposed in the form of a flow diagram that should be relatively easy to implement in a computer program. Furthermore, an alternative simplified press selection process was developed and implemented in the FBC Spreadsheet mentioned before.

Another important challenge encountered in this research project consisted in the extrusion speed estimation, especially due to the hot shortness (i.e. surface cracking) limit that the material imposes on the process. The complexity of the thermomechanical phenomena occurring in the hot extrusion process makes the corresponding governing equations fairly complex. Furthermore, even though simplified models relating the extrusion exit temperature to the extrusion speed do exist in the literature, no guidelines seem to be available regarding exit temperature limits to prevent hot shortness. An approach was proposed in this thesis (and implemented in the FBC Spreadsheet mentioned above) to estimate a "pseudo-limit" for the exit temperature (based on a series of assumptions deemed reasonable) and then solve for the corresponding extrusion exit speed. The validation of this specific part of the FBC model was beyond the scope of this thesis.

The cost model was successfully validated by showing close agreement between its cost predictions and actual cost data obtained from US extruders' quotations of eleven different designs, covering a fairly large domain of the GCDs. The errors observed in Piece Part Costs predictions were within 3%, whereas the ones observed in Tooling Costs were within 20% (for the most part). Fortunately, as the Total Production Volume increases to typical levels, the error in Tooling Costs predictions is wiped out (as a result of amortization of Non-Recurring Costs) and becomes much less significant for the accuracy of the Manufacturing Cost estimations.

The analysis of the FBC model predictions for the eleven designs aforementioned showed that the Material Cost is the dominant factor in the Manufacturing Cost, representing about 82% to 86% of the Piece Part Cost, and 76% to 84% of the Manufacturing Cost. The Direct Overhead Cost was the next most significant item, contributing with 12% to 17% of the Manufacturing Cost, and finally the Amortized Investment ranged from 1% to 12% of the Manufacturing Cost. Labor Costs constituted less than 1% of the Manufacturing Cost, as the cycle times predicted were very short (ranging from 4.2 to 32.7 sec per part). Likewise, the other direct costs (i.e. Setup Cost and Waste Time Cost) represented less than 1% of the Manufacturing Cost. Nevertheless, the significance reported above for the various cost items is

based exclusively on the results observed for the sample of designs quoted, which were all made of Al-6063. In the case of more difficult-to-extrude alloys (e.g. hard alloys), the Overhead, Labor and Tooling Costs may become more significant in the Manufacturing Cost. Also, as the Total Production Volume is decreased from the one arbitrarily assumed (2000 parts) the Amortized Investment becomes a bigger contributor to the Manufacturing Cost. Moreover, the highly fluctuating nature of Raw Material Prices in the market may definitely have an impact on the dominance of the Material Cost.

## 7.2 Future Work Recommendations

While the research work performed in this thesis covered a lot of ground regarding "Feature Based Costing of Extruded Parts", it is virtually impossible to address every single detail related to the topic. Therefore, the objective of this last section is to outline the recommended future work on this field, from the author's perspective.

First of all, the cost model developed in this thesis does not consider the effect of costs incurred on secondary cut-off operations, which are usually required whenever the length of the part is shorter than 3 ft (914 mm), as discussed before. While some (limited) data obtained from extruders (via quotes) on short design configurations suggests that the secondary cut-off operation costs may not be significant compared to the primary extrusion process costs, further research on this matter is considered necessary.

Secondly, based on discussions held with extruders during the request-for-quotation process, surface finish plays an important role in the manufacturing cost of aluminum extrusions. The FBC model developed in this thesis does not take into account the effect of such secondary operation, assuming a mill (as extruded) surface finish. Alternative surface finishing options (e.g. Anodize, Paint) could be incorporated in the model in the future, as an optional secondary operation cost.

As regards to improvements in the FBC model developed, the empirical Tooling Cost equation could be refined in the future by gathering more quotes to improve the regression accuracy. Alternatively, a Feature Based Cost Model for the tooling manufacturing itself could be developed, especially if more accurate cost predictions are required for the Amortized Investment (e.g. Low Production Volumes). Furthermore, the Tooling Costs for extrusion of hard alloys (e.g. 2XXX and 7XXX aluminum alloys) should be investigated, as the dies involved are usually of the "Shaped" type design, which are more difficult and costly to manufacture than the "Flat-face Dies" used for soft aluminum alloys.

Another area of opportunity for future work is the incorporation of Multi-hole Dies option in the FBC Model. This would certainly add to the complexity of the optimal press selection and billet sizing process, adding one more independent variable to the problem (the number of holes in the die). Also, if Multi-hole Dies are considered, additional constraints should be included in the model, specifically the "Table Weight" capacity of the Runout Table and handling equipment, as well as some "economic feasibility criterion" to decide if it is worth it or not to produce multiple strands in a die (given the extrusion handling difficulties it implies) based on the anticipated production volume. Additionally, the Tooling Cost would likely be sensitive to the number of strands (a.k.a. holes) in the die; therefore, it should be considered in the optimization process.

Regarding the Extrusion Press Database developed in this thesis, additional data should be added to cover a larger domain of extrusion's CCD. While the billet diameter range in the press database (from 3.5 to 18 inches) already covers the majority of aluminum extrusion work (i.e. CCD between 1 and 10 inches), larger presses with billet diameters up to 29 inches (737 mm) are known to exist in the market. The incorporation of such presses in the database would further extend the applicability of the FBC Spreadsheet (attached to this thesis) to those extreme cases where the CCD and/or the Cross Sectional Area of the extrusion demand the use of a press with a billet diameter larger than 18 inches (457 mm).

To complement the Manufacturing Cost Estimation, an enhanced FBC tool should include Producibility Constraints and a feedback mechanism that lets the user know what

makes the design unfeasible to manufacture (if that is the case). Producibility guidelines for hot extrusion are documented extensively in the literature in various sources like [3], [8], [22], [24], [26], [43], [55] and [60].

In order to automate the input of GCDs into the Cost Model, an interface with a CAD software is necessary, so that the relevant geometric parameters can be extracted from the CAD Model and imported into the Cost Model, without the need of manual input from the user. Such integration process is patented in [20]. If the automation task aforementioned is pursued in the future, it should consider the creation of an algorithm to automatically classify the Shape Type of the extrusion (e.g. Solid, Semihollow Class 1, Semihollow Class 2, etc.), based on the corresponding criteria documented in this thesis.

Finally, the FBC Model developed here for Hot Extrusion of Aluminum Alloys could be adapted to extend its use for other commonly extruded materials like Steel, Copper, Lead, Tin, Zinc, Magnesium, Titanium, and others. In doing so, not only would the corresponding material properties have to be gathered, but the differences in processing, equipment, tooling and overall cost modeling assumptions would have to be reviewed. Likewise, the development of FBC Models for other extrusion process types like Cold Extrusion, Impact Extrusion, Hydrostatic Extrusion, Coextrusion, Equal Channel Angular Extrusion and even Indirect (Backwards) Hot Extrusion would require a detailed understanding of the characteristics of each process. In any of the cases mentioned above, the research work documented in this thesis should be helpful as a reference.

# APPENDIX A: EXIT TEMPERATURE VS. EXTRUSION RATIO

The following numerical example was performed in Mathcad Software, as a sanity check to verify the value of the extrusion ratio *R* that minimizes *ΔT* (and hence the exit temperature):

**Table A.1** Input data used in numerical example.

| Material | Aluminum 6063 |
|---|---|
| Extrusion Exit Speed, $v_f$ (m/min) | 80 |
| Billet Length, $L_o$ (mm) | 810 |
| Billet Diameter, $D_o$ (mm) | 210 |
| Die Land Length, s (mm) | 3 |
| Strength Coefficient, C (MPa) | 24 |
| Strain Rate Sensitivity Exponent, m | 0.17 |
| Density, ρ (kg/m$^3$) | 2700 |
| Specific Heat, $c_p$ (J/kg-°C) | 900 |
| Thermal Diffusivity, α (m$^2$/s) | 8.23E-05 |

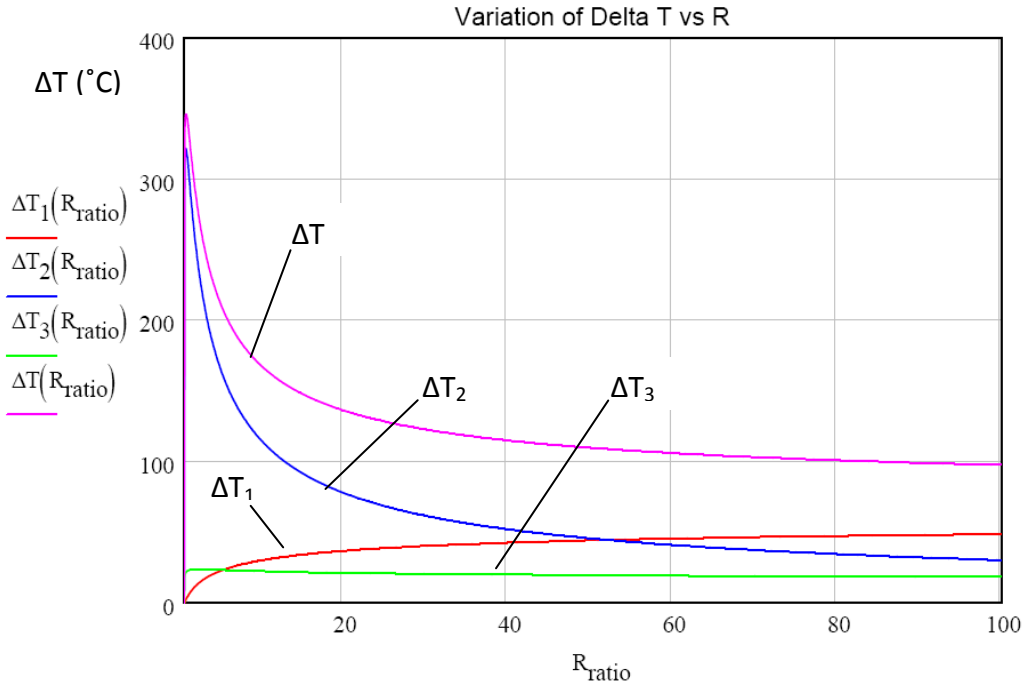


**Figure A.1** Variation of *ΔT* with Extrusion Ratio *R*.

Note in Figure A.1 that the total $\Delta T$ is always decreasing as $R$ increases (in the range of $R$=10-100). Thus, the minimum $\Delta T$ in that range occurs at $R$=100. The global maximum for $\Delta T$ occurs at $R$≈1.3. At low values of $R$ (0-10), $\Delta T_2$ dominates the total $\Delta T$, while at higher values of $R$ (30-100) the three $\Delta T$'s have significant contributions to the total $\Delta T$. Also, additional calculations were carried out with different values of billet length, $L_o$ and the decreasing trend of $\Delta T$ vs. $R$ was maintained. As $L_o$ increases, the $\Delta T_2$ term becomes more dominant; conversely, as $L_o$ decreases, the $\Delta T_2$ term becomes less dominant. For very low values of $L_o$ (around 8 mm), the trend of $\Delta T$ changes, and it increases with $R$, because $\Delta T_1$ becomes dominant. However, such low values of $L_o$ are impractical, so it can be concluded that $\Delta T$ is practically always decreasing as $R$ increases.

# APPENDIX B: EXTRUSION PRESS DATABASE

The data compiled in Table B.1 below (3 pages) contains the main technical specifications of direct hot extrusion presses available for aluminum alloys, as provided by different press manufacturers in the world (SMS, UBE, THMC, TS PLZEN). For some presses, the Dead-Cycle Time and Minimum Billet Length data was not available directly from the press manufacturer, so it was estimated based on the assumptions and methods described in Sections 4.1.3 and 4.2.1. The data is sorted in descending order of billet diameter.

**Table B.1** Extrusion Press Database

| Machine Name | Press Force Capacity (MN) | Press Force Capacity (US ton) | Billet Diameter (mm) | Billet Diameter (in) | Max Billet Length (mm) | Min Billet Length (mm) | Max Extrusion Speed (mm/s) | Dead Cycle Time (sec) |
|---|---|---|---|---|---|---|---|---|
| THMC AL 75-460 | 75 | 8431 | 460 | 18.1 | 1650 | 825 | 20.0 | 22.7 |
| SMS 101-18 | 101 | 11308 | 457 | 18.0 | 1800 | 900 | 15.0 | 30.4 |
| UBE NPC-SS 9000-18 | 80 | 9000 | 457 | 18.0 | 1600 | 800 | 25.0 | 29.9 |
| UBE NPC-SS 9000-17 | 80 | 9000 | 432 | 17.0 | 1600 | 800 | 25.0 | 29.9 |
| SMS 82-16 | 82 | 9206 | 406 | 16.0 | 1800 | 900 | 19.0 | 25.0 |
| UBE NPC-SS 9000-16 | 80 | 9000 | 406 | 16.0 | 1600 | 800 | 25.0 | 29.9 |
| UBE NPC-SS 5500-15 | 49 | 5500 | 381 | 15.0 | 1511 | 756 | 25.0 | 21.7 |
| UBE NPC-SS 6000-15 | 54 | 6016 | 381 | 15.0 | 1524 | 762 | 28.9 | 23.0 |
| TS PLZEN CXP 3200-360 | 31 | 3518 | 360 | 14.2 | 1000 | 500 | 25.0 | 14.3 |
| TS PLZEN CXT 3200-200 | 31 | 3490 | 360 | 14.2 | 1000 | 500 | 50.0 | 14.3 |
| UBE NPC-SS 5000-14 | 44 | 5000 | 356 | 14.0 | 1486 | 743 | 25.0 | 20.5 |
| UBE NPC-SS 5500-14 | 49 | 5500 | 356 | 14.0 | 1511 | 756 | 25.0 | 21.7 |
| SMS 66-14 | 66 | 7442 | 356 | 14.0 | 1600 | 800 | 20.0 | 19.1 |
| UBE NPC-SS 6000-14 | 54 | 6016 | 356 | 14.0 | 1524 | 500 | 28.9 | 23.0 |
| SMS 55-13 | 55 | 6228 | 330 | 13.0 | 1600 | 800 | 21.0 | 18.6 |
| TS PLZEN CXP 3200-330 | 31 | 3518 | 330 | 13.0 | 1000 | 500 | 25.0 | 14.3 |
| UBE NPC-SS 4400-13 | 39 | 4400 | 330 | 13.0 | 1410 | 705 | 25.0 | 19.1 |
| UBE NPC-SS 5000-13 | 44 | 5000 | 330 | 13.0 | 1486 | 743 | 25.0 | 20.5 |
| UBE NPC-SS 5500-13 | 49 | 5500 | 330 | 13.0 | 1511 | 756 | 25.0 | 21.7 |
| UBE NPC-SS 6000-13 | 54 | 6016 | 330 | 13.0 | 1524 | 762 | 28.9 | 22.9 |
| TS PLZEN CXT 3200-200 | 31 | 3490 | 330 | 13.0 | 1000 | 500 | 50.0 | 14.3 |
| THMC AL 36-320 | 36 | 4047 | 320 | 12.6 | 1200 | 600 | 18.0 | 14.9 |
| UBE NPC-SS 4000-12 | 36 | 4012 | 305 | 12.0 | 1334 | 667 | 24.7 | 18.2 |
| TS PLZEN CXP 3200-305 | 31 | 3518 | 305 | 12.0 | 1000 | 500 | 25.0 | 14.3 |

**Table B.1** (Cont.)

| Machine Name | Press Force Capacity (MN) | Press Force Capacity (US ton) | Billet Diameter (mm) | Billet Diameter (in) | Max Billet Length (mm) | Min Billet Length (mm) | Max Extrusion Speed (mm/s) | Dead Cycle Time (sec) |
|---|---|---|---|---|---|---|---|---|
| UBE NPC-SS 4400-12 | 39 | 4400 | 305 | 12.0 | 1410 | 705 | 25.0 | 19.1 |
| UBE NPC-SS 5000-12 | 44 | 5000 | 305 | 12.0 | 1486 | 743 | 25.0 | 20.5 |
| TS PLZEN CXT 3200-200 | 31 | 3490 | 305 | 12.0 | 1000 | 500 | 50.0 | 14.3 |
| TS PLZEN CXP 3200-280 | 31 | 3518 | 280 | 11.0 | 1000 | 500 | 25.0 | 14.3 |
| TS PLZEN CXT 3200-200 | 31 | 3490 | 280 | 11.0 | 1000 | 500 | 50.0 | 14.3 |
| SMS 44-11 | 44 | 4969 | 279 | 11.0 | 1500 | 750 | 22.0 | 17.0 |
| UBE NPC-SS 4000-11 | 36 | 4012 | 279 | 11.0 | 1334 | 667 | 24.7 | 18.2 |
| UBE NPC-SS 4400-11 | 39 | 4400 | 279 | 11.0 | 1410 | 705 | 25.0 | 19.1 |
| UBE NPC-SS 3600-11 | 32 | 3615 | 279 | 11.0 | 1257 | 629 | 25.3 | 17.3 |
| TS PLZEN CXP 3200-255 | 31 | 3518 | 255 | 10.0 | 1000 | 500 | 25.0 | 14.3 |
| TS PLZEN CXT 3200-200 | 31 | 3490 | 255 | 10.0 | 1000 | 500 | 50.0 | 14.3 |
| SMS 35-10 | 35 | 3934 | 254 | 10.0 | 1400 | 700 | 22.0 | 14.4 |
| UBE NPC-SS 4000-10 | 36 | 4012 | 254 | 10.0 | 1334 | 667 | 24.7 | 18.2 |
| UBE NPC-SS 2750-10 | 24 | 2749 | 254 | 10.0 | 1054 | 527 | 24.9 | 15.3 |
| UBE NPC-SS 3000-10 | 27 | 3018 | 254 | 10.0 | 1118 | 559 | 24.9 | 15.9 |
| UBE NPC-SS 3600-10 | 32 | 3615 | 254 | 10.0 | 1257 | 629 | 25.3 | 17.3 |
| TS PLZEN CXP 2000-250 | 20 | 2266 | 250 | 9.8 | 800 | 400 | 25.0 | 13.1 |
| TS PLZEN CXT 2000-250 | 20 | 2219 | 250 | 9.8 | 800 | 400 | 50.0 | 13.0 |
| THMC AL 20-230 | 20 | 2248 | 230 | 9.1 | 810 | 405 | 22.0 | 13.1 |
| TS PLZEN CXP 2000-230 | 20 | 2266 | 230 | 9.1 | 800 | 400 | 25.0 | 13.1 |
| TS PLZEN CXP 3200-230 | 31 | 3518 | 230 | 9.1 | 1000 | 500 | 25.0 | 14.3 |
| SMS 30-9 | 30 | 3417 | 229 | 9.0 | 1300 | 650 | 19.0 | 14.5 |
| UBE NPC-SS 2750-9 | 24 | 2749 | 229 | 9.0 | 1054 | 527 | 24.9 | 15.3 |
| UBE NPC-SS 3000-9 | 27 | 3018 | 229 | 9.0 | 1118 | 400 | 24.9 | 15.6 |
| UBE NPC-SS 2500-9 | 22 | 2504 | 229 | 9.0 | 1003 | 502 | 25.0 | 14.7 |
| TS PLZEN CXP 1600-225 | 16 | 1810 | 225 | 8.9 | 750 | 375 | 25.0 | 12.7 |
| TS PLZEN CXT 1600-225 | 15 | 1731 | 225 | 8.9 | 750 | 375 | 50.0 | 12.7 |
| TS PLZEN CXT 2000-225 | 20 | 2219 | 225 | 8.9 | 800 | 400 | 50.0 | 13.0 |
| TS PLZEN CXT 3200-200 | 31 | 3490 | 225 | 8.9 | 1000 | 500 | 50.0 | 14.3 |
| THMC AL 16-210 | 16 | 1832 | 210 | 8.3 | 810 | 405 | 25.0 | 12.7 |
| SMS 27-8 | 27 | 3069 | 203 | 8.0 | 1300 | 650 | 21.0 | 14.0 |
| SMS 24-8 | 24 | 2732 | 203 | 8.0 | 1200 | 600 | 24.0 | 13.0 |
| UBE NPC-SS 2750-8 | 24 | 2749 | 203 | 8.0 | 1054 | 527 | 24.9 | 15.3 |
| UBE NPC-SS 2500-8 | 22 | 2504 | 203 | 8.0 | 1003 | 502 | 25.0 | 14.7 |
| THMC AL 20-200 | 20 | 2248 | 200 | 7.9 | 810 | 405 | 22.0 | 13.1 |
| TS PLZEN CXP 1600-200 | 16 | 1810 | 200 | 7.9 | 750 | 375 | 25.0 | 12.7 |
| TS PLZEN CXP 2000-200 | 20 | 2266 | 200 | 7.9 | 800 | 400 | 25.0 | 13.1 |

**Table B.1** (Cont.)

| Machine Name | Press Force Capacity (MN) | Press Force Capacity (US ton) | Billet Diameter (mm) | Billet Diameter (in) | Max Billet Length (mm) | Min Billet Length (mm) | Max Extrusion Speed (mm/s) | Dead Cycle Time (sec) |
|---|---|---|---|---|---|---|---|---|
| TS PLZEN CXP 3200-200 | 31 | 3518 | 200 | 7.9 | 1000 | 500 | 25.0 | 14.3 |
| TS PLZEN CXT 1600-200 | 15 | 1731 | 200 | 7.9 | 750 | 375 | 50.0 | 12.7 |
| TS PLZEN CXT 2000-200 | 20 | 2219 | 200 | 7.9 | 800 | 400 | 50.0 | 13.0 |
| TS PLZEN CXT 3200-200 | 31 | 3490 | 200 | 7.9 | 1000 | 500 | 50.0 | 14.3 |
| TS PLZEN CXP 1250-180 | 13 | 1419 | 180 | 7.1 | 710 | 355 | 25.0 | 12.4 |
| THMC AL 16-180 | 16 | 1832 | 180 | 7.1 | 810 | 405 | 25.0 | 12.7 |
| TS PLZEN CXT 1250-180 | 12 | 1382 | 180 | 7.1 | 710 | 355 | 50.0 | 12.4 |
| TS PLZEN CXT 1600-180 | 15 | 1731 | 180 | 7.1 | 750 | 375 | 50.0 | 12.7 |
| TS PLZEN CXT 2000-180 | 20 | 2219 | 180 | 7.1 | 800 | 400 | 50.0 | 13.0 |
| UBE NPC-SS 2000-7 | 18 | 1989 | 178 | 7.0 | 1016 | 300 | 23.0 | 13.7 |
| UBE NPC-SS 1800-7 | 16 | 1793 | 178 | 7.0 | 813 | 407 | 25.5 | 13.0 |
| SMS 18-7 | 18 | 1967 | 178 | 7.0 | 1000 | 500 | 22.0 | 12.9 |
| SMS 20-7 | 20 | 2248 | 178 | 7.0 | 1000 | 500 | 22.0 | 12.9 |
| TS PLZEN CXP 1600-175 | 16 | 1810 | 175 | 6.9 | 750 | 375 | 25.0 | 12.7 |
| TS PLZEN CXP 2000-175 | 20 | 2266 | 175 | 6.9 | 800 | 400 | 25.0 | 13.1 |
| THMC AL 20-170 | 20 | 2248 | 170 | 6.7 | 810 | 405 | 22.0 | 13.1 |
| THMC AL 16-160 | 16 | 1832 | 160 | 6.3 | 810 | 405 | 25.0 | 12.7 |
| TS PLZEN CXP 2000-160 | 20 | 2266 | 160 | 6.3 | 800 | 400 | 25.0 | 13.1 |
| TS PLZEN CXT 2000-160 | 20 | 2219 | 160 | 6.3 | 800 | 400 | 50.0 | 13.0 |
| TS PLZEN CXP 1250-155 | 13 | 1419 | 155 | 6.1 | 710 | 355 | 25.0 | 12.4 |
| TS PLZEN CXT 1250-155 | 12 | 1382 | 155 | 6.1 | 710 | 355 | 50.0 | 12.4 |
| THMC AL 8-150 | 8 | 899 | 150 | 5.9 | 750 | 375 | 21.0 | 12.1 |
| TS PLZEN CXP 1600-145 | 16 | 1810 | 145 | 5.7 | 750 | 375 | 25.0 | 12.7 |
| TS PLZEN CXT 1600-145 | 15 | 1731 | 145 | 5.7 | 750 | 375 | 50.0 | 12.7 |
| TS PLZEN CXP 800-140 | 9 | 975 | 140 | 5.5 | 560 | 280 | 25.0 | 12.2 |
| TS PLZEN CXP 1250-130 | 13 | 1419 | 130 | 5.1 | 710 | 355 | 25.0 | 12.4 |
| TS PLZEN CXT 1250-130 | 12 | 1382 | 130 | 5.1 | 710 | 355 | 50.0 | 12.4 |
| TS PLZEN CXP 800-126 | 9 | 975 | 126 | 5.0 | 560 | 280 | 25.0 | 12.2 |
| TS PLZEN CXT 630-125 | 6 | 708 | 125 | 4.9 | 500 | 250 | 50.0 | 12.0 |
| THMC AL 8-120 | 8 | 899 | 120 | 4.7 | 750 | 375 | 21.0 | 12.1 |
| THMC AL 6-100 | 6 | 618 | 100 | 3.9 | 450 | 225 | 20.0 | 12.0 |
| THMC AL 8-100 | 8 | 899 | 100 | 3.9 | 750 | 375 | 21.0 | 12.1 |
| TS PLZEN CXP 800-100 | 9 | 975 | 100 | 3.9 | 560 | 280 | 25.0 | 12.2 |
| TS PLZEN CXT 630-90 | 6 | 708 | 90 | 3.5 | 500 | 250 | 50.0 | 12.0 |

# APPENDIX C: WASTE TIME ESTIMATION

The estimation of waste time per batch was done by calibrating the cost model to benchmark productivity data on a section extruded from an 8" (203 mm) diameter billet. For simplicity of the geometrical properties calculation, an angle shape was assumed, as shown in Figure C.1. The dimensions of the section were set to provide the average extrusion ratio (R=55) for Al-6063 extrusions (soft alloys range: R=10-100).

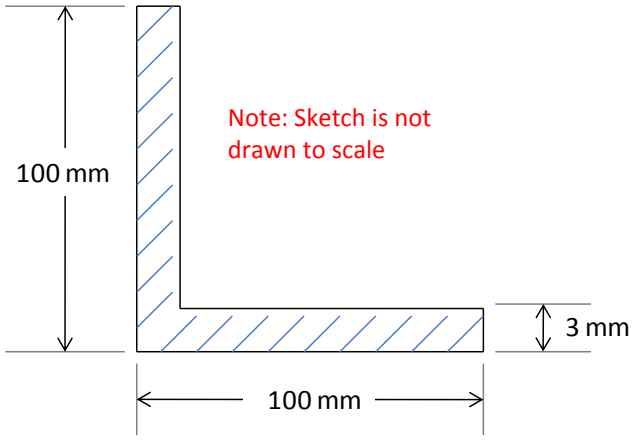


**Figure C.1** Cross-section shape and size used for model calibration

The geometrical properties of the design and the billet are shown in Table C.1, along with the batch size. The latter was intentionally assigned to result in a cycle time per batch close to 0.8 hr, as commonly encountered in extrusion plants (having 10 batches per 8 hr shift [26]). Extrusion Speed Calculations were carried out according to the method described in Section 4.1.2; they are shown in Table C.2 for reference. Note that the extrusion exit speed ($v_f$) resulted in 52.3 m/min, which is fairly close to the average extrusion exit speed for Al-6063 (57.5 m/min, from the range of 35-80 m/min).

**Table C.1** Design Input Data, Billet Size and Extrusion Ratio.

| DESIGN INPUT DATA | |
|---|---|
| Cross Sectional Area, $A_f$ ($mm^2$) | 591 |
| Circumscribing Circle Diameter, *CCD* (mm) | 141 |
| Length, $L_{part}$ (mm) | 3000 |
| External Perimeter, $P_{ext}$ (mm) | 400 |
| Maximum Wall Thickness (mm) | 3.0 |
| Material | Aluminum 6063 |
| Batch Size, $N_{parts\_batch}$ (qty) | 500 |
| **BILLET SIZE AND EXTRUSION RATIO** | |
| Standard Billet Diameter, $D_o$ (mm) | 203.2 |
| Billet Length, $L_o$ (mm) | 1003 |
| Cross Sectional Area of Billet, $A_o$ ($mm^2$) | 32429 |
| Extrusion Ratio, *R* | 55 |

**Table C.2** Extrusion Speed Calculations.

| EXTRUSION SPEED CALCULATIONS | | |
|---|---|---|
| **Variable** | **Value** | **Eqn # or Source** |
| Max Extrusion Ram Speed of Press, $v_{o\_press}$ (mm/s) | 25.0 | Press Data |
| Max Extrusion Exit Speed without Hot Shortness, $v_{f\_hs}$ (m/min) | 52.3 | 4.14 |
| Max Extrusion Ram Speed without Hot Shortness, $v_{o\_hs}$ (mm/s) | 15.9 | 4.15 |
| Extrusion Ram Speed, $v_o$ (mm/s) | 15.9 | 4.16 |
| Extrusion Exit Speed, $v_f$ (m/min) | 52.3 | 4.17 |

The cycle time calculations were performed based on the approach presented in Section 4.2. The results are shown in Table C.3, where it can be seen that the estimated cycle time per batch is 0.75 hr, which is relatively close to 0.8 hr, as intended. Finally, the waste time per batch was found by assuming a benchmark productivity of 6000 lb/hr (2721 kg/hr) [53] and solving equation 4.46 for $t_{waste\_batch}$. The results are shown in Table C.4, where a waste time per batch of 6.8 minutes is indicated. For practical purposes, the waste time per batch may be assumed to be 7 minutes.

**Table C.3** Cycle Time per Batch Calculations.

| CYCLE TIME CALCULATIONS | | |
|---|---|---|
| **Variable** | **Value** | **Eqn # or Source** |
| Extruded Length of one Billet, $L_f$ (m) | 49.5 | 4.19 |
| Runout Table Length, $L_{runout\_table}$ (m) | 35 | Assumed |
| Length scrapped per extrusion, $L_{scrap}$ (m) | 2 | Assumed |
| Number of Parts per Extrusion, $N_{parts\_ext}$ (qty) | 11 | 4.25 |
| Length of Continuous Extrusion, $L_{cont\_ext}$ (m) | 35.0 | 4.26 |
| Number of Billets per Extrusion, $n_{billets\_ext}$ (qty) | 0.7 | 4.27 |
| Quality Scrap (%) | 6% | Assumed |
| Number of Parts per Billet, $n_{parts\_billet}$ (qty) | 15.6 | 4.24 |
| Number of Billets per Batch, $n_{billets\_batch}$ (qty) | 34.2 | 4.23 |
| Extrusion Time per Billet, $t_{ext\_billet}$ (sec) | 56.8 | 4.18 |
| Ram Acceleration Time per Billet, $t_{accel\_billet}$ (sec) | 7 | Assumed |
| Dead Cycle Time per Billet, $t_{dead\_billet}$ (sec) | 14.7 | Press Data |
| Cycle Time per Batch, $t_{cycle\_batch}$ (hrs) | 0.75 | 4.21 |

**Table C.4** Productivity and Waste Time per Batch Calculations.

| PRODUCTIVITY CALCULATIONS | | |
|---|---|---|
| **Variable** | **Value** | **Eqn # or Source** |
| Part Mass, $m_{part}$ (kg) | 4.79 | $=\rho A_f L_{part}$ |
| Setup Time per Batch, $t_{setup\_batch}$ (min) | 1.0 | Assumed |
| Waste Time per Batch, $t_{waste\_batch}$ (min) | 6.8 | 4.46 |
| Net Mass per Batch, $m_{net\_batch}$ (kg) | 2394 | 4.39 |
| Productivity (kg/hr) | 2722 | Assumed |
| Productivity (lb/hr) | 6000 | Assumed |

# APPENDIX D: DETAILED DRAWINGS OF EXTRUDED SHAPES QUOTED

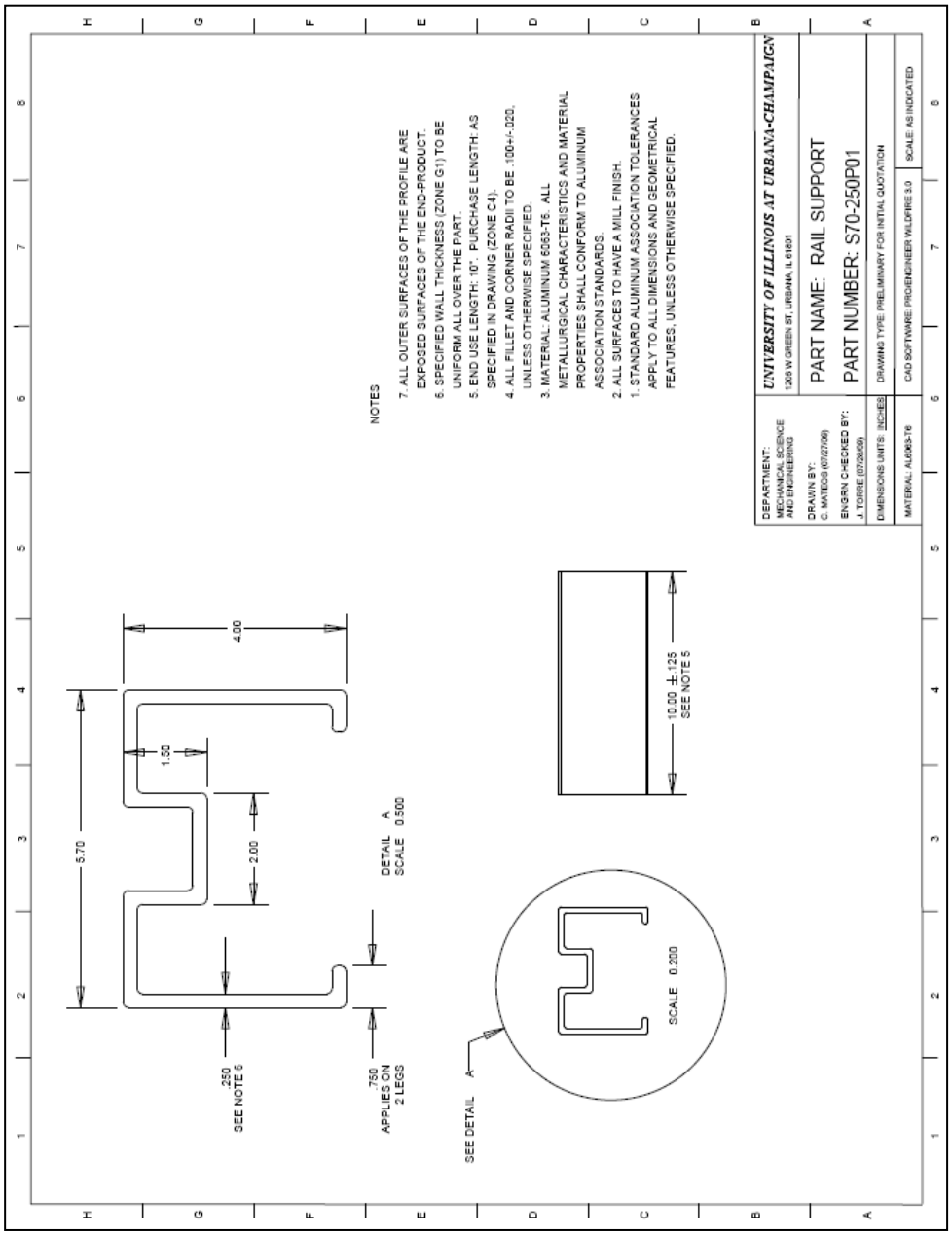


**Figure D.1** Detail Drawing for Design #1.

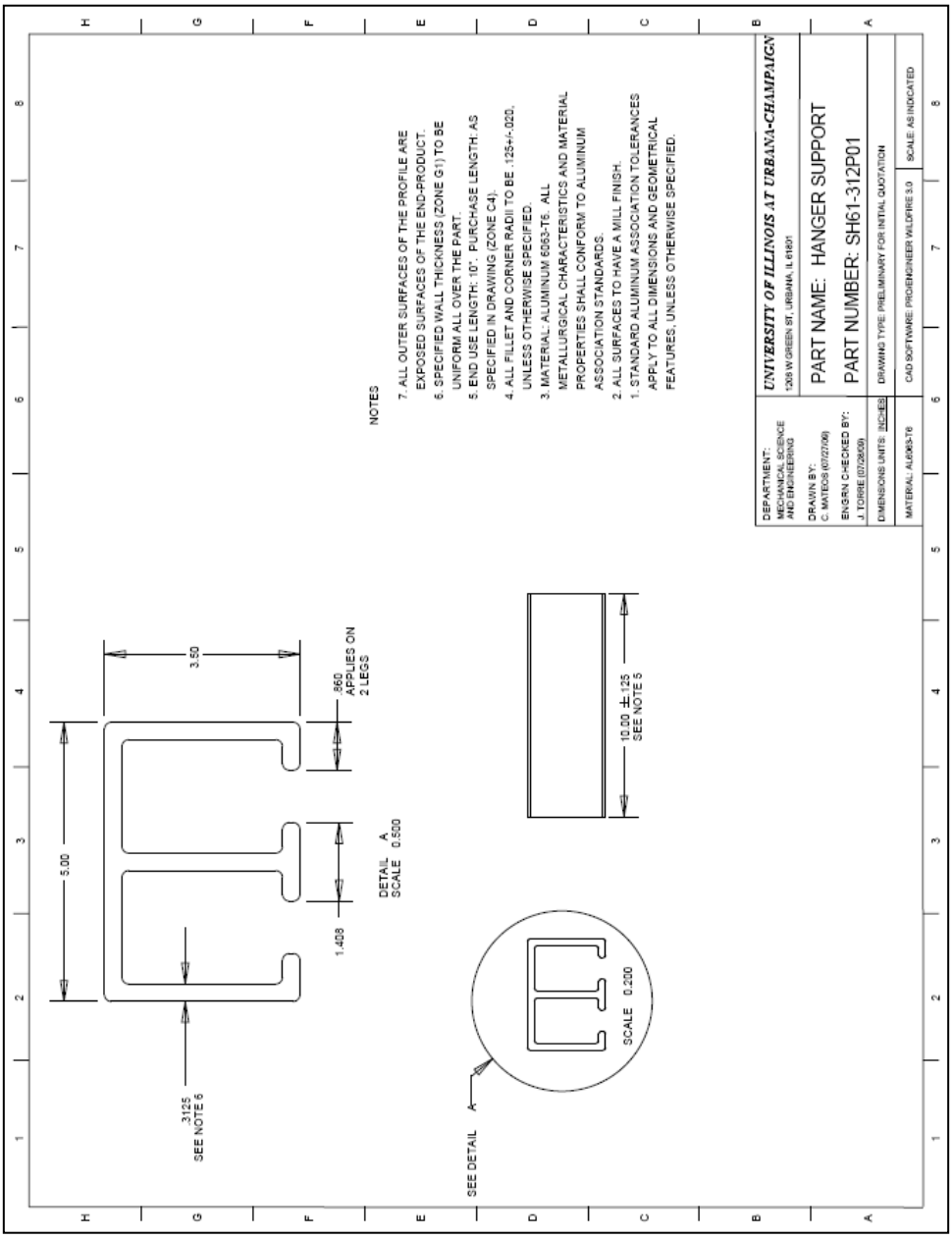


**Figure D.2** Detail Drawing for Design #2.

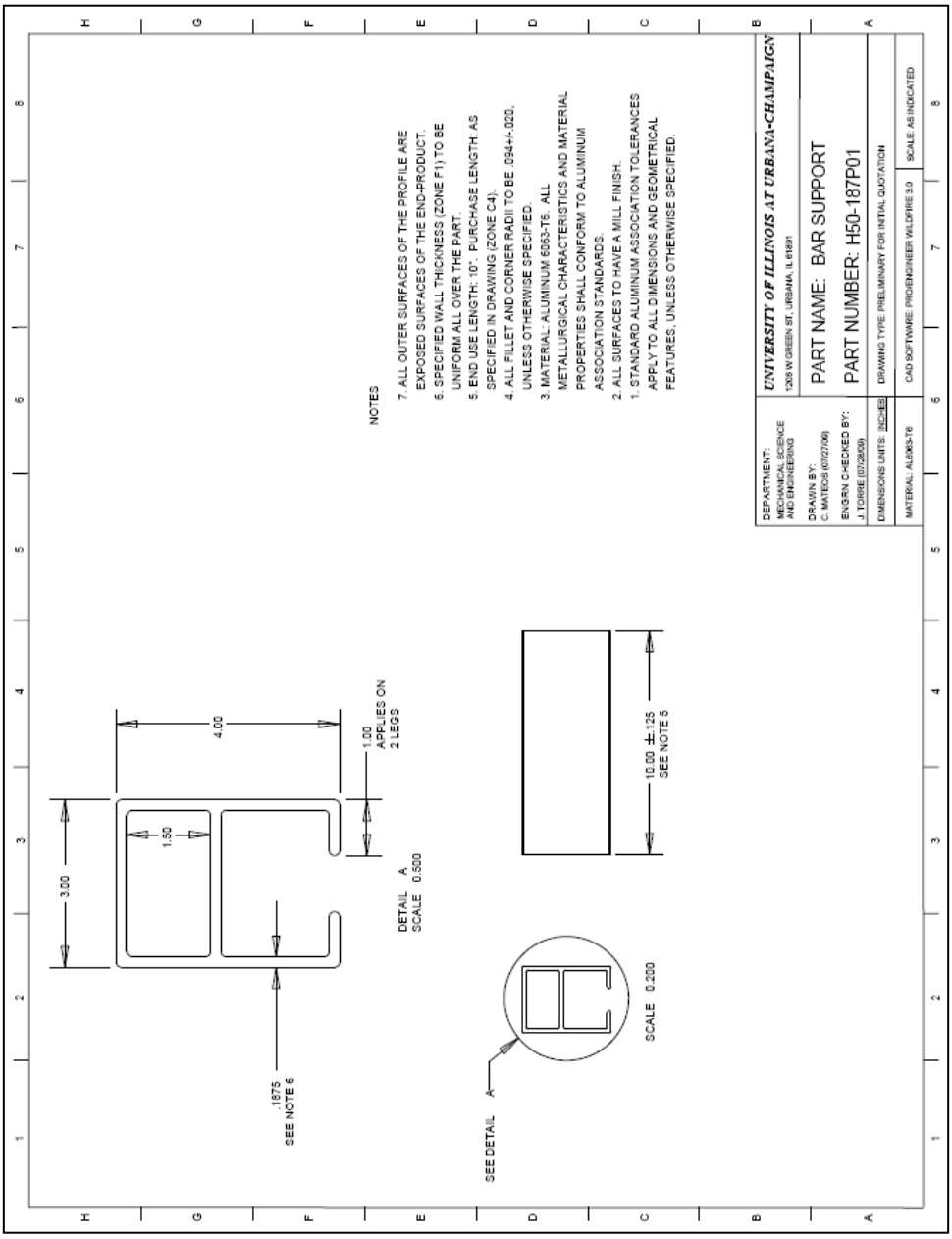


**Figure D.3** Detail Drawing for Design #3.

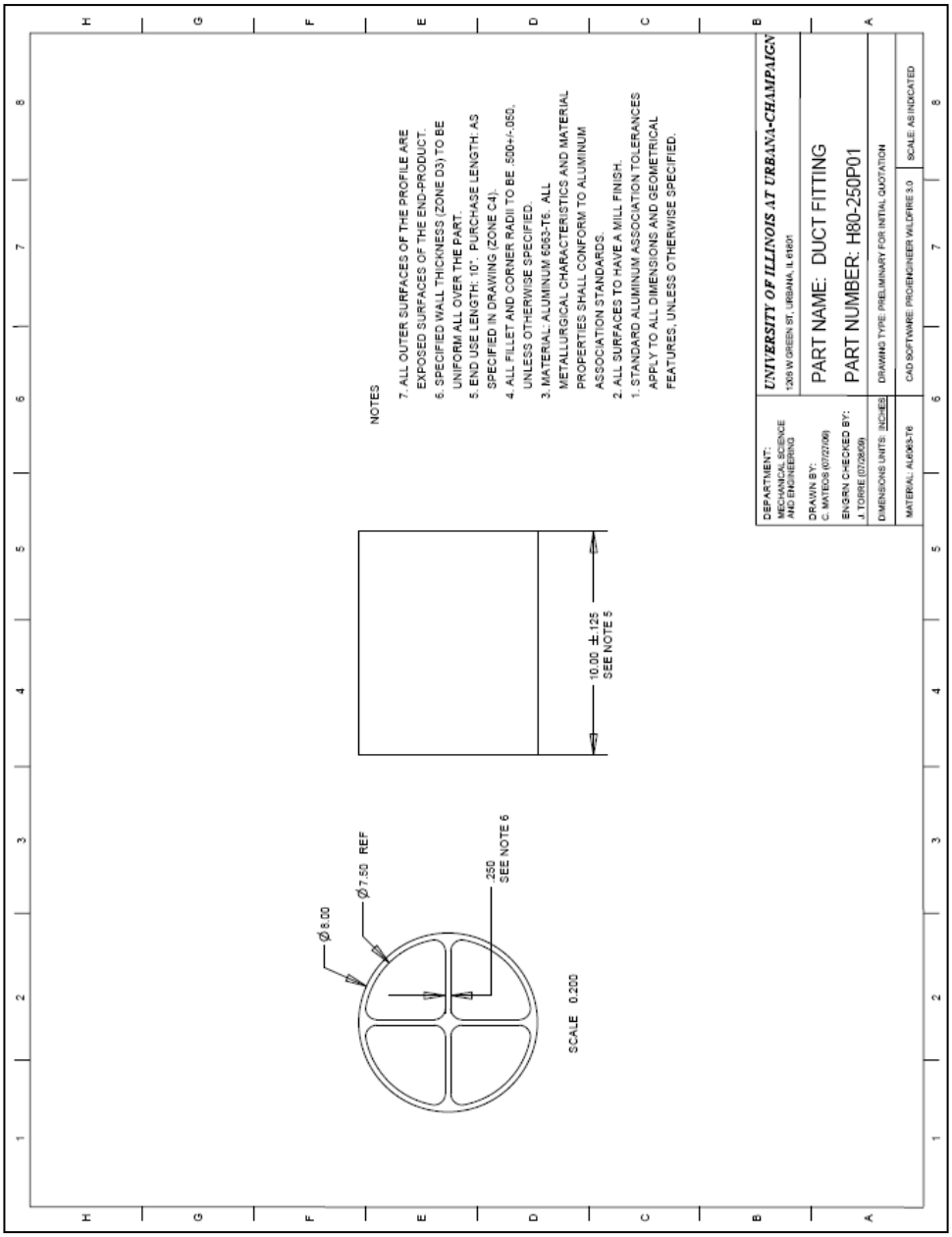


**Figure D.4** Detail Drawing for Design #4.

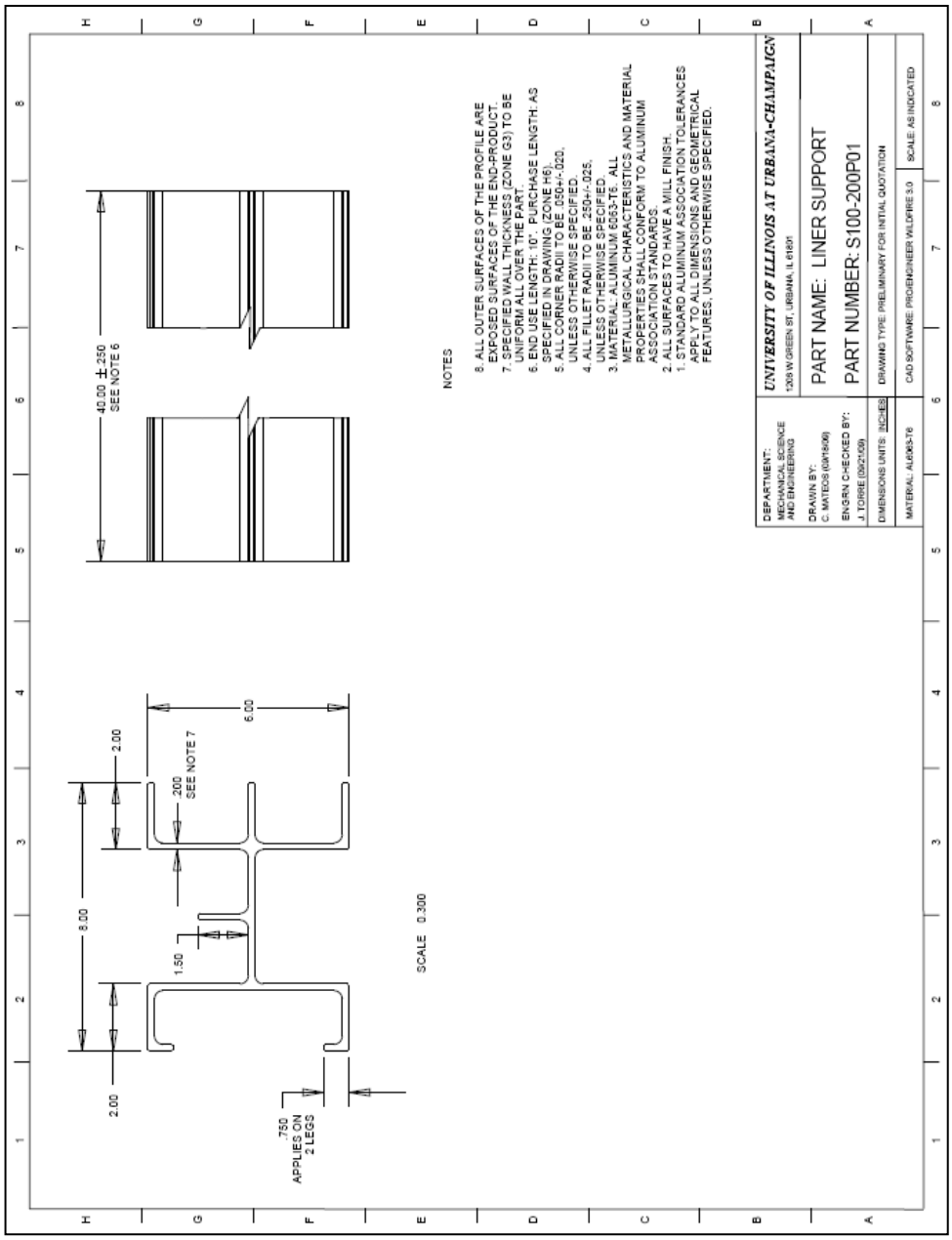


**Figure D.5** Detail Drawing for Design #5.

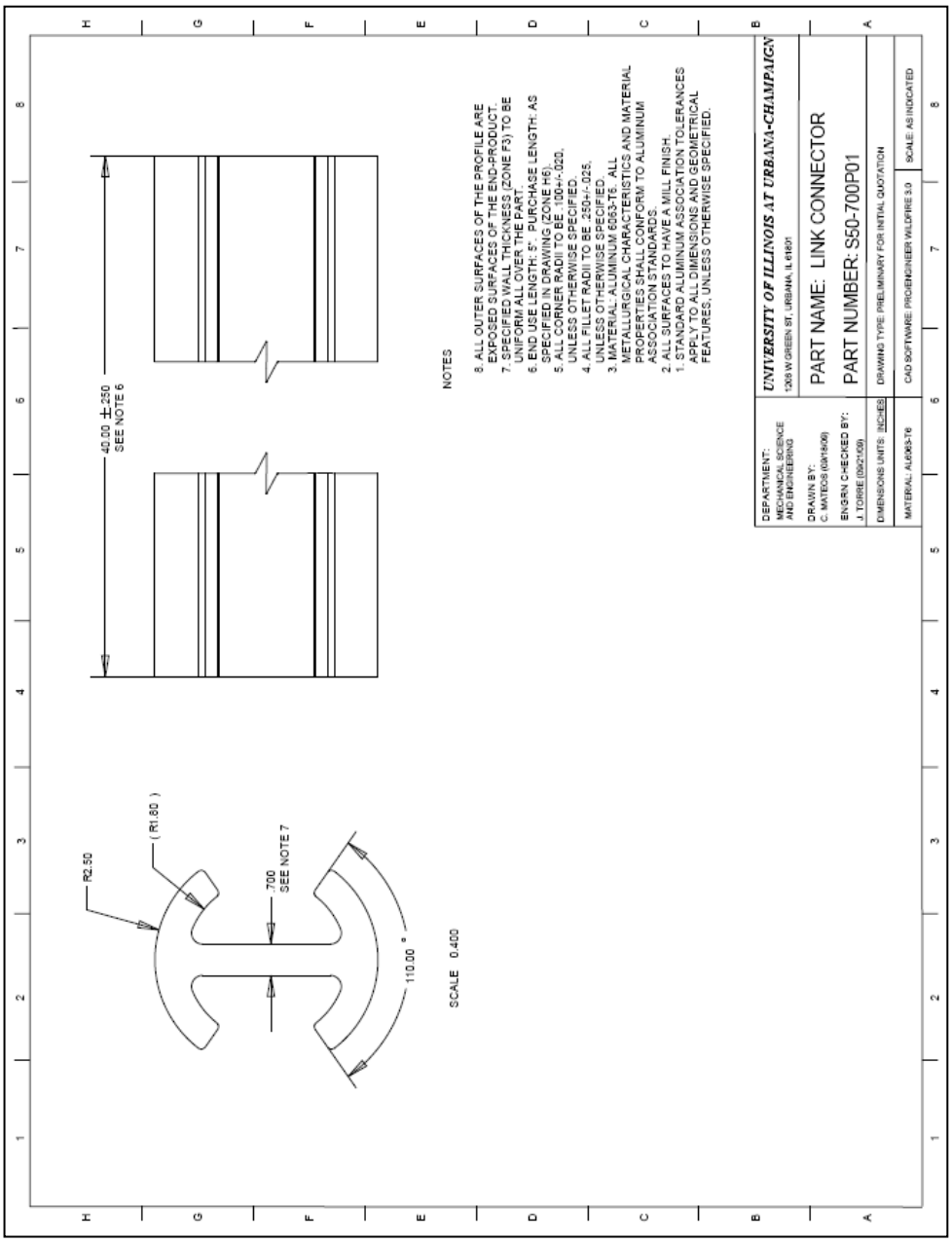


**Figure D.6** Detail Drawing for Design #6.

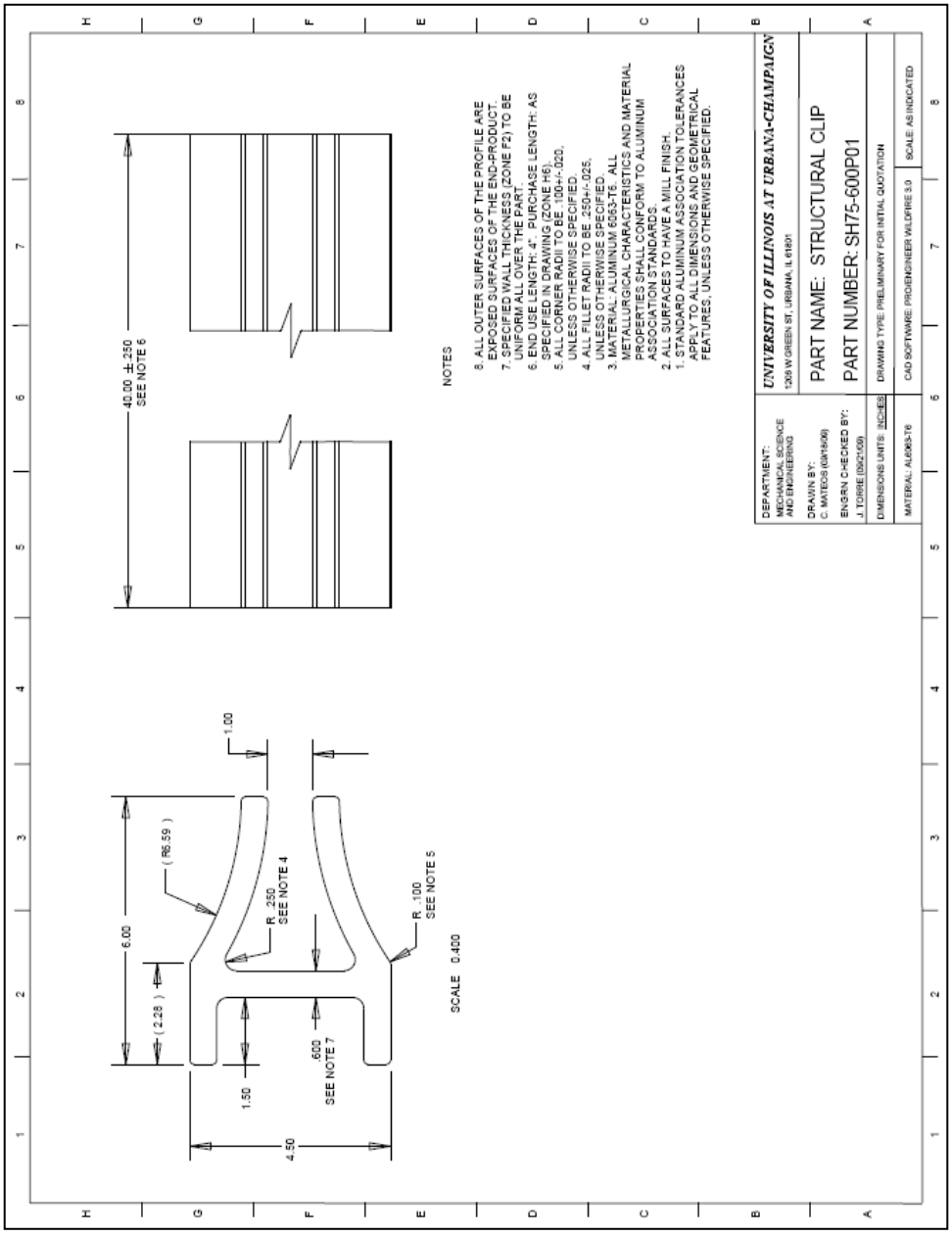


**Figure D.7** Detail Drawing for Design #7.

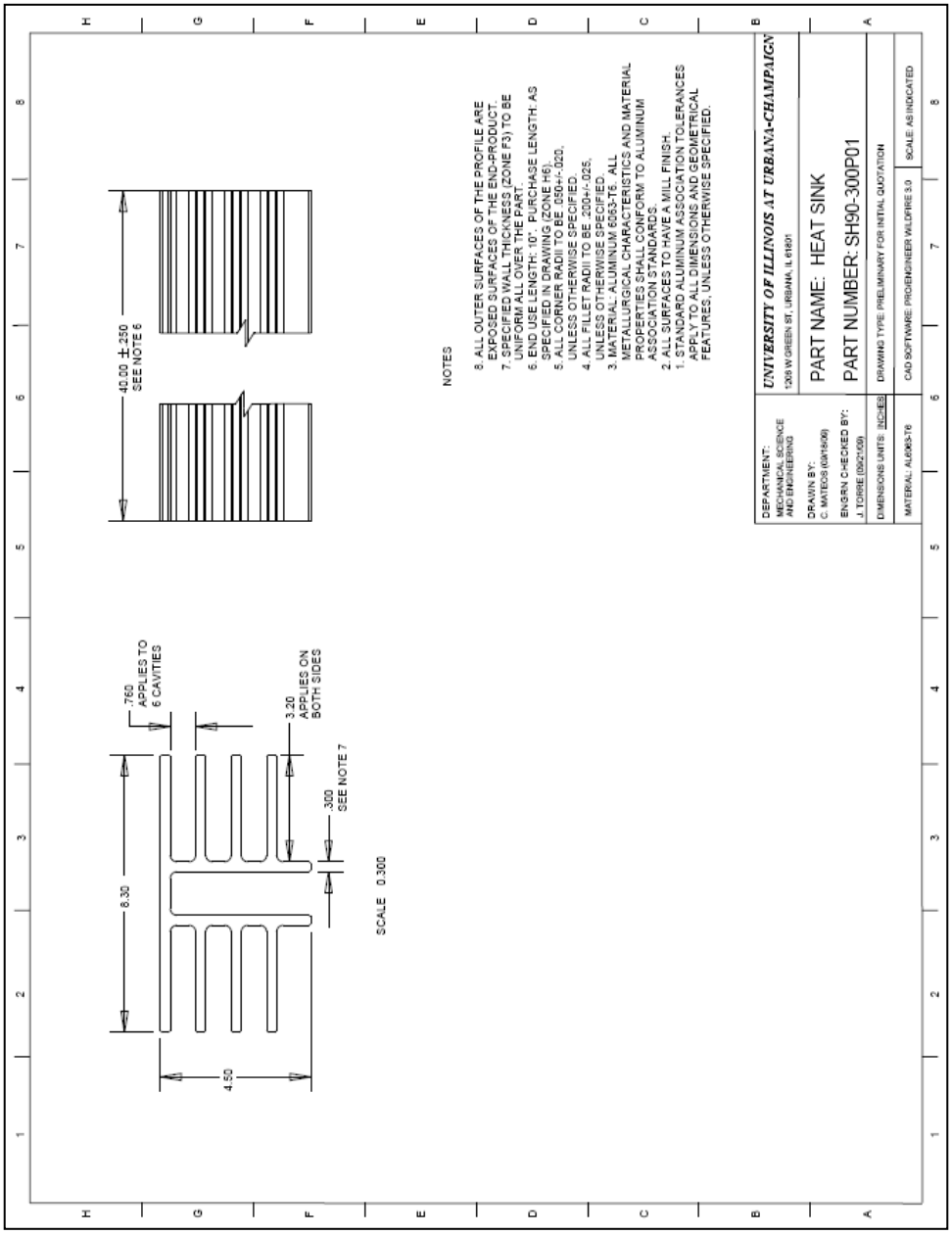


**Figure D.8** Detail Drawing for Design #8.

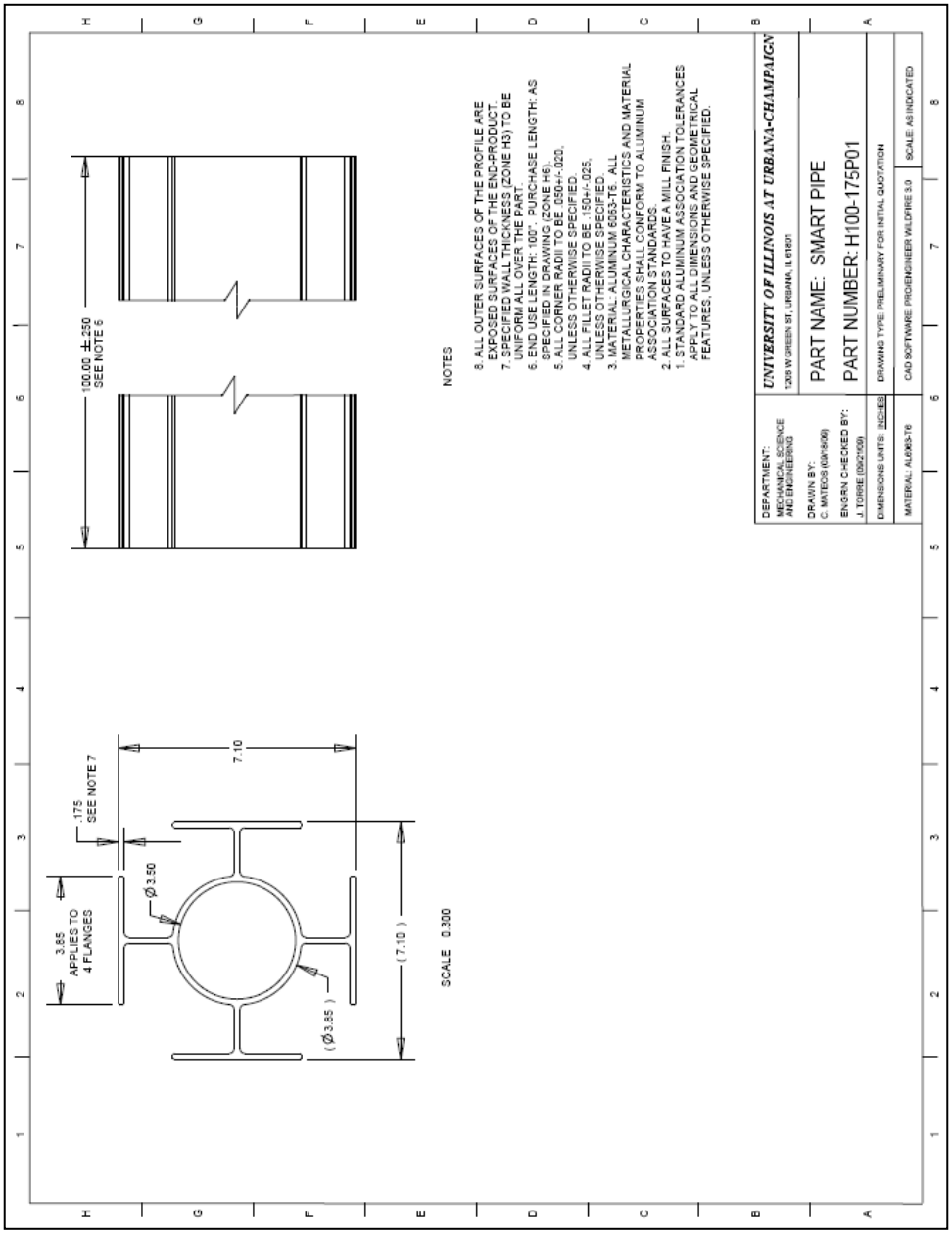


**Figure D.9** Detail Drawing for Design #9.

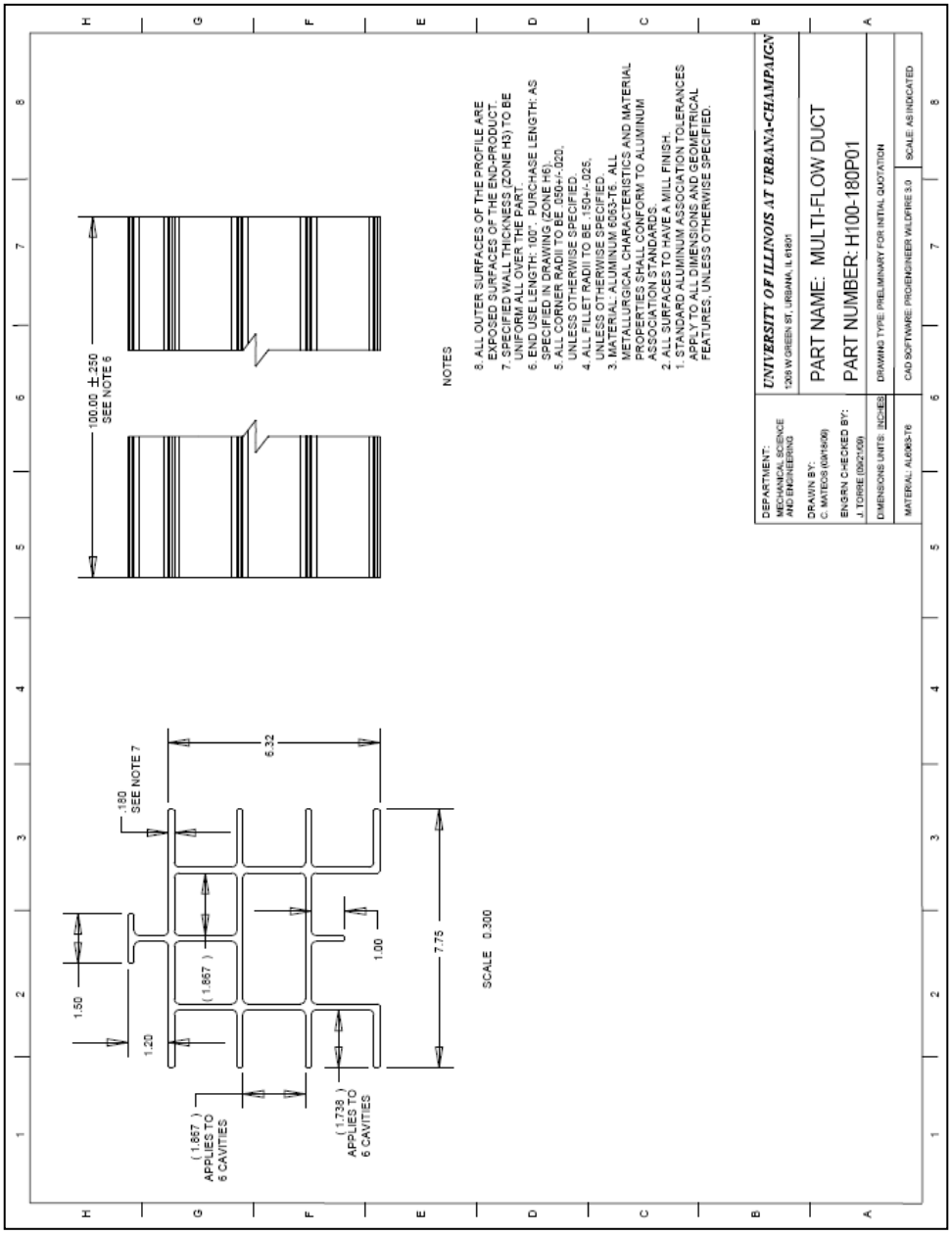


**Figure D.10** Detail Drawing for Design #10.

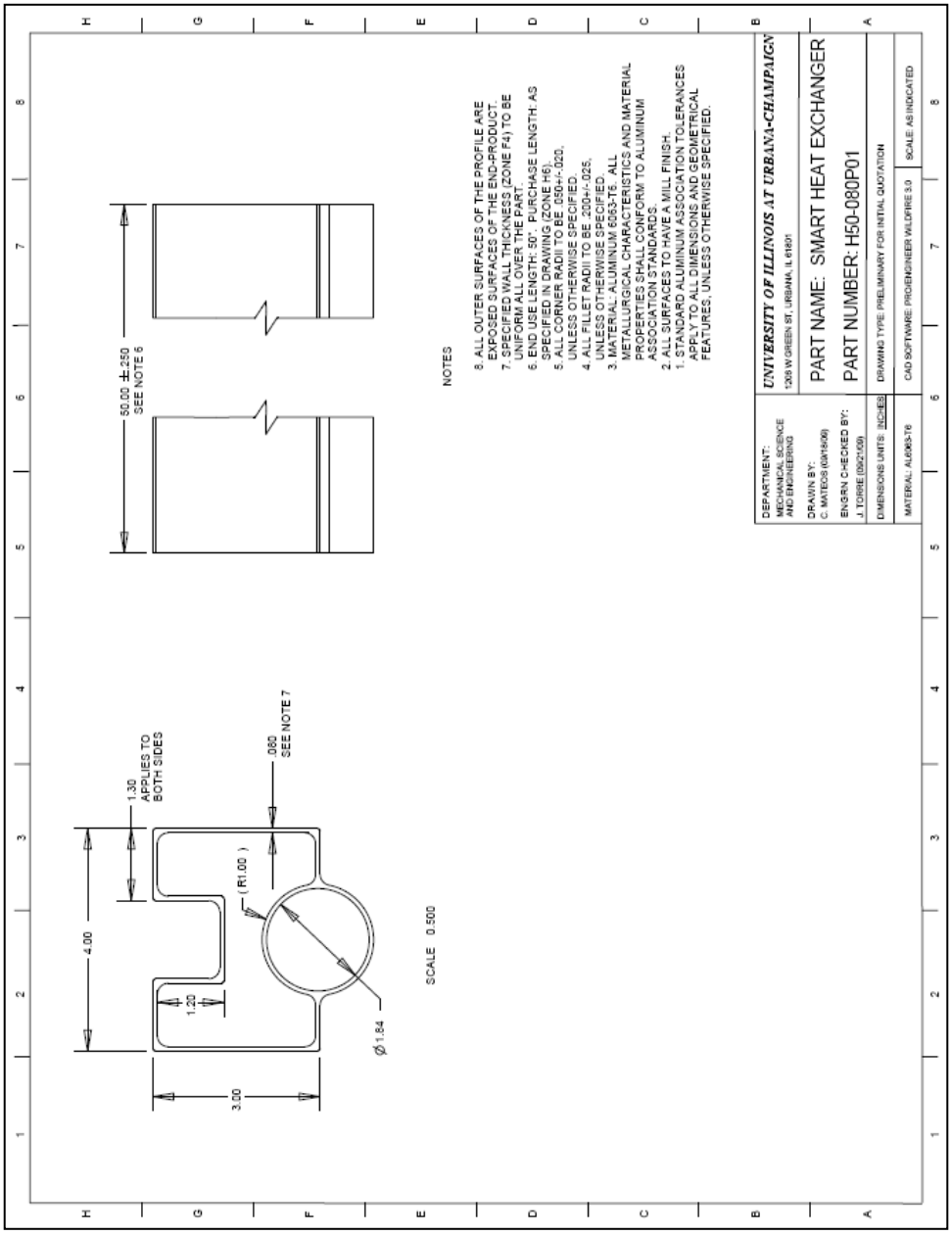


**Figure D.11** Detail Drawing for Design #11.

# APPENDIX E: HOT EXTRUSION FBC SPREADSHEET

The author of this thesis created a spreadsheet (in Microsoft Office Excel 2007) that performs Feature Based Costing of Hot Extruded Parts made of Aluminum Alloys, using the methods described in Chapters 4-6. The spreadsheet can be found in a supplemental file named **Hot_Extrusion_FBC_Model.xlsm**.

Note that in order for the spreadsheet to function properly, Excel's "Solver Add-In" must be activated; otherwise the macros embedded in the file will not work and you may get an error message like the one shown in Figure E.1 after executing the spreadsheet's "Press Selection and Extrusion Speed Solver Macro". Please refer to Excel's Help Function for detailed instructions on how to activate Excel's Solver Add-Inn.

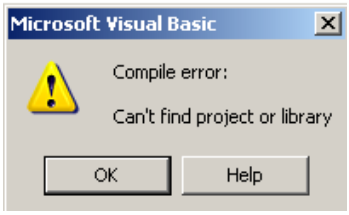


**Figure E.1** Error Message displayed by Excel when Solver Add-Inn is not activated.

If after loading Excel's Solver Add-Inn (and restarting Excel) macros in the spreadsheet are still not working properly, you may need to "add the Solver Reference" in VBA. To do so, follow these steps:

1) Press Alt+F11 to open up VBA in Excel.
2) Add the Solver reference in Visual Basic (Tools > References..., then make sure that SOLVER is checked).

# REFERENCES

[1] Kalpakjian, S., and Schmid, S.R., 2003, "Manufacturing Processes for Engineering Materials", Pearson Education, USA, pp. 954.

[2] Vasiliou, V. C., and Milner, D. A., 1986, "Computer-Integrated Manufacture for Cold Roll Forming", Advances in Manufacturing Technology, pp. 79-85.

[3] Bralla, J.G., 1998, "Design for Manufacturability Handbook", McGraw-Hill, USA, pp. 1368.

[4] Westney, R.E., 1997, "The Engineer's Cost Handbook: Tools for Managing Projects Costs", Marcel Dekker, USA, pp. 738.

[5] Sweeney, K., and Grunewald, U., 2003, "The Application of Roll Forming for Automotive Structural Parts", Journal of Materials Processing Technology, **132**(1-3) pp. 9-15.

[6] Semiatin, S.L., et al., 2005, "ASM Handbook Volume 14A, Metalworking: Bulk Forming", ASM International, USA, pp. 860.

[7] Azushima, A., Kopp, R., Korhonen, A., 2008, "Severe Plastic Deformation (SPD) Processes for Metals", CIRP Annals - Manufacturing Technology, **57**(2) pp. 716-735.

[8] Trucks, H.E., 1987, "Designing for Economical Production", Society of Manufacturing Engineers, pp. 366.

[9] Nagasekhar, A. V., and Kim, H. S., 2008, "Plastic Deformation Characteristics of Cross-Equal Channel Angular Pressing", Computational Materials Science, **43**(4) pp. 1069-1073.

[10] Paydar, M. H., Reihanian, M., Bagherpour, E., 2009, "Equal Channel Angular pressing–forward Extrusion (ECAP–FE) Consolidation of Al Particles", Materials & Design, **30**(3) pp. 429-432.

[11] Sugiyama, S., and Yanagimoto, J., 2008, "Feasibility of Recycling Aluminum Alloy Scrap by Semisolid Extrusion", Solid State Phenomena, **141-143** pp. 79-83.

[12] Fang, G., Zhou, J., and Duszczyk, J., 2009, "FEM Simulation of Aluminum Extrusion through Two-Hole Multi-Step Pocket Dies", Journal of Materials Processing Technology, **209**(4) pp. 1891-1900.

[13] Karamış, M. B., and Nair, F., 2008, "Effects of Reinforcement Particle Size in MMCs on Extrusion Die Wear", Wear, **265**(11-12) pp. 1741-1750.

[14] Zubizarreta, C., Giménez, S., Martín, J. M., 2009, "Effect of the Heat Treatment Prior to Extrusion on the Direct Hot-Extrusion of Aluminum Powder Compacts", Journal of Alloys and Compounds, **467**(1-2) pp. 191-201.

[15] Bonarski, J., Pospiech, J., Tarkowski, L., 2008, "Angular Extrusion of Double-Metal Ingot", Materials Science Forum, **584-586 PART 1** pp. 74-79.

[16] Lee, C. M., and Yang, D. Y., 2000, "A Three-Dimensional Steady-State Finite Element Analysis of Square Die Extrusion by using Automatic Mesh Generation", International Journal of Machine Tools and Manufacture, **40**(1) pp. 33-47.

[17] Balasundar, I., Sudhakara Rao, M., and Raghu, T., 2009, "Equal Channel Angular Pressing Die to Extrude a Variety of Materials", Materials & Design, **30**(4) pp. 1050-1059.

[18] Wilson, F., and Harvey, P., 1963, "Manufacturing Planning and Estimating Handbook", American Society of Tool and Manufacturing Engineers, McGraw-Hill, USA, pp. 854.

[19] Malstrom, E.M., 1984, "Manufacturing Cost Engineering Handbook", Marcel Dekker, USA, pp. 447.

[20] Philpott, M. L., Schrader, R. S., Subbarao, G., 2004, "Integrated Real-Time Feature Based Costing (FBC)", **10/993,406** (US Patent #7065420).

[21] Dallas, D.B., 1976, "Tool and Manufacturing Engineers Handbook", Society of Manufacturing Engineers, McGraw-Hill, USA, pp. 2952.

[22] Saha, P.K., 2000, "Aluminum Extrusion Technology", ASM International, USA, pp. 259.

[23] Totten, G.E., Funatani, K., and Xie, L., 2004, "Handbook of Metallurgical Process Design", Marcel Dekker, USA, pp. 966.

[24] Aluminum Company of Canada, 1964, "Shape Design Manual: Aluminum Extrusion", ALCAN, Canada, pp. 87.

[25] Aluminum Extruders Council, 1998, "Aluminum Extrusion Manual", Aluminum Extruders Council and The Aluminum Association, USA, pp. 200.

[26] Laue, K., and Stenger, H., 1981, "Extrusion: Processes, Machinery, Tooling", American Society for Metals, USA, pp. 457.

[27] www.aec.org/techinfo/expro.html, "Aluminum Extruders Council, Technical Information", 2009.

[28] www.grancoclark.com/aluminum-extrusion-equipment/integral-cooling.html, "Granco Clark Integral Runout Cooling Systems", 2009.

[29] www.grancoclark.com/aluminum-extrusion-equipment/profile-stretcher.html, "Granco Clark, Stretchers", 2009.

[30] www.grancoclark.com/aluminum-extrusion-equipment/cut-off-saw.html, "Granko Clark, Cutoff Saw and Gage Systems", 2009.

[31] www.grancoclark.com/aluminum-extrusion-equipment/rack-handling.html, "Granco Clark, Rack Handling Systems", 2009.

[32] www.giaet.com/maduracion.php, "GiA CLECIM Press, Aging Ovens", 2009.

[33] www.grancoclark.com/aluminum-extrusion-equipment/continuous-aging-oven.html, "Granco Clark, Continuous Aging Oven", 2009.

[34] Qamar, S. Z., 2004, "Modeling and Analysis of Extrusion Pressure and Die Life for Complex Aluminum Profiles", PhD Dissertation, King Fahd University of Petroleum & Minerals, pp. 320.

[35] Altan, T., Oh, S., and Gegel, H.L., 1983, "Metal Forming: Fundamentals and Applications", American Society for Metals, USA, pp. 353.

[36] Akeret, R., Jung, H., and Scharf, G., 1978, "Atlas of Hot Working Properties of Nonferrous Metals", Deutsche Gesellschaft für Metallkunde (DGM), Germany, pp. 600.

[37] Semiatin, S. L., Frey, N., Walker, N. D., 1986, "Effect of Deformation Heating and Strain Rate Sensitivity on Flow Localization during the Torsion Testing of 6061 Aluminum", Acta Metallurgica, **34**(1) pp. 167-176.

[38] Prasad, Y.V.R.K., and Sasidhara, S., 1997, "Hot Working Guide: A Compendium of Processing Maps", ASM International, USA, pp. 545.

[39] Qamar, S. Z., Arif, A. F. M., and Sheikh, A. K., 2004, "A New Definition of Shape Complexity for Metal Extrusion", Journal of Materials Processing Technology, **155-156** pp. 1734-1739.

[40] Vater, M., and Heil, H. P., 1969, "Effect of Section Shape on Energy Requirements for Extrusion (Der Einfluss Der Profilform Auf Den Kraftbedarf Beim Strangpressen)", Aluminium, **45**(3) pp. 141-149.

[41] Ohgashi, H., and Yamashita, H., 1962, "A Study on the Extrusion Force for Aluminum Alloys", Sumitomo Light Metal Technical Reports, **3**(2) pp. 87-93.

[42] Sheppard, T., 1999, "Extrusion of Aluminium Alloys", Kluwer Academic Publishers, The Netherlands, pp. 220.

[43] Balasubramaniam, L., and Ulrich, K. T., 1998, "Producibility Analysis using Metrics Based on Physical Process Models", Research in Engineering Design, **10**(4) pp. 210.

[44] www.bonlalum.com/Login/SlsMfg/extrusion_process.jsp, "Bonnell Aluminum Products: Extrusion Process Description", 2009.

[45] Stüwe, H. P., 1968, "Einige Abschätzungen Zum Strangpressen", Metall, **22** pp. 1197-1200.

[46] www.aec.org/index.cfm, "Aluminum Extruders Council Website", 2009.

[47] www.aec.org/techinfo/faqs.html, "Aluminum Extruders Council, Technical Info, FAQs" 2009.

[48] www.bls.gov/oes/2008/may/oes_nat.htm#b51-0000, "US Bureau of Labor Statistics: May 2008 National Occupational Employment and Wage Estimates", 2009 (Jun 25, 2009) .

[49] www.amm.com/, "American Metal Market (AMM)", 2009 (11/10) .

[50] www.platts.com/CommodityHome.aspx?Commodity=Metals, "Platts, Metal Prices", 2009 (11/10).

[51] www.lme.co.uk, "LME Free Market Data: Nonferrous Metal Official Prices", 2009 (Jun/30) .

[52] www.platts.com/IM.Platts.Content/MethodologyReferences/MethodologySpecs/metals.pdf, "Platts, Metals Week: Price Methodology and Specifications Guide", 2009 (11/10) pp. 19.

[53] Fielding, R. A. P., Johannes, M., and Fielding, P. H., 2005, "Extrusion Productivity", Light Metal Age, **63**(3) pp. 6-19.

[54] Fielding, R. A. P., 2004, "Managing the Performance of an Extrusion Plant", International Aluminum Extrusion Technology Seminar: Exploring Innovations, Aluminum Extruders Council, USA, **1,** pp. 565-570.

[55] The Aluminum Association, 1982, "Aluminum Standards and Data", The Aluminum Association, USA, pp. 211.

[56] Oakdale Engineering, 2006, "DataFit", 8.2.79.

[57] www.statistics.com/resources/glossary/c/correlcoeff.php, "Statistics.Com Statistical Glossary", 2009.

[58] Oakdale Engineering, 2006, "DataFit: Understanding and Interpreting Regression Results", 8.2.

[59] Rekab, K., and Shaikh, M., 2005, "Statistical Design of Experiments with Engineering Applications", CRC Press, pp. 252.

[60] Balasubramaniam, L., 1993, "Producibility Analysis using Analytical and Empirical Process Models", PhD Dissertation, MIT, pp. 167.

# AUTHOR'S BIOGRAPHY

Jose Torre Nieto was born in Celaya, Mexico, but grew up in Mazatlan, Mexico. He graduated from *Tec de Monterrey* (in Monterrey, Mexico) in 2002 with a Bachelor of Science Degree in Mechanical Engineering and a minor in Electrical Engineering, and was distinguished with a Mention of Excellence, the maximum academic recognition that *Tec de Monterrey* grants to undergraduate students upon graduation. In early 2003, Jose joined General Electric (GE) to work as a Design Engineer of Static Structures in the Aircraft Engines Division, in one of GE's Global Tech Centers located in Queretaro, Mexico. In 2005, he was promoted to a Lead Engineer Position in the same organization, where he led and supervised a team of 7 engineers for 2 years to redesign structural hardware of the newly developed *GEnx* engine (for Boeing's *787 Dreamliner*), achieving manufacturing cost savings of $1.7M USD annually and about 27 lbs of engine weight reduction. During that time, Jose received numerous recognitions in GE, including the prestigious "Illumination Award on Material Cost Productivity" in 2008, handed by the VP of Engineering in GE Aviation, and the "GE Engineering Recognition Day (ERD) Award" in 2006, 2007 and 2008, given by the General Director of GE's Tech Center in Mexico.

In 2008, after 5+ years working for GE, Jose decided to go to graduate school to further enhance his technical knowledge in the Mechanical Design discipline. He was awarded with a Fulbright Fellowship to pursue a Master of Science Degree in Mechanical Engineering at the University of Illinois at Urbana-Champaign (UIUC). In 2009, he was appointed as a Teaching Assistant in the Department of Mechanical Science and Engineering at UIUC, where he taught the Lab Section of *ME 371-Mechanical Design II* (Fall 2009) and various Lecture-Discussion sessions of *ME 431–Mechanical Component Failure* (Spring 2010).

Jose is happily married to Cynthia since December of 2005. He enjoys practicing sports, especially tennis, basketball and soccer. He also loves to play guitar, both electric and acoustic, and loves to spend time with his family and friends.